X-Hab 2026: LiDAR-Powered Autonomous Charging Service Capability for Surface Rovers and Systems

Georgia Southern University

Department of Mechanical Engineering

1332 Southern Drive, Statesboro, GA 30458

May 2026

Authors:

Megan Steele, Rafe Hamilton, Kyle Henderson, Abigeal McCarthy, Aidan Real, Amadou Mbye, Austen Almeida, Austin Barnes, Austin Herndon, Austin Nobis, Axel Salazar, Ayden Perez, BaJeah Rhoden, Bryan Acosta, Bryce Freeman, Christopher Proctor, Clinton Madden, Cohen Cox, Cole Vandiver, Coleman Norton, Collin Thompson, Dawson Peek Ethan Brown, Garrett Murdock, Hunder Mace, Isaiah Lee, Jacob Allan, James Young, Javier Bejarano, Javon Montford, Josh Hawkins, Justin Tyre, Katie Brown, Kevin McElrath, Liam Fox, Matt Langley, Matthew Walvoord, Michael Taylor, Nichole Christian, Noah Barker, Payton Fuller, Peyton Sperier, Petyon Stanfield, Reasun Allah-U-Akbar, Stephen Nicholas, Timothy Mayo, Tristan Graham, Wesley Powell, Zach Davis

Principal Investigator:

Valentin Soloiu, Ph.D.

Senior Personnel:

Brian Vlcek, Ph.D.

Marcel Ilie, Ph.D.

MSc Student Supervisor:

Timothy Sutton

Table of Contents

1. Executive Summary

This document details the timeline of the LiDAR-Powered Autonomous Charging Service Capability for Surface Rovers and Systems project, initiated by the Fall 2025 semester class and completed by the Spring 2026 semester classs. This project focuses on developing a fully autonomous system composed of a mobile surface rover and an induction charging station with a robotic arm, both controlled by their own NVIDIA Jetson Orin Nano.

Structural improvements to the rover suspension system and body eliminated excessive camber, reduced stress and strain on the plexiglass body, and improved maneuverability and durability of the rover. The charging station robotic arm was fully redesigned to increase reach while minimizing weight and increasing misalignment tolerance during docking on uneven terrain. Electrical system improvements addressed previous torque and power limitations of both the rover and charging station arm. High-torque servo motors were selected based on updated calculations which incorporated terrain slope and Factor of Safety, enabling zero-point turning for the rover and increased payload capacity of the charging station arm. Significant progress was made in autonomy and perception. The rover now employs 3D LiDAR and SLAM mapping for localization, mapping, and path planning.

The Battery Monitoring System (BMS) was created to coordinate battery management between the rover and charging station. The BMS provides continuous monitoring of battery state of charge, temperature, current, and will enable the autonomous initiation, execution, and termination of the charging cycle via Bluetooth communication. Testing of the WIBOTIC induction charging system demonstrated reliable power transfer under both aligned and misaligned conditions. This project demonstrated the ability of an autonomously navigating surface rover to independently plan a path to the charging station, dock, and the charging station to autonomously deploy a robotic charging arm and initiate charging of the rover. This work details the progress made to demonstrate the feasibility of autonomous surface rover navigation and recharging systems.

Figure 1: Autonomous Rover and Charging Station CAD Model

1.1 Problem Identification

Current extraterrestrial rovers do not possess strong capabilities to recharge their onboard batteries, thus limiting their lifespan to the power capacity of their battery or radioisotope power source. Size constraints limit the size and capacity of any onboard batteries or solar panels used to recharge the rover. Battery capacity is currently directly linked to the size of the battery, making large and long lasting batteries impractical for surface rovers. In addition, autonomous battery monitoring would ensure the safety of the rover and prevent mission critical failures. The ability to quickly and reliably recharge a surface rover would drastically improve its useful lifespan, thus extending mission viability and improving cost efficiency.

Modern surface rovers are either directly or indirectly monitored and controlled by human operators millions of miles away. Transmission latency, blackout periods, and communication errors limit the speed and effectiveness of a rover's navigation decisions. Extending the rover's capabilities to include autonomous path planning would reduce the necessary manpower to operate surface rovers, thus increasing mission manpower efficiency.

1.2 Team Structure

2025 Project Manager - Abigeal McCarthy

Rover Team Lead - Katie Brown
Rover Team Members- Cohen Cox, Tristan Graham, Justin Tyre, Peyton Sperier, Aidan Real, Isaiah Lee, Jacob Allan, Austen Almeida, Bryce Freeman

Station Team Lead - Stephen Nicholas
Station Team Members - Peyton Stanfield, Kevin McElrath, Axel Salazar, Dawson Peek, Christopher Proctor, Austin Barnes, Javon Montford, Hunder Mace, Josh Hawkins

Perception Team Lead - Bryan Acosta
Perception Team Members - Zach Davis, Liam F., Nichole Christian, Micheal Taylor, Noah Barker, Austin Herndon, Clinton Madden, Timothy Mayo

2026 Project Manager - Megan Steele

Rover Team Lead - Kyle Henderson
Rover Team Members - Matt Langley, Garrett Murdock, Ethan Brown, Javier Bejarano, Matthew Walvoord, Reasun Allah-U-Akbar, Coleman Norton, Austin Nobis

Station Team Lead - Rafe Hamilton

Station Team Members - Payton Fuller, James Young, Wesley Powell, Cole Vandiver, Collin Thompson, Amadou Mbye, Ayden Perez, BaJeah Rhoden

2. Project Definition

This project aims to design an autonomous surface rover with autonomous induction charging capabilities. As a subsystem of future moon exploration and habitation missions, the autonomous charging station should be scalable and able to accommodate and fully charge various types of rovers. The surface rover should be capable of fully autonomous navigation, including obstacle avoidance, cost mapping, path planning, and battery management as a part of navigation planning. The subsystems should communicate consistently and reliably over a specified range, communicating data such as battery level and usage, and odometry.

2.1 Customer Requirements

The National Aeronautics and Space Administration (NASA) requires an extraterrestrial rover capable of autonomous navigation including obstacle avoidance, path planning, and battery monitoring utilizing LiDAR technology. In addition, the charging station should be capable of autonomous charging initiation, robotic arm deployment, and charging termination. Both systems should communicate critical battery health information, including voltage, current, and temperature. Consideration of the extreme lunar environment in design generation and verification is also required.

2.2 Engineering Constraints

The rover must be lightweight and of a size to be compatible with the charging station arm. The rover must be capable of traversing rough terrain without risking the safety of critical electronics components. Rover suspension must be strong enough to support the main rover body, as well as possess the ability to articulate over terrain. Motors must be capable of overcoming terrain given the rover weight and an incline of 30°. LiDAR integration must include Simultaneous Localization and Mapping (SLAM) capabilities, as well as cost mapping and path planning to a specified target location.

The charging station arm links must be lightweight yet strong enough to support the induction charger. Arm design must include an interior channel for wire management, but the channel must not compromise structural integrity of the arm. Servo motors must be capable of supporting payload weight based upon torque calculations, and must be precisely controlled during operation to minimize jerk and risk for component damage.

The Battery Monitoring System (BMS) must communicate battery voltage, current, and temperature consistently and accurately over a specified Bluetooth receiver range. The entire

project must be completed within the specified budget and timeframe, as well as maintain safety to humans and components during machining and operation.

2.3 Quality Function Diagrams

The seven components making up the rover QFD are the customer's requirements, customer requirement rankings, technical requirements, relationship matrix, co-relationship matrix, and technical evaluations. The QFD was used to evaluate the importance of customer requirements and the relationships between customer requirements and technical specifications, used later in the rover decision matrix. The rover QFD is shown in Figure 2.

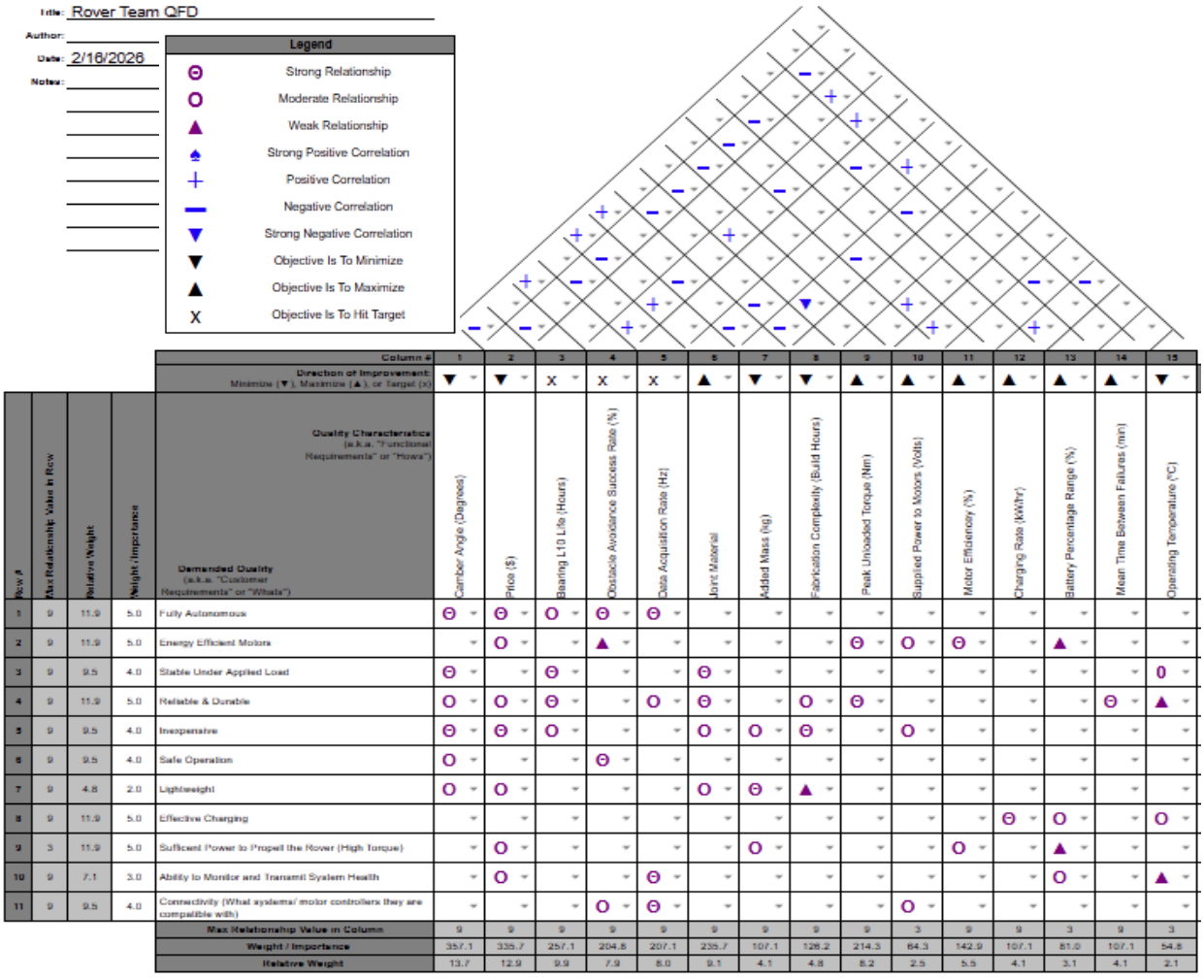

Figure 2. Rover QFD

The customer requirements are listed under the "Demanded Quality" section and describe what the customer wants out of the Rover. The customer requirements include, full autonomy, efficient motors, stability, reliability and durability, inexpensive, safe operation, lightweight, effective charging, sufficient power, ability to monitor health, and full connectivity. These

customer requirements were chosen based on the initial project application to NASA. The weight - importance assigned to each customer requirement was determined based on previous NASA progress reports and an analysis of the fall 2025 rover.

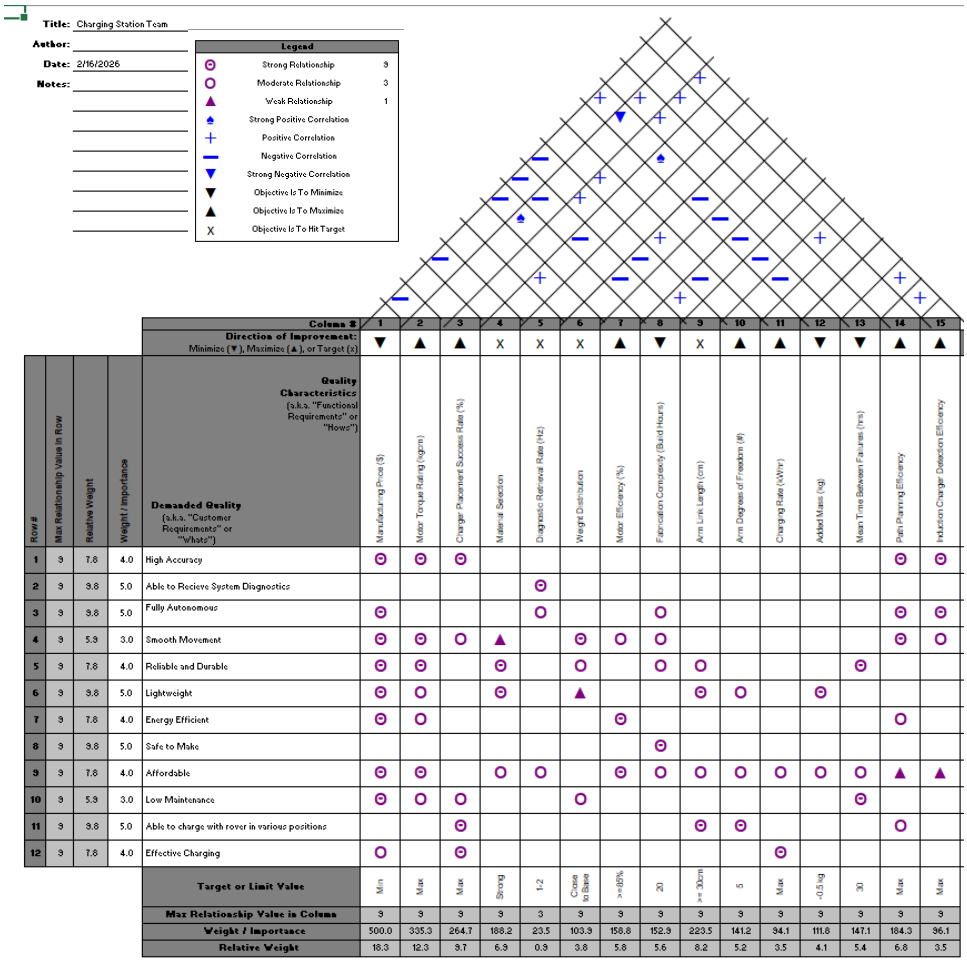

Title: Charging Station Team
Author:
Date: 2/16/2026
Notes:

Legend		
⊙	Strong Relationship	9
○	Moderate Relationship	3
▲	Weak Relationship	1
♠	Strong Positive Correlation	
+	Positive Correlation	
—	Negative Correlation	
▼	Strong Negative Correlation	
▼	Objective Is To Minimize	
▲	Objective Is To Maximize	
X	Objective Is To Hit Target	

Row #	Max Relationship Value in Row	Relative Weight	Weight / Importance	Demanded Quality (a.k.a. "Customer Requirements" or "Whats")	Manufacturing Price ($)	Motor Torque Rating (kgcm)	Charger Placement Success Rate (%)	Material Selection	Diagnostic Retrieval Rate (Hz)	Weight Distribution	Motor Efficiency (%)	Fabrication Complexity (Build Hours)	Arm Link Length (cm)	Arm Degrees of Freedom (#)	Charging Rate (kWhr)	Added Mass (kg)	Mean Time Between Failures (hrs)	Path Planning Efficiency	Induction Charger Detection Efficiency
				Column #	1	2	3	4	5	6	7	8	9	10	11	12	13	14	15
				Direction of Improvement: Minimize (▼), Maximize (▲), or Target (x)	▼	▲	▲	x	x	x	▲	▼	x	▲	▲	▼	▼	▲	▲
1	9	7.8	4.0	High Accuracy	⊙	⊙	⊙											⊙	⊙
2	9	9.8	5.0	Able to Recieve System Diagnostics					⊙										
3	9	9.8	5.0	Fully Autonomous	⊙				○			○						⊙	⊙
4	9	5.9	3.0	Smooth Movement	⊙	⊙	○	▲		⊙	○	○						⊙	○
5	9	7.8	4.0	Reliable and Durable	⊙	⊙		⊙		○		○	○				⊙		
6	9	9.8	5.0	Lightweight	⊙	○		⊙		▲			⊙	○		⊙			
7	9	7.8	4.0	Energy Efficient	⊙	○					⊙							○	
8	9	9.8	5.0	Safe to Make								⊙							
9	9	7.8	4.0	Affordable	⊙	⊙		○	○		⊙	○	○	○	○	○	○	▲	▲
10	9	5.9	3.0	Low Maintenance	⊙	○	○			○							⊙		
11	9	9.8	5.0	Able to charge with rover in various positions			⊙						⊙	⊙				○	
12	9	7.8	4.0	Effective Charging	○		⊙								⊙				
				Target or Limit Value	Min	Max	Max	Strong	1-2	Close to Base	>=85%	20	>= 30cm	5	Max	~0.5 kg	30	Max	Max
				Max Relationship Value in Column	9	9	9	9	9	9	9	9	9	9	9	9	9	9	9
				Weight / Importance	500.0	335.3	264.7	188.2	23.5	103.9	156.8	152.9	223.5	141.2	94.1	111.8	147.1	184.3	96.1
				Relative Weight	18.3	12.3	9.7	6.9	0.9	3.8	5.8	5.6	8.2	5.2	3.5	4.1	5.4	6.8	3.5

Figure 3: Charging station QFD

Similar to the rover QFD, the charging station QFD translates customer requirements into product characteristics. For example, the payload capacity of the charging arm strongly correlates with the torque rating and price of motors. The QFD also compares each product characteristic with other product characteristics, and ranks how they relate to each other. For example, charger placement success rate has a strong positive correlation with charging station efficiency as a whole.

2.4 Safety Requirements

Each team member will observe all requirements for basic lab safety, including wearing long pants, close-toed shoes, and securing hair longer than shoulder length. In addition, special

care will be taken during any machining including proper Personal Protective Equipment (PPE), such as safety glasses, ear protection, and gloves, and machining in the shop using the buddy system at all times.

The rover and charging station will be designed in accordance with all pertinent OSHA electrical wiring requirements, including but not limited to:

- **29 CFR §1910.303** - Proper grounding of all electrical components, all live parts will be secured and guarded
- **29 CFR §1910.304 -** Electrical components will be designed and selected to accommodate maximum power draw to prevent overheating and damage
- **29 CFR §1910.305** - Reduce strain on all wires, temporary wiring must be reasonably secured
- **29 CFR 1910** - The movement of a robotic arm will be taken into consideration when wiring components [1]

Both subsystem designs have been created with fundamental engineering codes and canons of safety in mind, including but not limited to:

- **Code of Ethics for Robotics Engineers, Principle #2:** "Consider and respect peoples' physical well-being and rights." [3]
- **ASME Fundamental Canon #1: "**Engineers shall hold paramount the safety, health, and welfare of the public in the performance of their professional duties." [4]

The rover design considers the safety of the onboard electrical components, and has included secure attachment points and pertinent shielding/cases. Safety of operators has been considered in the speed of the rover, it is not too fast so as to run into and hurt anyone. The charging station design has included electrical organization structures. Both subsystems have been equipped with emergency circuit breaker switches in easily accessible locations, as shown in Figure X.

Figure 4: Charging station emergency circuit breaker switch

2.5 Impacts

The social impacts of this project can be seen both within and outside the team structure. Within the project team, significant time was spent working cooperatively to accomplish difficult tasks, many of which were completely new to the team. Significant time was spent troubleshooting, planning, and collaborating as a team. As stated in ASME Fundamental Canon #10, "Engineers shall, in all matters related to their profession, treat all persons equitably and encourage and support participation by all…" [4] This project has produced a team of professional, creative, and determined young engineers who are capable of participating in constructive disagreements and working as a member of a diverse team.

Outside of the team structure, the NASA M2M X-HAB Academic Innovation Challenge itself is an inspiring and community-building project designed to build up the next generation of engineers. Many of NASA's innovative technologies go on to become mainstream products and services, thus furthering human scientific advancement as a whole.

The primary economic goal of this project was to stay within the prescribed budget set forth by the NASA M2M X-HAB project, and supplemented by Georgia Southern's Dr. Soloiu. The team accomplished this goal through reusing all possible materials and components from the previous semester's work, comparing pricing among multiple stores, and purchasing only what was needed for the project's success.

The environmental impact of the engineering work in this project may be considered small-scale, but it is important nonetheless. From design to manufacturing, environmental impacts and waste reduction were considered, in accordance with ASME Fundamental Canon #8 which states "Engineers shall consider environmental impact and sustainable development in the performance of their professional duties." [4] Waste reduction was considered when designing the new rover joints for CNC machining, and they were sized to fit closely in standard-sized aluminum stock pieces to minimize materials waste. During manual machining processes, all scrap and waste was thoroughly cleaned and placed in appropriate containers for recycling, when applicable.

3. Design Selection

Both rover and charging station teams developed three unique concept designs, including physical modifications, motor selections, and electronics component selection. Each team created a decision matrix to weigh the aspects of each design concept and select the best performing design for further development.

3.1 Initial Design Concepts

The design solution for the X-Hab 2026 Academic Innovation Challenge is a charging station supplied by 120 volts alternating current wall power equipped with induction-based charging to supply power to the battery located on the rover. The charging station's base is a

hexagonal design intended to permit multiple docking stations. In the center, a 3D printed mechanical arm with 300 degree horizontal position is used to transmit power through an induction transmitter coil located on its last link. The mechanical arm is equipped with five motors and a stereo camera connected to the Jetson Orin Nano Super for precise positioning and navigational requirements. In figure 4, the finalized 3D model for the Charging Station is shown.

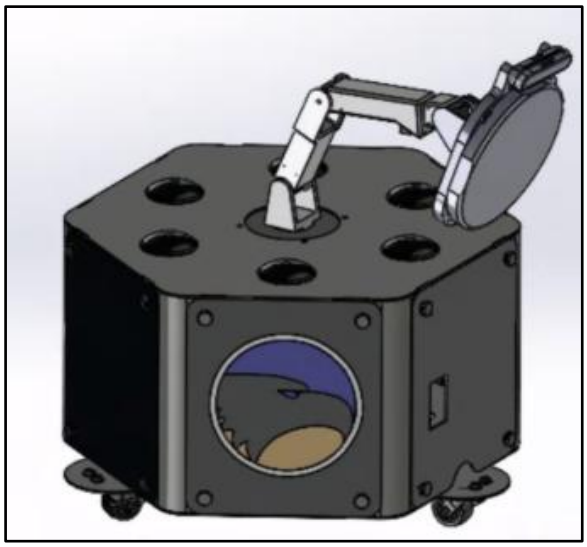

Figure 4: 3D Assembly of station

The first subassembly is the base. The base has six side panels designed to be removable for ease of access to the inner components. One of these panels contains the ground fault circuit interrupter (GFCI). This is intended for cable extension and is considered the troubleshooting panel. The main frame is a hexagonal design and the circular cut-outs placed on the top and bottom plates are used for weight reduction. Three ground stabilizers are used to secure the station's position, and for scalability purposes, have the ability to be mounted to the terrain.

The station's hexagonal top and base plates are made of Steel A36 due to its price and material properties. The base supports connecting the top and base plates are constructed of Aluminum 5052-H32 and are bent in house to a precise fit. Each base support has four weldnuts located on either side of the angled aluminum to permit a stable connection point for the side panels to be attached. In figure 5, the 3D model of the base assembly is shown.

Redacted due to Export Control/CUI requirements.

Figure 5: 3D CAD of Base Assembly

The mechanical arm was originally designed to have six motors and six degrees of freedom. Due to torque constraints, the finalized design is fitted with five motors and links and an updated mounting link to reduce weight constraints. The arm was 3D printed with ABS filament to reduce costs and for weight reduction. The five motors are daisy-chained along the link mounts and consist of two 50 kg-cm torque motors placed on links 1 and 2, and three 30 kg-cm torque motors on the remaining links. The finalized 3D model of the mechanical arm and the updated mounting link is shown in figure 6.

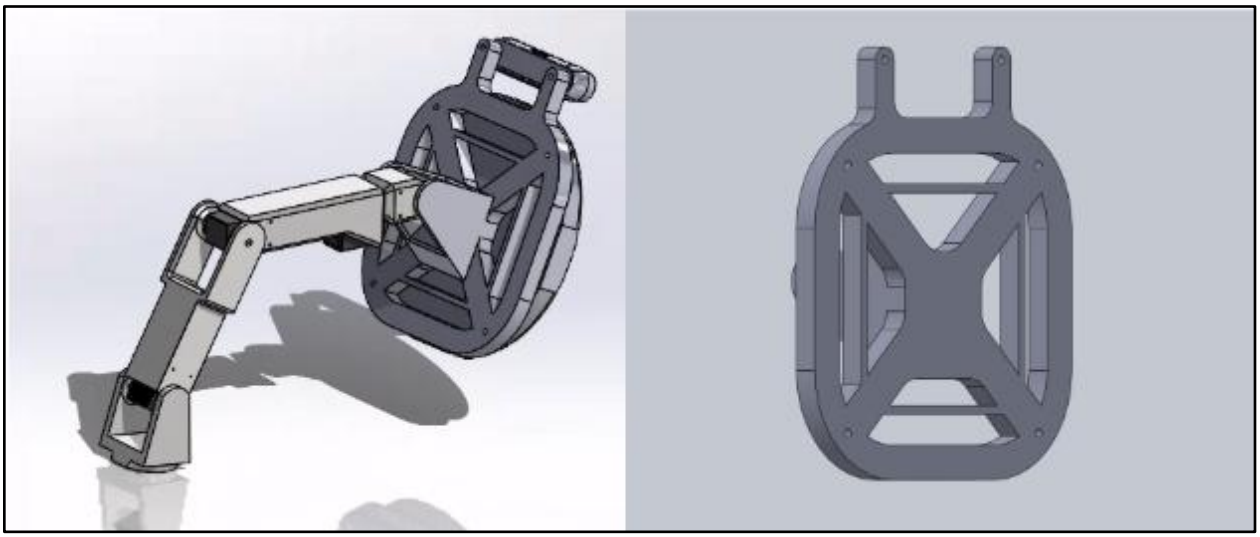

Figure 6: 3D Model of 5 Link Arm and Mounting Face

The servicing rover's design is consistent with those used in space exploration missions. The rocker-bogie design enables complex navigational capabilities not seen in other vehicular designs. The rocker and bogie links are connected on a differential joint which allows vertical maneuverability while maintaining all wheels on the ground . For the project's requirements, the servicing rover was developed to have six zero-turn wheels, so that the rover has precise rover positioning for charging protocols. The motors that govern wheel movement are six GM37 geared motors with encoders rated for 12 volts and 38 rotations per minute.

Due to the tire profile having more significant tire wells than originally anticipated, the original motor mounts experienced high levels of friction and reduced speed capabilities in the motors. To resolve this new 3D printed motor mounts were manufactured to extend the socket region and cutouts were designed to reduce manufacturing time. Thus the motor axle can extend towards the rim without adding any significant load. This can be seen in figure 9. Part drawings and tolerances have been created for the servicing rover, in addition to the current bill of materials which is shown in the appendix. The servicing rover's main subassemblies include leg infrastructure, controls and charging system, and the frame.

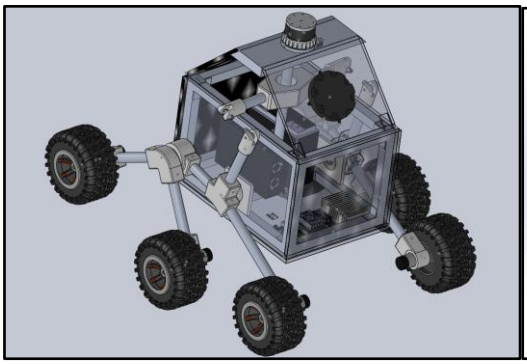

Figure 7: Rover 3D Model

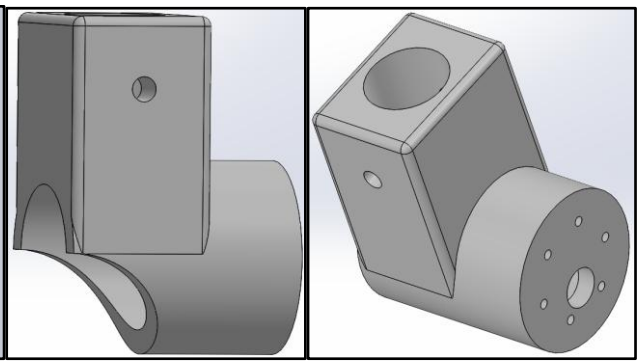

Figure 8-9: 3D Models Motor of Mounts

The leg infrastructure is connected through multiple differing joints all which is to be 3D printed using PLA Filament. The links that connect the leg assembly together are made out of 6061 aluminum piping to reduce the overall weight of the servicing rover. Due to the limited structural strength of 3D printed parts, the leg joints and links underwent strict stress analysis to ensure the structural integrity of the leg assembly. The frame is to be constructed out of aluminum framing fixed with plexiglass walls. The main body contains the microprocessors, battery, and electric equipment designed to transfer power. The main materials used for constructing the main body are plexiglass and aluminum. These materials were chosen due to weight reduction, and cost reduction. The charging receiver is placed on one of the 45 degree plexiglass framing sheets enclosing the main body to limit the distance the arm must reach. The 3D Lidar is placed on a flat surface on top of the servicing rover's main body. The controls and charging system pertains to the motor system, battery system, microprocessors, and the induction charge receiver. The main source of power for the servicing rover is a 24 V 10 Ah battery, that is to be recharged by the station. The estimated battery life of the servicing rover is approximately 42 minutes.

The 2026 semester team evaluated each design for both the station and the rover, and generated new design concepts for both. Further decision making was performed to select the best of the new design concepts for further model development and manufacturing.

The charging station team developed three SolidWorks concept models to solve design issues identified from previous semester design for the induction charging arm. The design requirements for the charging station arm include: being able to accurately and consistently place the induction charger onto the rover, having enough length and degrees of freedom to place the charger in a variety of positions, being able to receive and transmit rover diagnostics, knowing when to stop charging protocols, and performing all actions autonomously. Changes to the physical structure of the station arm may be able to meet the requirement for length and degrees of freedom. Through physical analysis of the previous group's final station arm concept, it was determined that, assuming a 76.2mm gap between the front wheel of the rover and the front face of the station body, the maximum extension of the arm possesses an approximately 253mm gap between its induction charging plate and the charging plate of the rover. The second link in the 5

link arm setup was measured at 220mm and may be observed in Figure 10. The third link in the 5 link setup was measured at 145mm and may be observed in Figure 11.

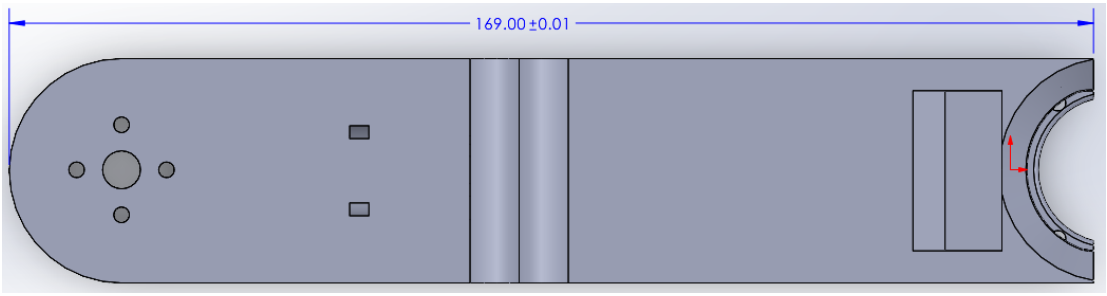

Fig 10. Link 2 on Fall 2025 Charging Station Final CAD Model

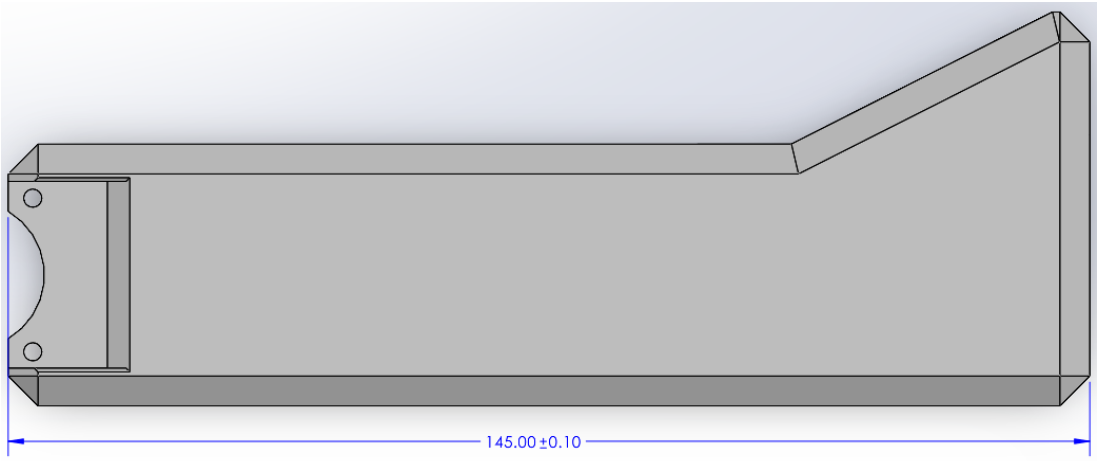

Fig 11. Link 3 on Fall 2025 Charging Station Final CAD Model

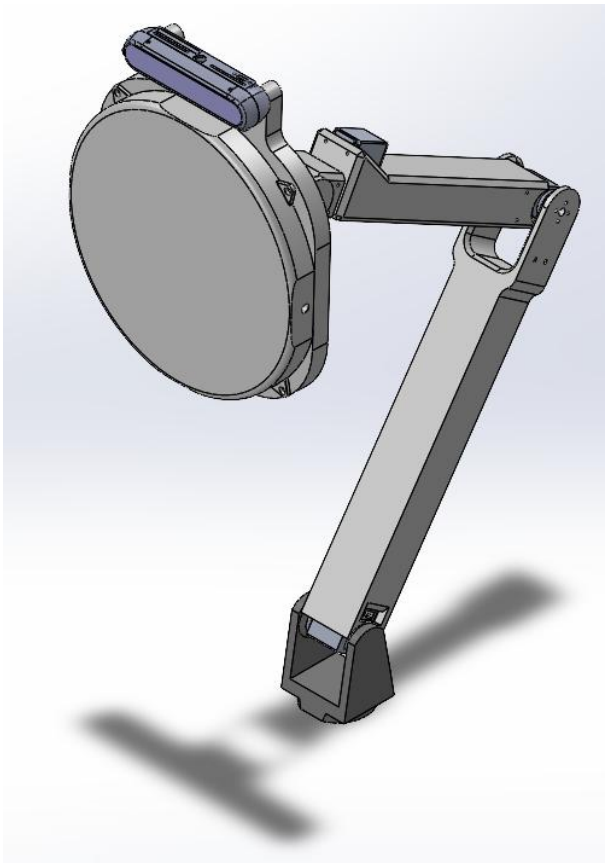

Fig 12. Concept 1 Charging Station, 5 Link Arm Full Assembly

Upon calculating the requirements for torque from each servo motor in the arm, it was determined that the torque ratings of the servos were insufficient for proper operations, but the existing motors do possess the capability to move the arm. These problems aimed to be solved by the three concepts to differing degrees. Concept 1 aimed to have the least amount of change to the existing CAD models by lengthening the second and third links to close the gap observed in the previous semester final models. Additionally, the arms are to be redesigned to fit new motors of 50kg and 95kg torque capacity. The second link was increased in length by 178mm and the third was lengthened by 75mm. The new size of the second link may be seen in Figure 13. The new size of the third link may be seen in Figure 14. The full SolidWorks assembly of the Concept 1 arm may be seen in Figure 15.

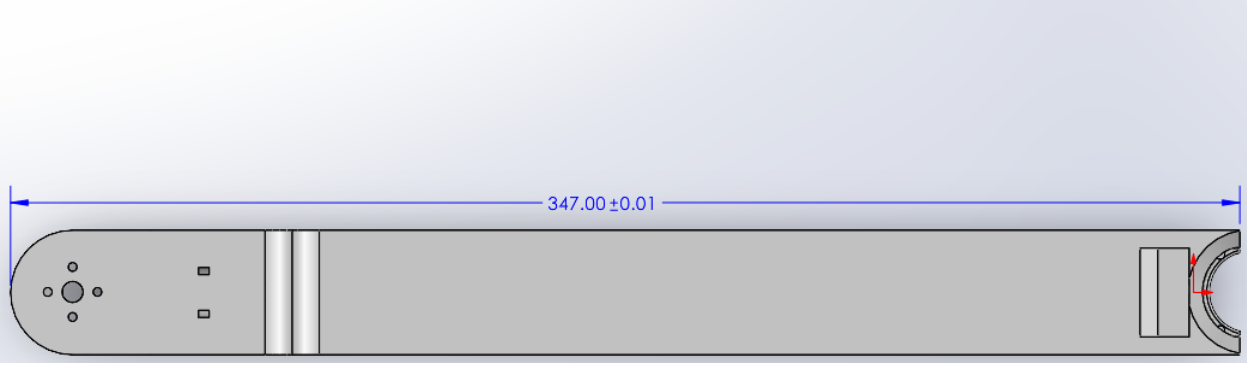

Fig 13. Concept 1 Link 2 CAD Model

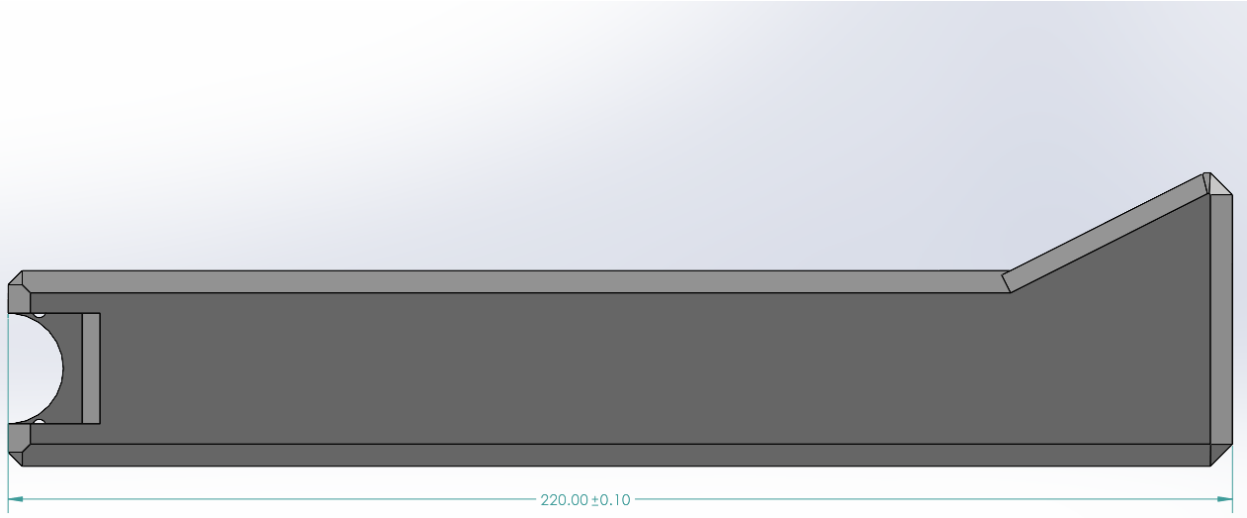

Fig 14: Concept 1 Link 3 CAD Model

Concept 2 aimed to be a more in depth modification to the original CAD models. This concept aims to reduce material on the induction charging pad to alleviate torsional stress on servo motors, hollow out the center of the links for further torsional stress relief and for cable management, and lengthen the second and third links to meet the 253mm overall length increase requirement. All modifications are to be done assuming no change to the original motors, unlike Concept 1. The full SolidWorks assembly file for Concept 2 may be seen in Figure 16 A bottom-up view of link 2 on the 5 link arm seen in Figure 17. shows how the concept reduces overall weight and material expense by hollowing out the center of the arms. This will also serve as cable management structures. The hollow space allowable for cables has a minimum cross sectional area of $1444.32mm^2$ which is sufficient for the cables used for this induction charging system.

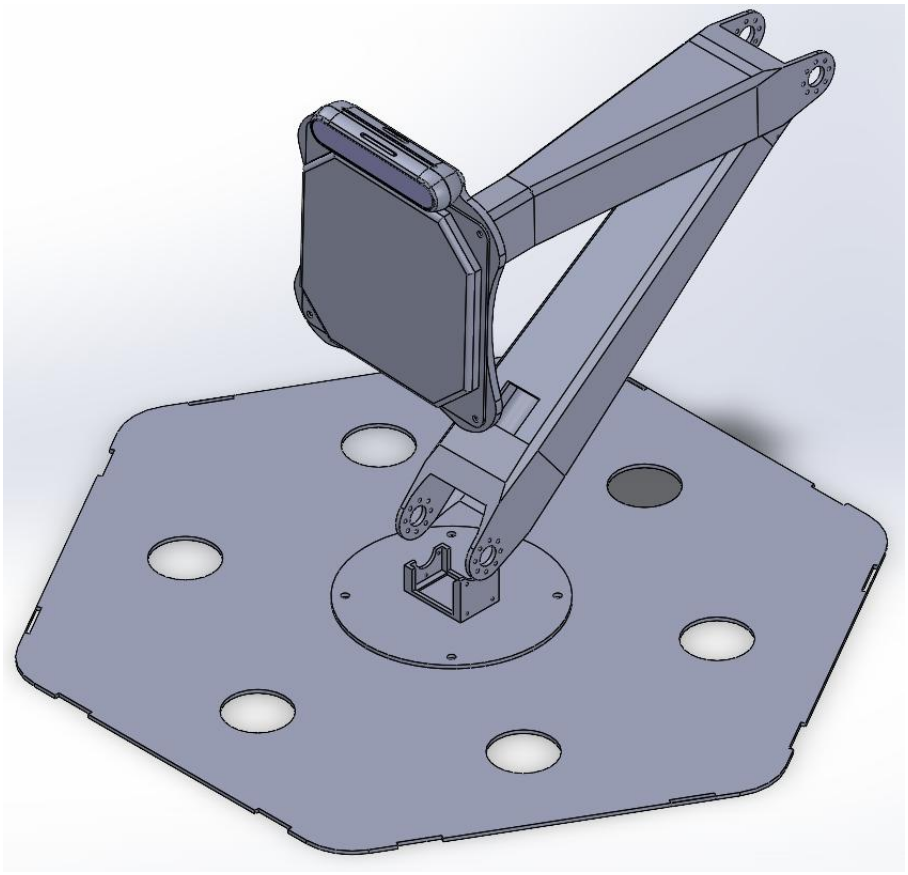

Fig 16. Concept 2 Version 1 Full Assembly

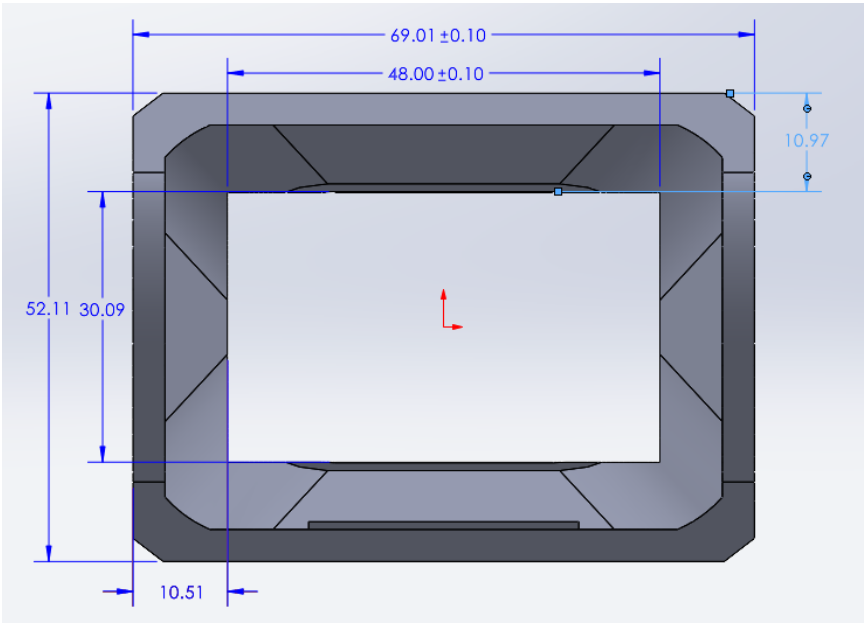

Fig 17. Concept 2 Version 1 Link 2, detail view of wire management channel

Concept 3 aimed to make the most modifications to the original design. The first and second links were to be redesigned to fit an upgraded servo capable of 95kg torque capacity while the existing 50kg servos were moved to the upper link joints. Cutouts were made along the length of Links 2 and 3 for weight reduction without compromising strength and payload capacity. In addition, a Link 1 to base structural reinforcement plate was designed to improve stability at this joint, especially at full arm extension. A full assembly CAD model of the Concept 3 design in an isometric viewpoint may be seen inFigure 18

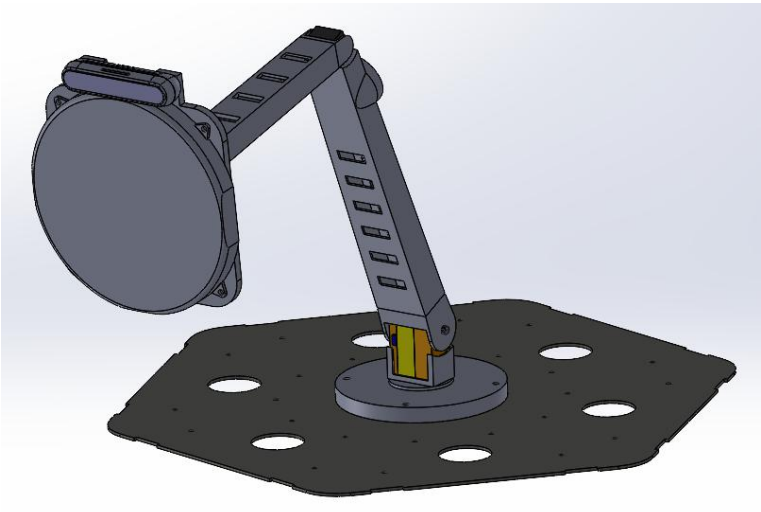

Figure 18: Concept 3 fully assembly model

The rover team also developed three design concepts in order to solve the issues identified with the prior design. Amongst all three concepts, due to most issues being primarily concentrated on the mechanical and software side. All existing sensors and controls were maintained. The Ouster OS0-128 Lidar Scanner would remain as the primary sensor for navigation and the motor controls would remain on the Arduino Uno with the Nvidia Jetson Orin Nano Super operating the rover. The current 24V 10Ah lithium battery would also remain in use. In order to showcase the possibility of thermal controls, all concepts would implement mylar sheeting to insulate the electronics and deploy K type thermocouple to monitor temperature of key components.

Concept 1 focuses on changing the joint design to ensure all motors are in line with each other. The main joint connecting the rocker and chassis would be changed to be machined aluminum and the joint between the rocker and bogie would be changed to an aluminum knuckle joint in order to reduce the camber at said joint Figure 19. Additionally, an aluminum plate would be used to ensure that the weight of the body was not transferred through plexiglass Figure 20. The motors would continue to be DC motors, however, with a higher torque and lower RPM. Additionally, in order to protect the electronics from extreme temperatures mylar sheeting would be implemented on the main chassis. The positives of the first concept is that the in-line knuckle join reduces potential camber and failure at the joint, the insulation helps maintain ideal temperature for the electronics, and the DC motors allow for simpler controls and electrical. As a negative, the knuckle joint could interfere at extreme angles, extra weight would be added by

reinforcing aspects with aluminum, and the higher torque motors would also reduce the top speed of the rover.

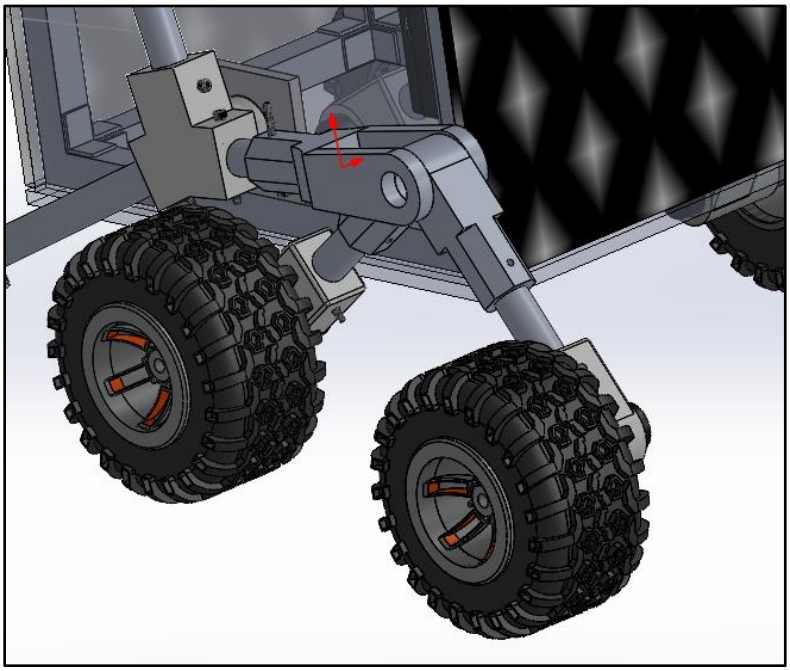

Figure 19: Concept 1 Knuckle joint at rocker-bogie node

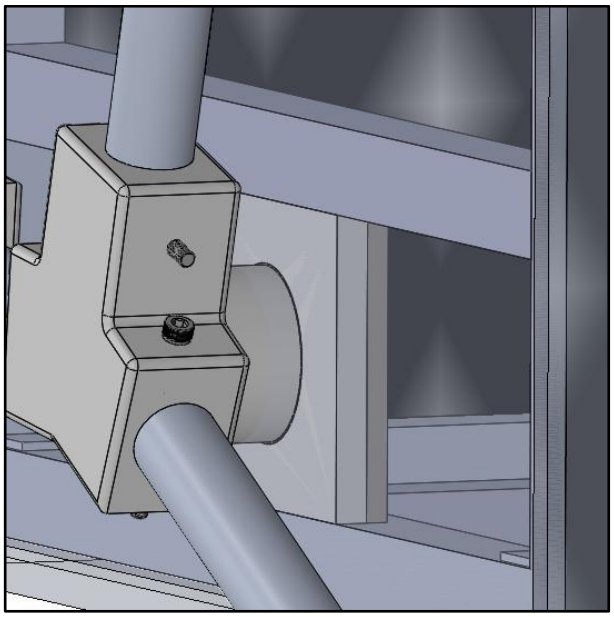

Figure 20: Concept 1 Plexiglass reinforcement plate

The second concept for the rover would make use of AC servo motors instead of the prior DC motors. Additionally, the existing plastic joints would be machined out of aluminum and vertical aluminum extrusion supports would be used to reduce flex in the plexiglass, as shown in Figure 21. The AC motors would allow for superior positioning accuracy and dynamic response as well as reduced maintenance due the the brushless design, however these benefits come with

greater control and integration complexity, requiring tuning and electromagnetic interference mitigation. Additionally, the aluminum joints would provide better durability and wear resistance as well as better alignment retention and reduced camber due to higher stiffness in the parts. These improvements would come at the cost of higher manufacturing costs and complexity, as well as increasing the overall mass of the rover.

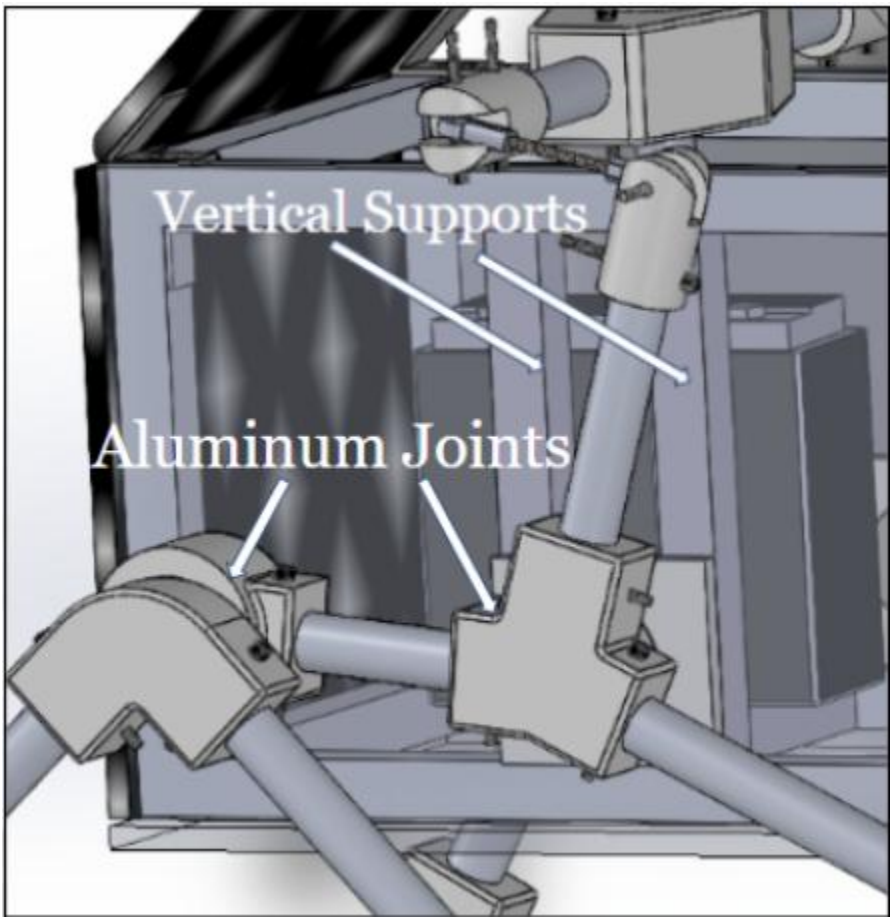

Figure 21: CNC aluminum joints with vertical supports for mounting rocker-bogie to frame

The third rover concept would make use of full in-fill 3D printed components in order to address the inadequacies of the prior 50% in-fill joints Figure 22. This increased in-fill alongside vertical aluminum extrusions as supports for the plexiglass to prevent bending would aid in addressing the camber of the wheels. Additionally, the design would use stepper motors for precise movement and high torque at lower rpm. This concept would be simple to manufacture and would increase the strength in the joints without significantly affecting the mass. The cons of this design would be that the 3D printed parts are more susceptible to wear and the parts obtain larger tolerances, additionally, stepper motors are high cost, maintain constant current draw when idle, low torque at higher rpm, and are complex to control.

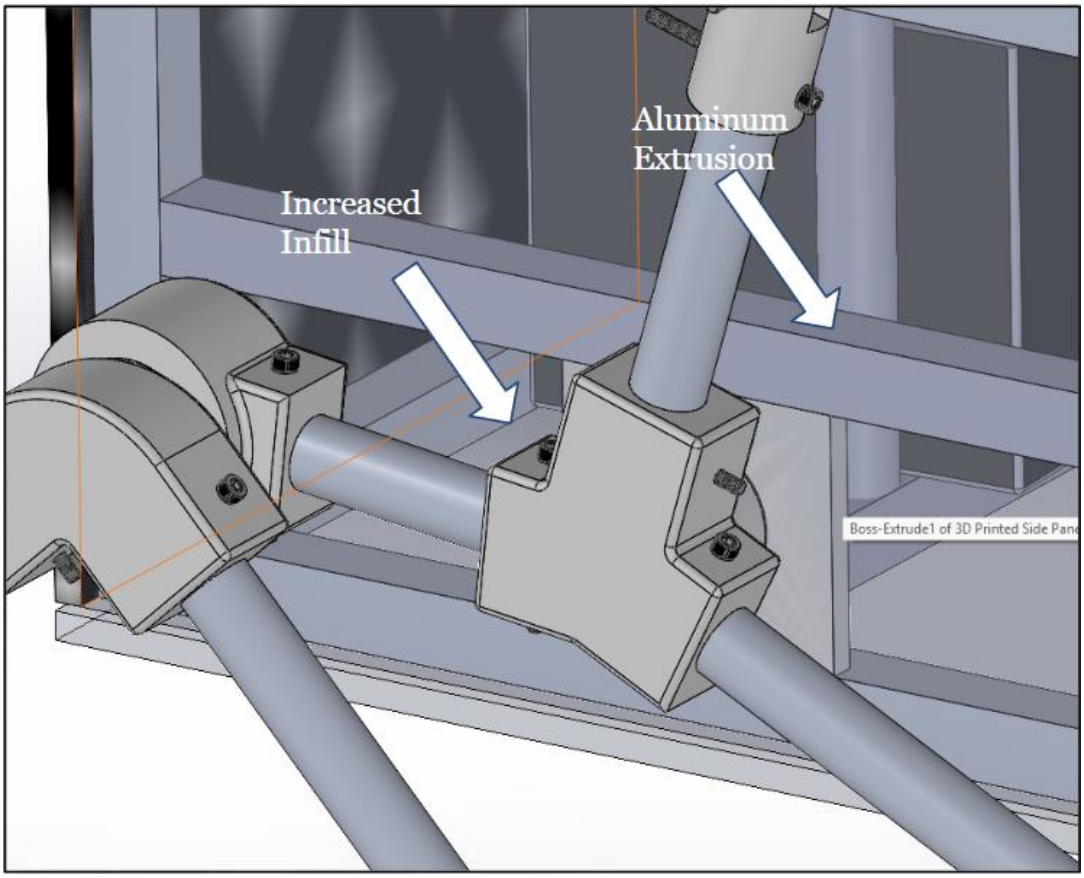

Figure 22: Rocker Bogie w/ Aluminum Extrusion Reinforcement

3.2 Decision Making

In order to determine the most optimal design for the charging station arm, a list of requirements was established, including reach capability and reliable operation. These requirements were used to form a decision matrix for design evaluation. Original design analysis revealed two major shortcomings. First, the induction charger could not reach the rover when the original charging arm was at full extension. To resolve this issue, all concept generations included increased link lengths to ensure the rover could align with the station at different orientations. Secondly, the motors on the original design were not strong enough to support the combined weight of the arm and induction charger assembly. This led to an overhaul of the motor selection as the motors were required to easily be able to maneuver the arm structure. Weight optimization and motor selection were primary motivators for the new designs. The updated motor requirements were established to achieve a higher factor of safety (3).

Station		Concept 1		Concept 2		Concept 3	
Criteria	Weight	Score	Weighted Score	Score	Weighted Score	Score	Weighted Score
Wire Management	3	2	6	5	15	2	6
Length	5	5	25	4	20	4	20
Diagnostic Retrieval	3	3	9	3	9	3	9
Motor Torque	5	4	20	5	25	5	25
DOF	4	5	20	5	20	4	16
Affordability	5	4	20	4	20	3	15
Maintenance	4	3	12	3	12	4	16
Manufacturing Complexity	2	2	4	2	4	3	6
Durability and Reliability	3	3	9	4	12	4	12
Weight Distribution	3	1	3	5	15	4	12
Total Weight	5	2	10	4	20	5	25
Final Weighted Score			138		172		162

Figure 23: Charging Station Arm Decision Matrix

Three conceptual designs were created to address the aforementioned issues. Concept 1 kept the original design while increasing the length of each arm link, but it was unable to resolve material usage/weight requirements. Concept 2 included an updated arm design that increased link lengths while accounting for weight requirements by hollowing out the center portions of each link and trimming down the thickness of the induction charger plate. This design also accounts for wire management as the wires present on the charging arm can be rearranged to the inside of the links. Concept 3 completely redesigned the charging station arm with less material but also one less degree of freedom as the wrist joint was removed. By extending the link length and using stronger motors, the structural strength was decreased due to the added weight and distribution methods. A decision matrix was created to impartially determine the best overall design concept to move forward with. The decision matrix used to evaluate the three concepts is shown in Figure 23.

Rover		Concept 1		Concept 2		Concept 3	
Criteria	Weight	Score	Weighted Score	Score	Weighted Score	Score	Weighted Score
Fully Autonomous	5	5	25	3	15	5	25
Energy Efficient Motors	5	5	25	3	15	1	5
Stable Under Applied Load	4	5	20	5	20	3	12
Reliable & Durable	5	3	15	5	25	3	15
Inexpensive	4	5	20	3	12	1	4
Safe Operation	4	5	20	5	20	5	20
Lightweight	2	1	2	1	2	3	6
Effective Charging	5	3	15	3	15	3	15
Sufficient Power to Propell the Rover (High Torque)	5	5	25	3	15	1	5
Ability to Monitor and Transmit System Health	3	3	9	1	3	5	15
Connectivity (what systems/motor controllers they are compatible with)	4	5	20	5	20	3	12
Final Weighted Score			91		75		73

Figure 24. Rover Decision Matrix

The decision matrix used the criteria identified in the Rover QFD and was assigned an adjusted weight from 1-5, with 5 being the most important. Each concept was scored according to the criteria in column 1. Criteria such as Lightweight, Charging Effectiveness, and Motor Torque

were scored and compared. Concept 2 was selected as it had the highest score by balancing length, structural strength and motor capability while meeting the customer requirements.

3.3 Design Iterations

With Concept 2 of the station selected, the arm design that was selected featured an 11” link 2, an 11” link 3, as well as a 3” link 4 and a 3” link 5. Link 1 was mounted into the top of the charging station, with a rotating motor under it to power the arm’s scanning rotation. A motor is attached on top of link 1, joining links 1 and 2 together. This motor was calculated to have 160 kg*cm of torque to be able to sustain the moments placed upon it by the rest of the arm and move it effectively. Link 2 then extends upward where a 150 kg*cm motor is attached at the end of it, joining links 2 and 3 together. Link 4, the wrist component, was joined to link 3 with a 50 kg*cm motor, and then had a 50 kg*cm motor on the other end connecting it to link 5, the plate where the induction charger sits.

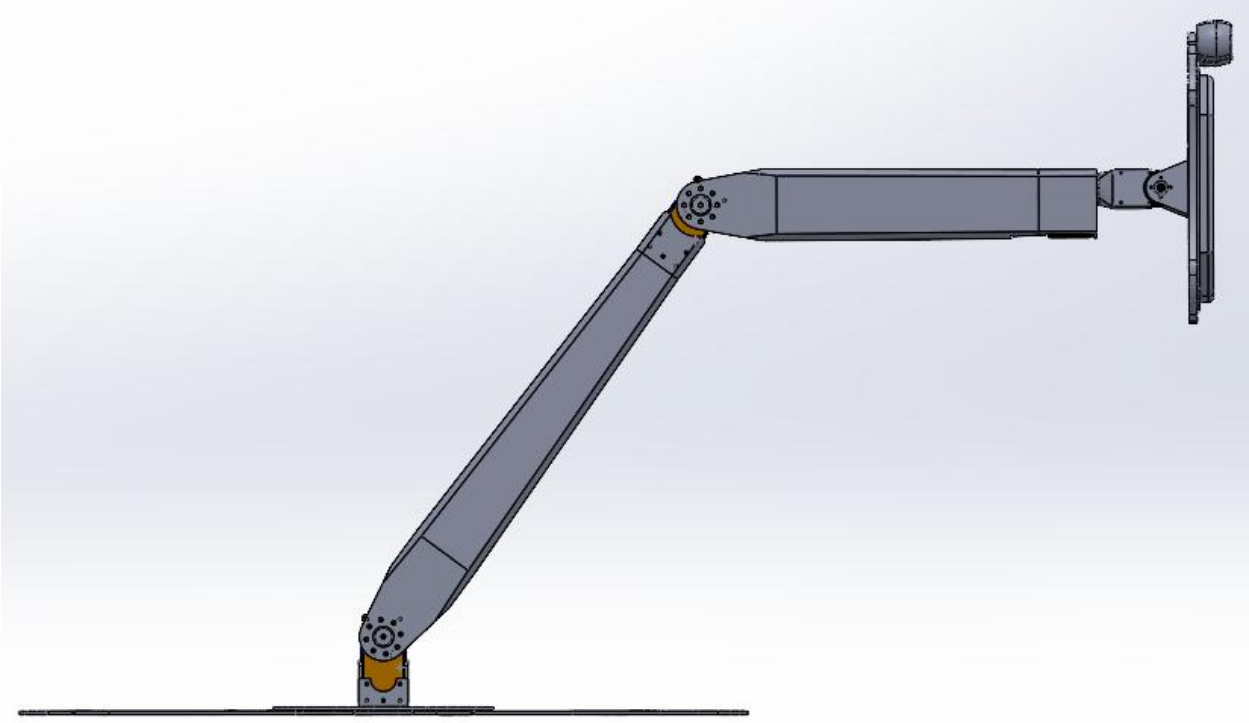

Figure 25. *Arm design Gen 2 V1*

This was the original design of the project, however it did not reach the required length necessary for consistent contact with the rover’s induction charger.

To address this length issue, four additional inches were added onto link 2 bringing it to a total of 15 inches. This brought the total length of the arm up to 32” meeting the requirement, however the 3-D printers accessible to the team could not print anything larger than 11”. Initially, link 2 was to be broken into two different sections to be printed separately and then joined together

in the assembly. After analyzing this in ANSYS, the group was not satisfied with the structural integrity of this plan and instead decided to reduce link 2 back to 11”.

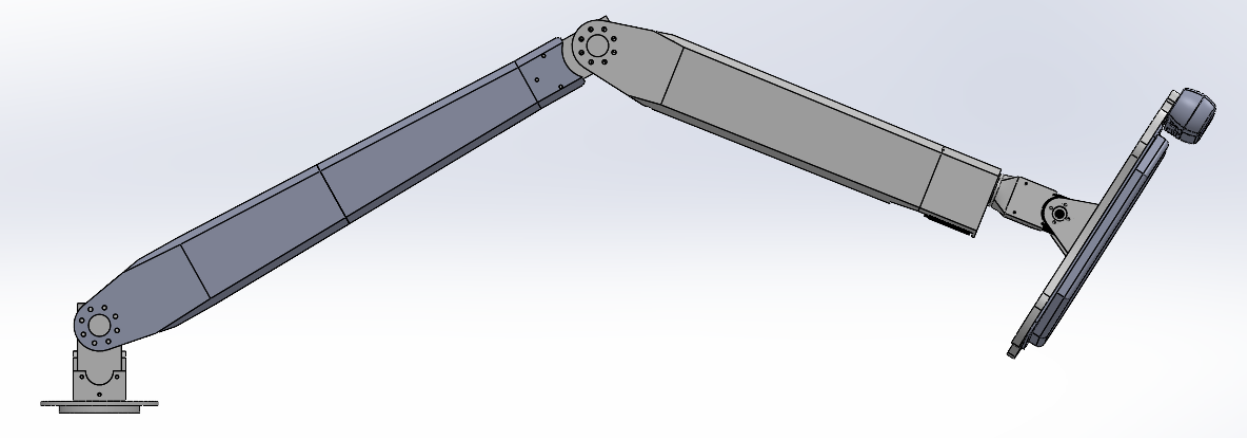

Figure 26. *Arm design Gen 2 V4*

This meant the additional length had to be redistributed throughout the other links on the arm, namely links 4 and 5. Upon adding this length, the torque calculations were done again to ensure the selected motor would be able to support the additional moment from this weight and length. With the torque calculations reaffirming that the motors would support, this is the design that moved forward. The links were hollow inside to reduce the weight and moment on the motors, allowing for motors with lower specs to be used. With additional analysis confirming that these lighter, less strong prints would be able to support the weight and movement necessary for the arm to function, this was the design that was finalized and printed for testing, and eventual use on the charging station.

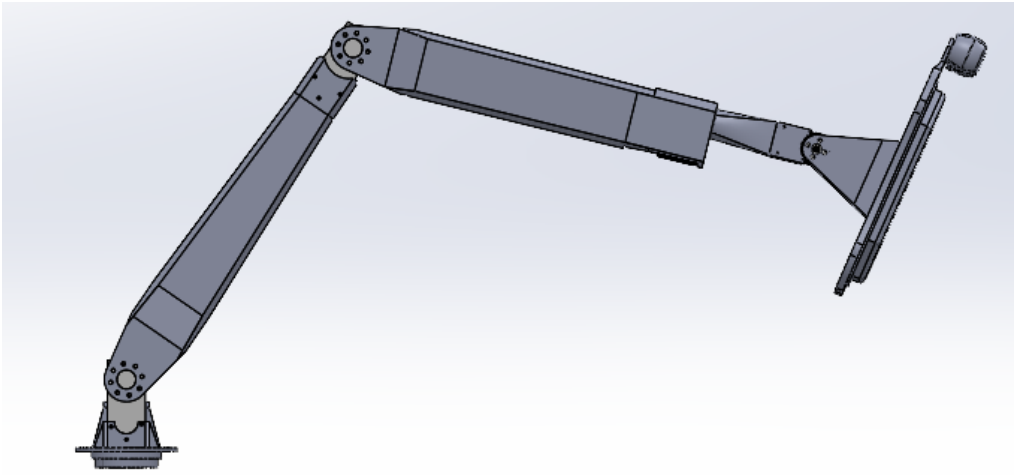

Figure 27. *Arm design Gen 2 V7*

4. Final Designs

This section details the final designs of the 2026 semester team.

4.1 Overview

The final design selection for the rover and charging station arm included rover concept 1 and station concept 2. Rover concept 1 includes critical structural modifications to the suspension system, as well as new higher torque motors and improved maneuverability control. Station concept 2 consists of a full arm redesign, increasing maximum reach by approximately 20 inches (to a new overall length of 30”), as well as features interior wire management capabilities and higher torque motors for increased payload capacity.

Figure 28: Full system assembly, final design

4.2 Mechanical Details

The most critical electrical component upgrades were the rover and charging station arm motors. In order to obtain servo motors with the proper torque ratings to support the combined weight of the material in the arm and the motors inside, torque calculations were necessary to complete. To do this, first a diagram of the arm was created to help derive the necessary equation.

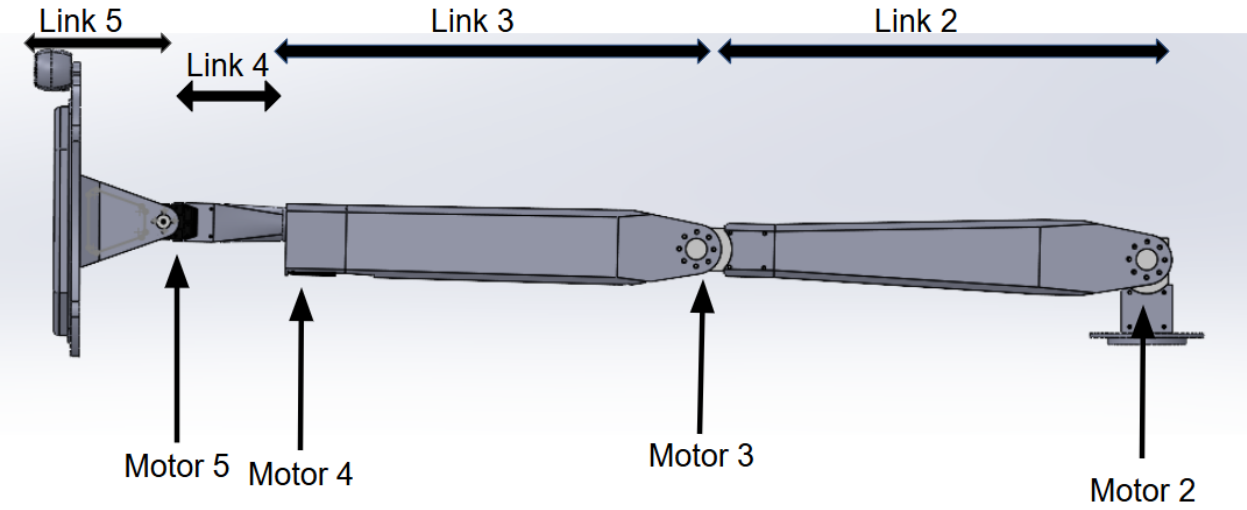

Figure 29: *Diagram of charging station arm*

With this diagram, a moment balance equation was created at each of the motor points on the arm. The force and distance of each component relative to the motor was added to the equation, and the resulting moment was the minimum torque required to support the arm. This equation was then inserted into MATLAB to do the calculations, and then convert the results from Newton-meters (Nm) to kilogram-centimeters (kg*cm), the units that the motors being selected from were listed in.

Figure/Table containing sensitive information has been removed.

Figure 30. *Torque Calculation MATLAB Code*

The results given from this equation gave the minimum torque value necessary to support the arm, but not to move it. To achieve a torque sustainable for movement, a minimum factor of safety of 1.7 was applied to each of the results when considering motor selection. The final motor selection included one 160kgcm ANNIMOS servo motor for Motor 2, 150kgcm ANNIMOS motors for Motor 3 as well as Motor 1 (located inside the station base), and repurposing two of the 50kgcm FEETECH motors from the previous semester's work for Motors 4 and 5. With this

equation to reference, the motor selection was completed with an additional motor 2 ordered in case the single motor couldn't support the weight of the entire arm.

The Gen. 1 rover was unable to perform zero-point turning; the primary cause of this was low-torque motors, and the secondary cause was the high traction wheels. The torque for the new rover motors were calculated for a thirty degree inclined surface with a Factor of Safety (FOS) of 2, as shown in Figure 10. The resulting torque for each motor was 47 kg.cm, and the new motors purchased for the Gen. 2 rover (shown in Figure 11) are rated at 51 kg.cm each.

Table 3: Rover Torque Calculations, Flat Terrain

Redacted due to Export Control/CUI requirements.

Table 4: Rover Torque Calculations, Inclined Terrain

Redacted due to Export Control/CUI requirements.

Redacted due to Export Control/CUI requirements.

Figures 31 and 32: Sample of Gen. 2 rover motor torque calculations, and CQRobot rover motors

The Gen. 1 rover joints were 3D printed out of PLA plastic with an infill of 50%. The previous rover design experienced significant camber issues caused by weak joints, which is shown in Figure 33.

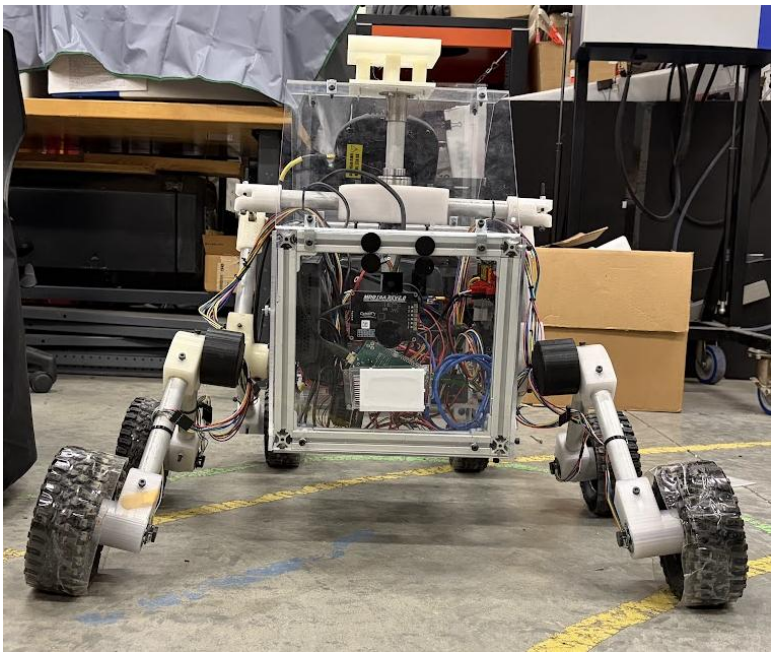

Figure 33. *Gen. 1 Rover Camber Example*

During the testing phase for the Gen. 2 rover, the joints from concept 1 were 3D printed and tested with the rover. The new design helped decrease overall camber, but during turns, the long forks of the outer knuckle joint would bend due to the 3D printed joints lower strength. The joints from concept 1 were CNC machined out of aluminum to improve their structural integrity. The material properties of aluminum are better suited to withstand the loads associated with rover movement, when compared to PLA. The improved camber is shown in Figure 34

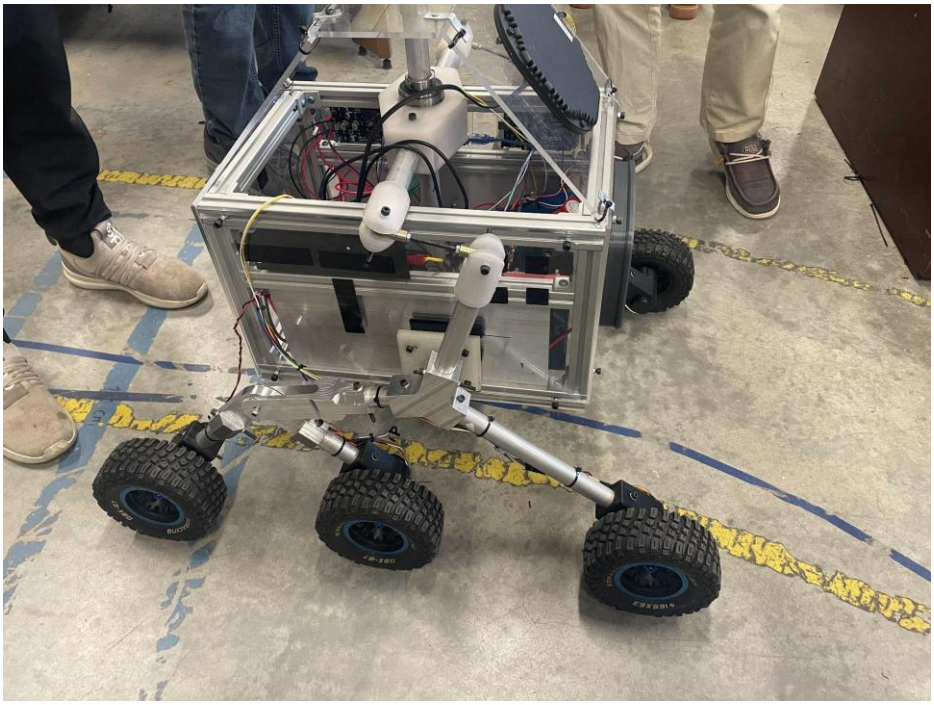

Figure 34. *Aluminum joints on rover*

The new rocker-bogie knuckle joint improves the structural stability in a few ways. Primarily the knuckle joint reduces the opportunity for camber at the join itself by ensuring that with the structural rigidity of aluminum, there is little opportunity for play in the horizontal axis. Additionally the joint moves the attached wheels in line with the main joint reducing the moment from the bogey wheels to the main connection to the rover. Furthermore, the forces on the join reduces the bending moment on the bearing which reduces wear and tear on the bearings.

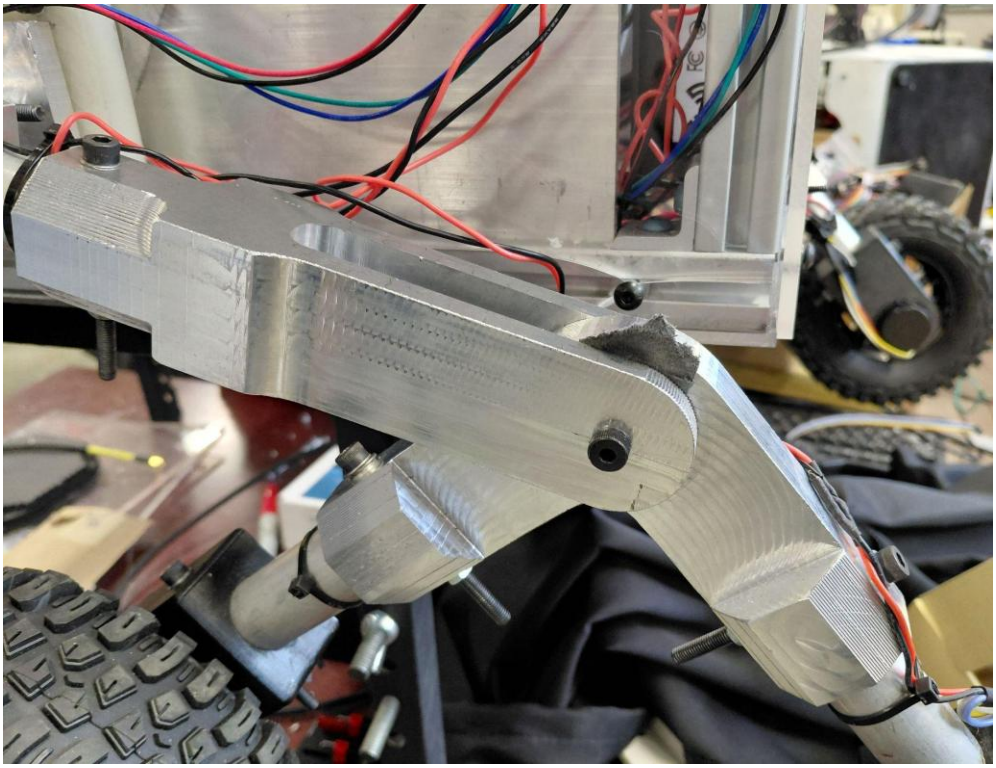

Figure 35: Aluminum Knuckle Joint

4.3 Electrical Details

The previous team made significant progress within the limited semester timeframe allowed for system development; however, certain design compromises were made to meet schedule constraints. During the initial evaluation phase of the previous semester's work, it was determined that the existing charging arm length was insufficient to reach the receiver coil on the rover. As a result, during the charging arm redesign, approximately 20" of length was added to the design by lengthening all of the arm links by varying amounts.

The additional length had cascading effects throughout the charging arm design, including the need for significantly higher torque motors to accommodate the increased torque from moving the arm's payload further away from the base. Additionally, a more capable power supply and updated motor control strategies were necessary to implement in the new design. The redesign effort provided an opportunity to incorporate internal wire management into the charging arm and incorporate additional safety features like an emergency circuit breaker switch, as shown in Figure 36.

Figure 36: Charging station emergency circuit breaker switch

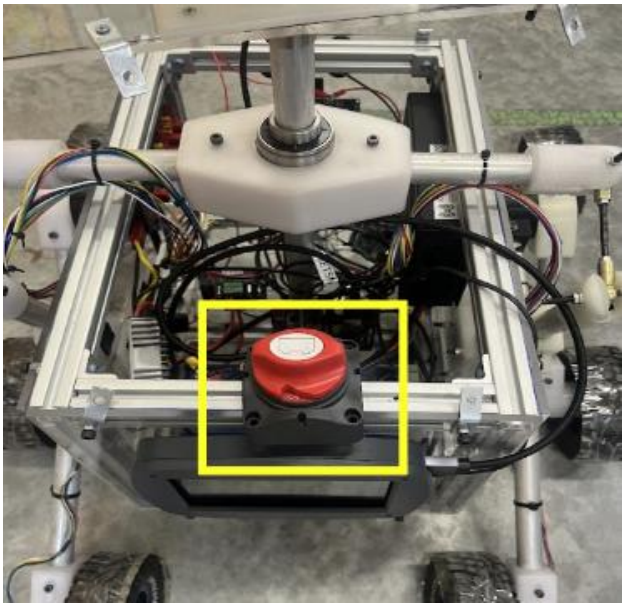

Figure 37: Circuit breaker switch on rover

The autonomous charging system leverages the technology of a WIBOTIC wireless power system. The system consists of a transmitter unit and transmitter coil for the charging station, and an onboard charger unit and receiver coil for the rover. The coils are tuned to a resonant frequency of approximately 6.7 MHz, which allows for maximum power transfer while utilizing carbon fiber as the induction coil material. [W] Design considerations were taken in the construction of the rover to avoid large, flat metal pieces near the receiver coil, as this would affect the coil tuning and charging efficiency.

The battery onboard the rover is a 25.6V, 256Wh battery, and the WIBOTIC charging system is capable of transmitting up to 1000W of power. To determine the charge time required to

charge the rover battery from 0% to 80%, divide the battery capacity by the charger output. (256 Wh / 25.6 V = 0.256 hr) This WIBOTIC charger is capable of charging the rover from 0% to 80% in approximately 15 minutes.

The WIBOTIC charger is capable of delivering full charging power with imperfect contact between the charging coils, which allows this autonomous charging system a wide range of effective rover docking and charging arm deployment positions. Having the ability to charge with imperfect contact gives room for error in rover docking due to terrain, as well as the constraint of the charging arm length.

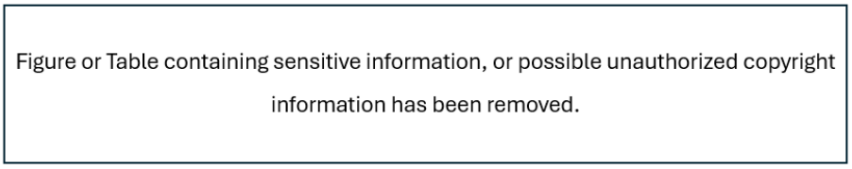

Figures 38 and 39 : WIBOTIC TR-1000 and AC/DC power converter

4.4 Programming Details

The programming for this project was conducted via the respective onboard NVIDIA Jetson Orin Nano for both the charging station and the rover. The Jetsons run on Linux, so a certain period of time at the beginning of the project was spent learning how to use and code using Linux.

The charging station and rover both utilize Python as well as Arduino code, two distinct programming languages with two different purposes. Python was used to write high-level functionality commands directly in the Visual Studio Code program. The station Python code included functions such as camera tracking and the distance to destination for the charging arm, as well as a critical ‘return to home’ protocol at the end of the charging deployment sequence to minimize strain on motors. The rover Python code included functions such as navigation and obstacle avoidance protocols, as well as the battery data transmission protocol.

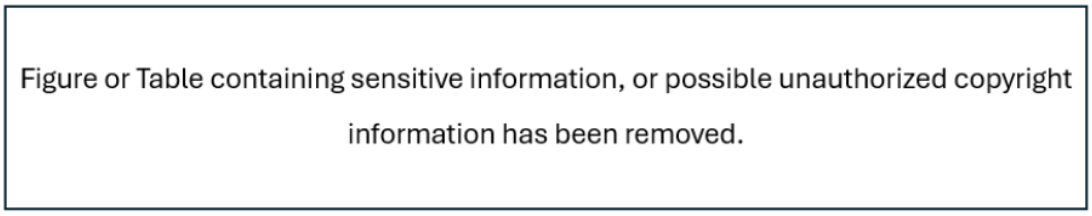

Figure 40: Charging arm ‘return to home’ Python code

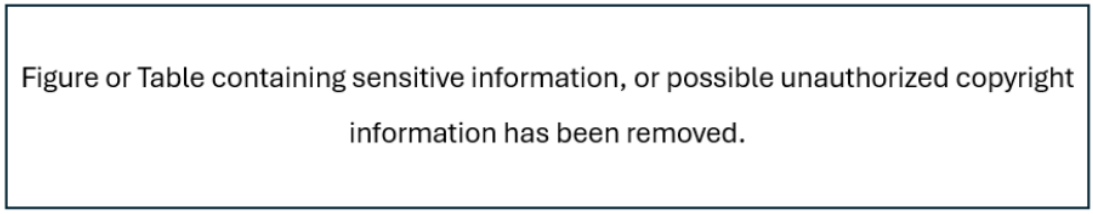

Figure 41: Charging station Arduino code for motor control

The Arduino code was primarily used to control and manage the motors of the charging station robotic arm and rover wheels. The Arduino code was critical for the charging arm, as the motors were uncontrollable without it and moved at full speed all the time, causing severe arm jerk and component damage. Significant time was spent developing the Arduino code for the station arm to control its movement and slow down the motors. The rover’s Arduino code controls the six motors of the rover wheels, evenly distributing power and coordinating motor speed for turning. The Arduinos onboard the rover were critical implementations to successfully generate zero-point turn functionality, significantly increasing the rover’s maneuvering capabilities.

Figure or Table containing sensitive information, or possible unauthorized copyright information has been removed.

Figure 42: Rover zero-point turning code section

5. Mechanical Design Analysis

In addition to physical testing and validation of the rover and charging station subsystems, computational design analysis was performed to verify the structural integrity of the new designs. Finite Element Analysis (FEA) was performed using the ANSYS Workbench software. Depending on the component, the simulations were performed using either ABS plastic or Aluminum Alloy from the ANSYS material library. FEA was conducted on each individual link of the station arm, as well as the full assembly of the arm. The full assembly was tested in both resting and a fully extended position. The specific types of analysis simulated for static structural integrity were total deformation, equivalent elastic strain, equivalent stress, structural error, and safety factor.

The majority of the FEA simulations and their results are included in the ANNEX.

5.1 Finite Element Analysis Simulations

The first part analyzed is the first major arm link, referred to as link 2. The part drawing may be seen in fig 43, and the mesh used for FEA results may be seen in fig. 44. The structural supports and applied forces used to simulate FEA may be seen in fig 45. This link serves as the upper-arm equivalent component on this structure. The FEA results for equivalent elastic strain may be seen in fig. 46. It may be observed that the elastic strain is mainly concentrated around the lower connection bolt holes and the upper connection wire management entry holes. Results for the Von-Mises stress may be seen in fig. 47. It may be seen that the results for Von-Mises stress have similar concentrations to the elastic strain with concentrations in the same areas. Results for the structural error may be seen in fig. 48. It may be observed that the structural error concentrations are found mostly at the upper connection area, with the maximum error being found

at the inside corner of the lower connection extrusions. The safety factor may be seen in fig 49. It may be observed that the safety factor remains 15 for every area, indicating safe operation during typical loading conditions. The total deformation is seen in fig 50. It may be observed that a relatively constant gradient of deformation occurs with increasing direction going from the lower to upper connection.

Redacted due to Export Control/CUI requirements.

Figure 43: Concept 2 Link 2 Dimensioned Part Drawing

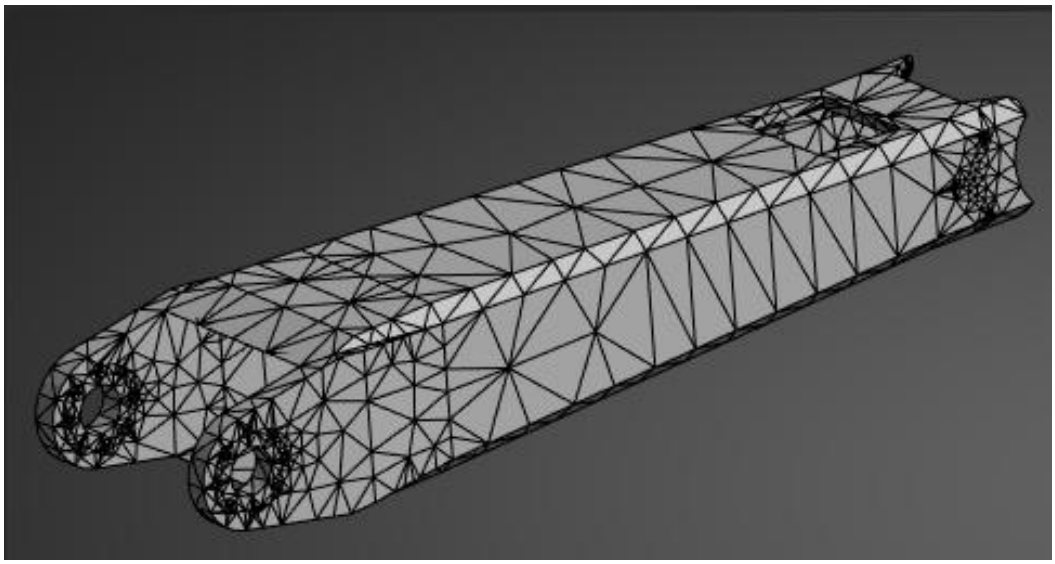

Figure 44: Concept 2 Link 2 Mesh

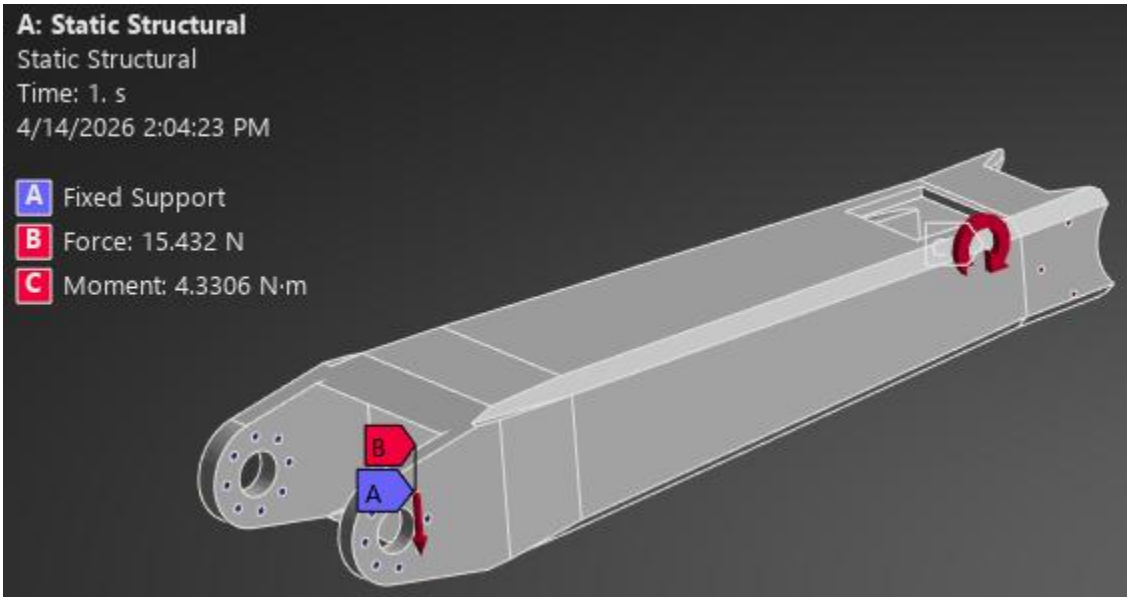

Figure 45: Concept 2 Link 2 Applied Forces and Fixed Support

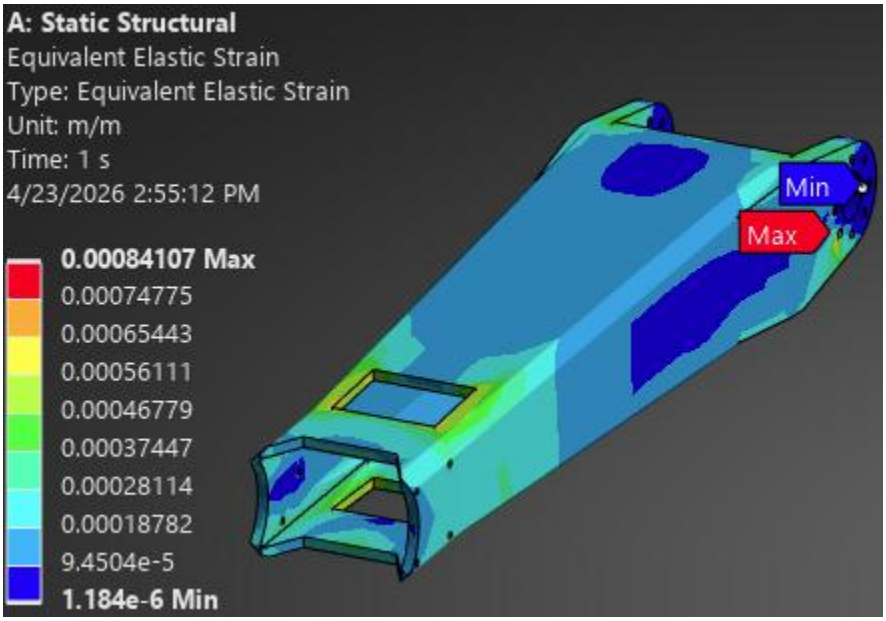

Figure 46. Concept 2 Link 2 FEA Results of Equivalent Elastic Strain

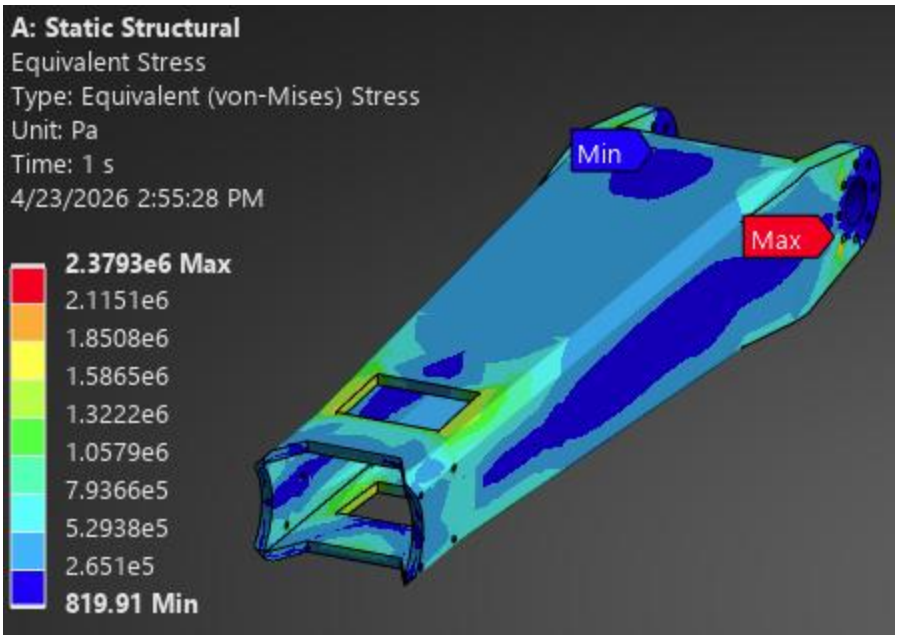

Figure 47. Concept 2 Link 2 FEA Results for Equivalent Stress

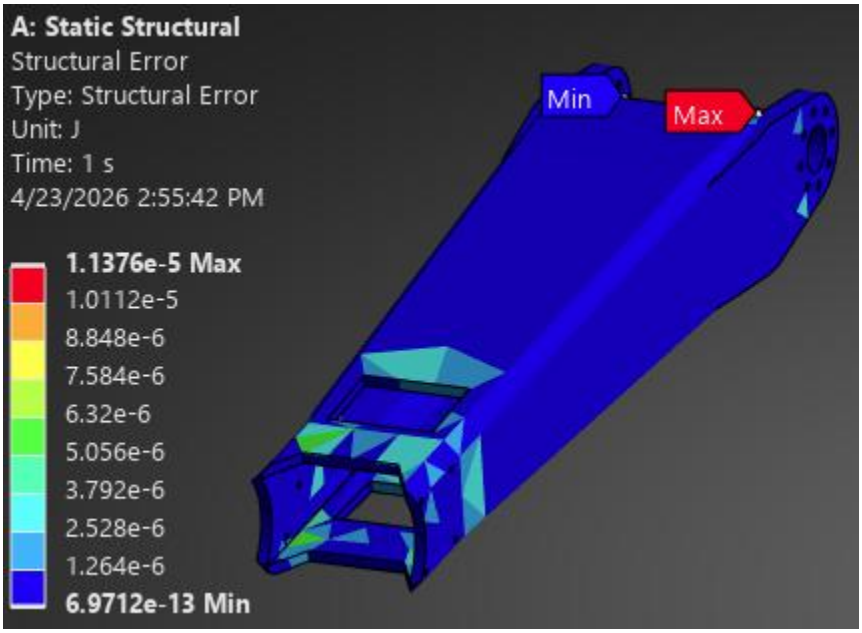

Figure 48. Concept 2 Link 2 FEA Results for Structural Error

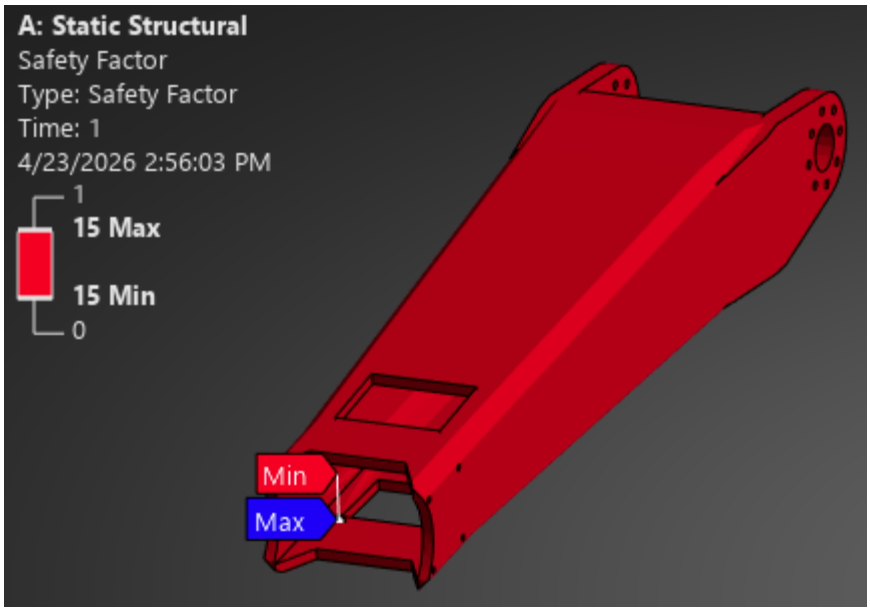

Figure 49: Concept 2 Link 2 FEA Results for Factor of Safety

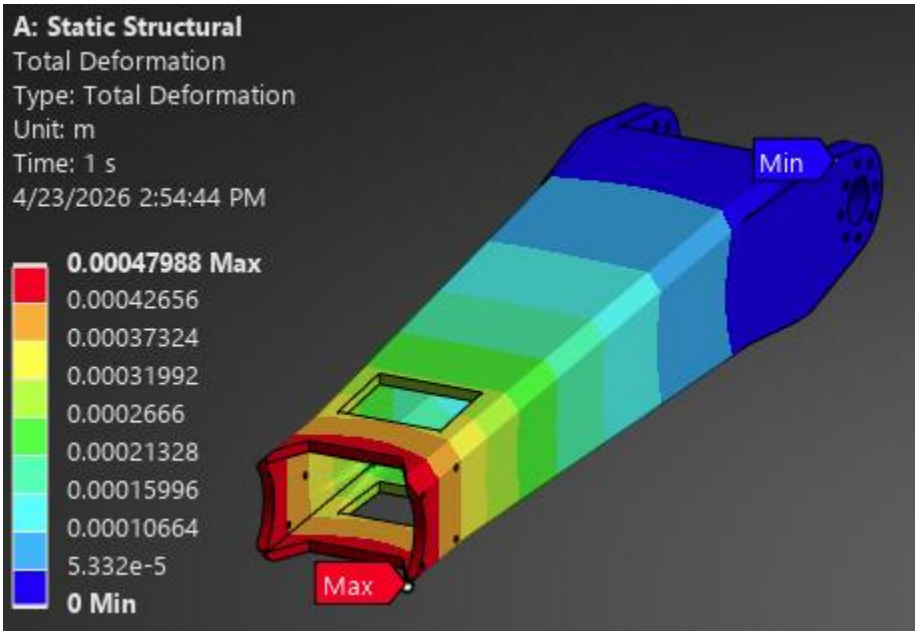

Figure 50. Concept 2 Link 2 FEA Results for Total Deformation

FEA was also performed on all new or changed rover components including the inner knuckle, outer knuckle, bearing housing, motor mounts, differential bracket, differential support bar, differential tube fitting, the main leg joint, and the aluminum support bracket as well as on a half model of the rover assembly. The total deformation, equivalent elastic strain, equivalent stress, and safety factor were simulated to ensure structural integrity. To ensure a proper mesh resolution, it was ensured that structural error remained low.

The FEA for the inner knuckle was performed using aluminum alloy as the material. The mesh was generated using the default mesh generation method with an element size of 2 mm for

both computational efficiency and the accuracy of the results, the generated mesh is shown in Figure 53. For the forces and supports, a fixed support was set at the pivot joint and the forces were placed at the connection to the cylindrical connection with a magnitude of 200 N in the positive Z direction in order to simulate the normal forces from the ground into the rocker-bogey joint. The knuckle analysis tree can be seen in Figure 52. This simulation provided a maximum equivalent stress of 1.98 MPa, a maximum equivalent strain of 3.3E-05 mm/mm, and a maximum total deformation of 0.0027 mm (Figures 53, 54, 55). The minimum factor of safety is 15 as shown in Figure 56 The meshing is also validated by a low structural error of only 3.87E-09 J as shown in Figure 57.

Figure 51: Inner Knuckle Joint Dimensioned Drawing

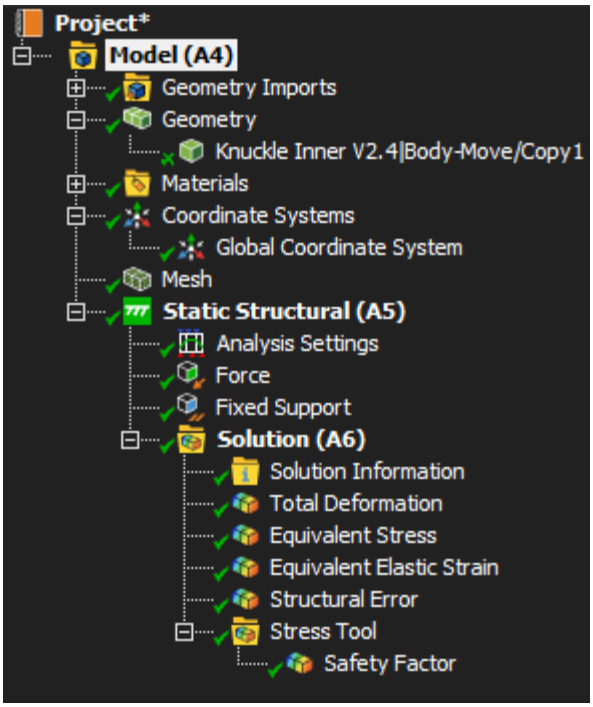

Figure 52: Inner Knuckle Analysis Tree

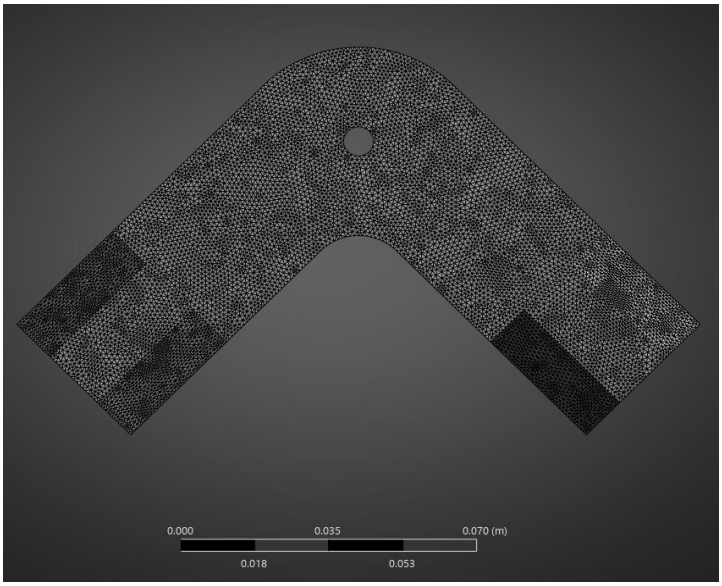

Figure 53: Inner Knuckle Joint Mesh

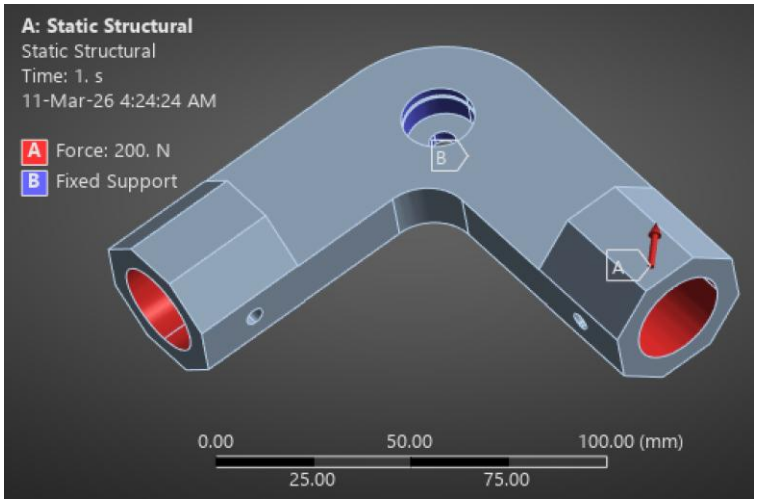

Figure 54: Inner Knuckle Joint Forces and Supports

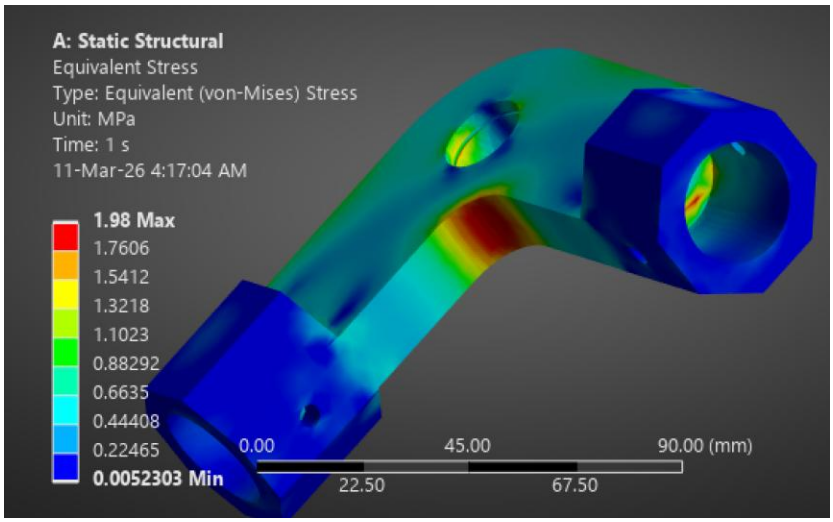

Figure 55: Inner Knuckle Joint Equivalent Stress

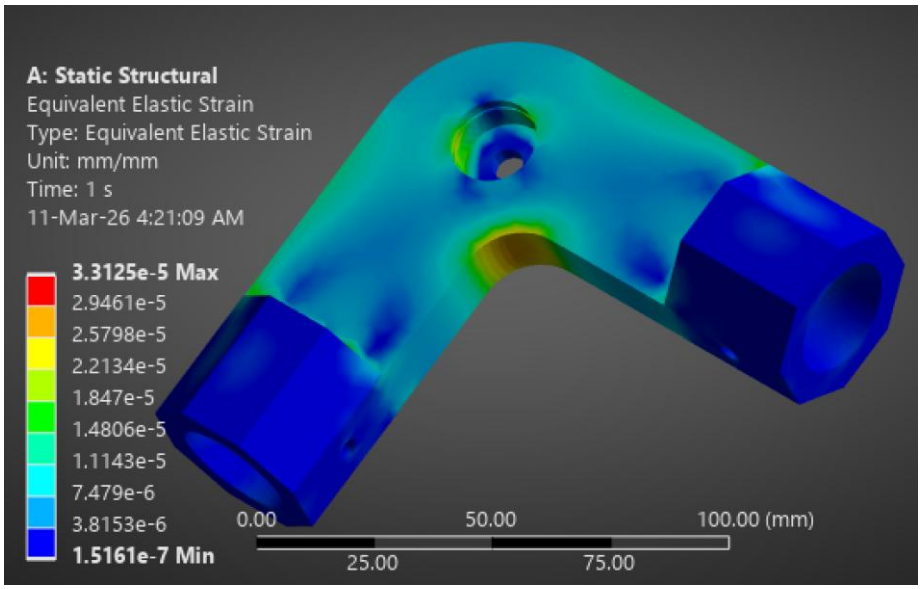

Figure 56: Inner Knuckle Joint Equivalent Strain

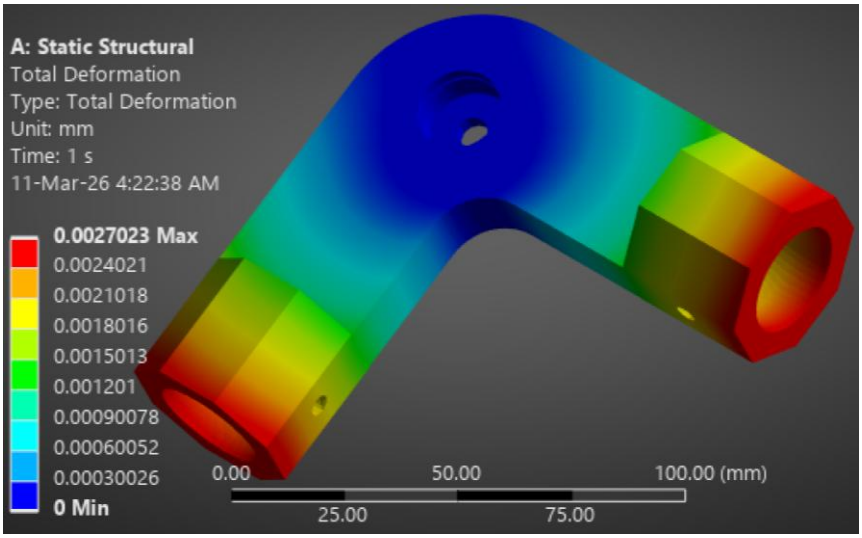

Figure 57: Inner Knuckle Joint Total Deformation

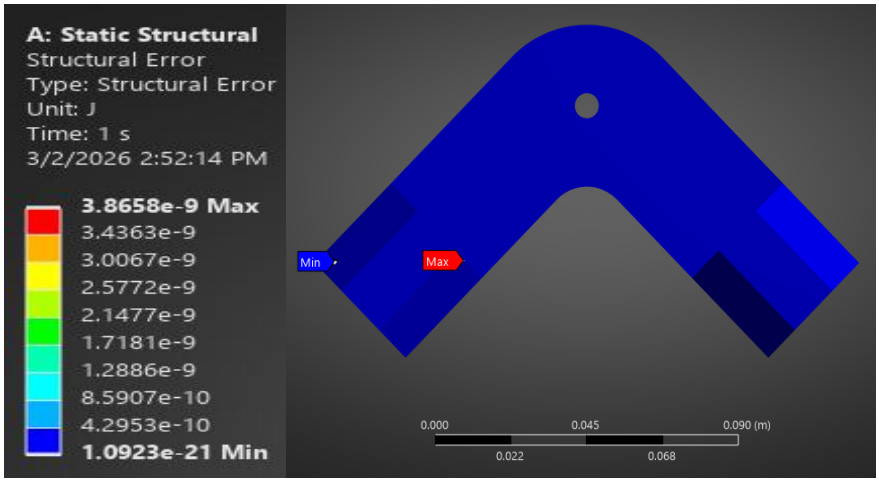

Figure 58: Inner Knuckle Joint Structural Error

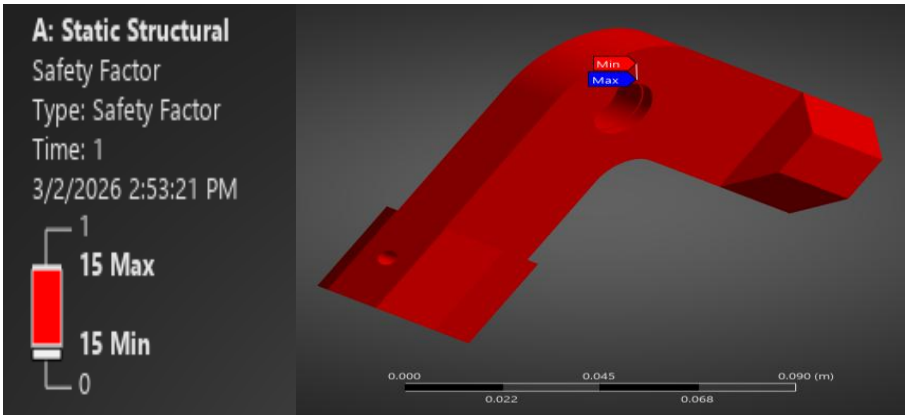

Figure 59: Inner Knuckle Joint Factor of Safety

The half body finite element analysis was performed using aluminum alloy and ABS plastic as the material. The mesh was generated using the default mesh generation method with an element

size of 20 mm for computational efficiency with the larger more complex body, the generated mesh is shown in Figure 60. Fixed supports were placed at the faces of the motor mounts where the rover tires are mounted and at the bottom of the rover as shown in Figures61 and 62. A force was placed on the inner cylinder between the main leg joint and the body with a magnitude of 107 N in the negative Z direction, as shown in Figure 63. This simulation provided a maximum equivalent stress of 4.26 MPa, a maximum equivalent strain of 4.01E-05 mm/mm, and a maximum total deformation of 0.013 mm (Figures X, X, and X). The minimum factor of safety is 15 as shown in Figure 64. The meshing is also validated by a low structural error of only 1.29E-06 J as shown in Figure 65.

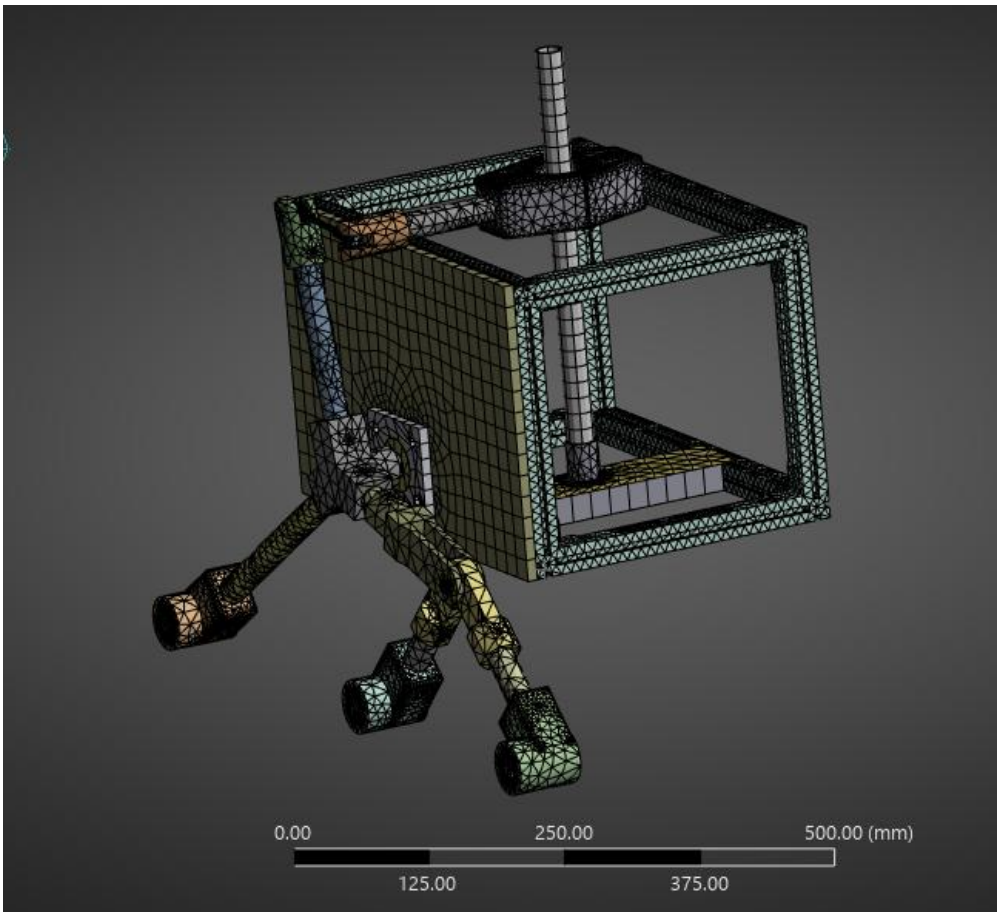

Figure 60: Half Body Simulation Mesh

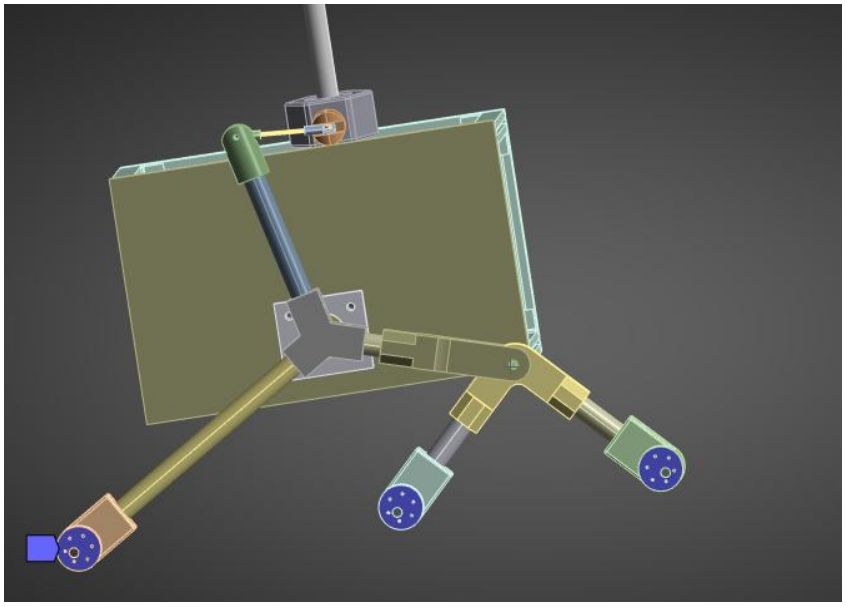

Figure 61: Half Body Simulation Leg Support

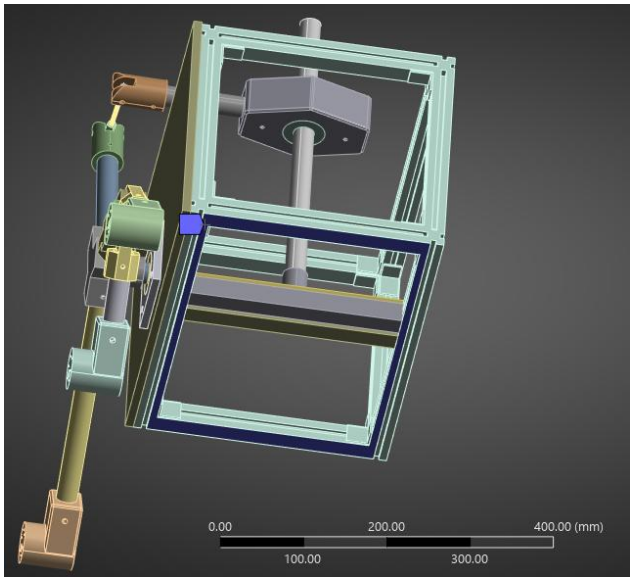

Figure 62: Half Body Simulation Bottom Support

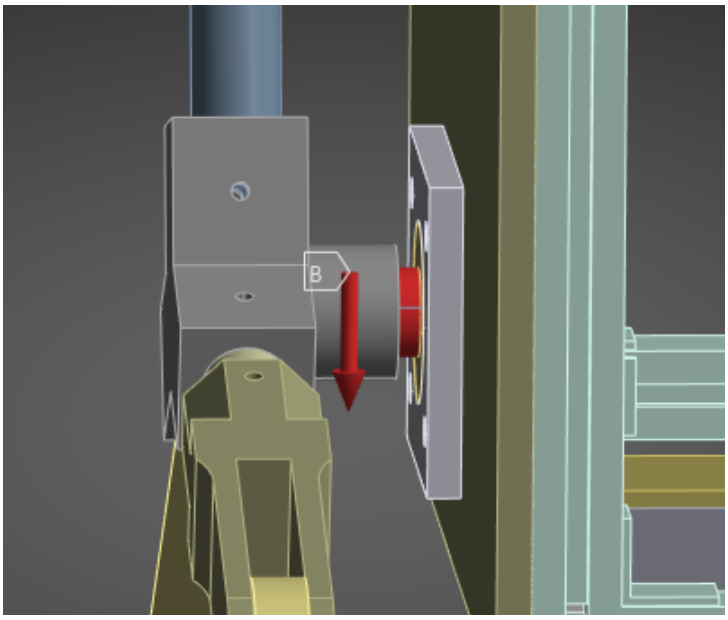

Figure 63: Half Body Simulation Forces

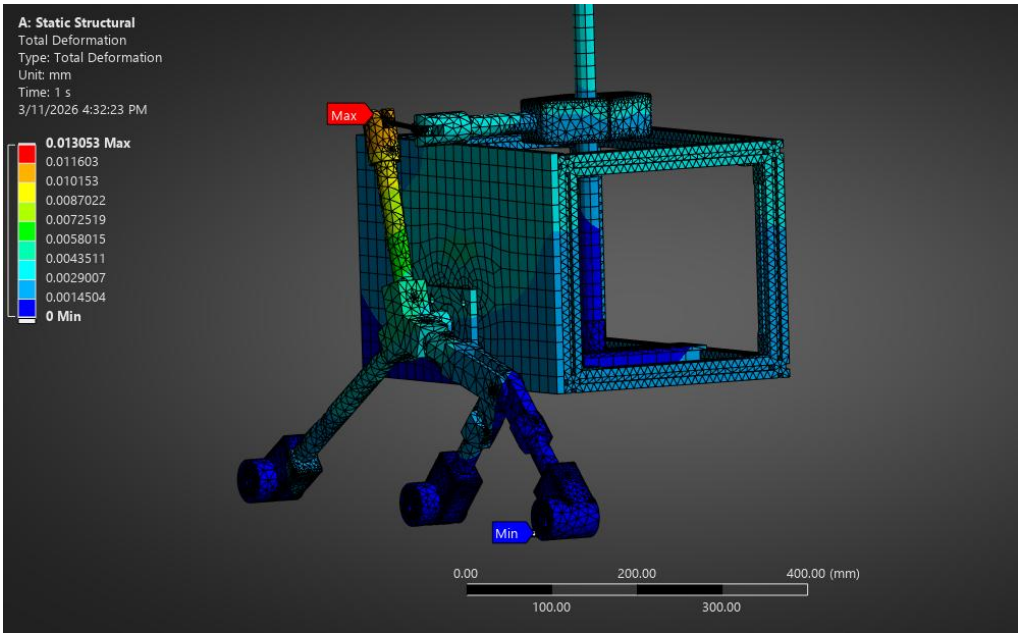

Figure 64: Half Body Simulation Total Deformation

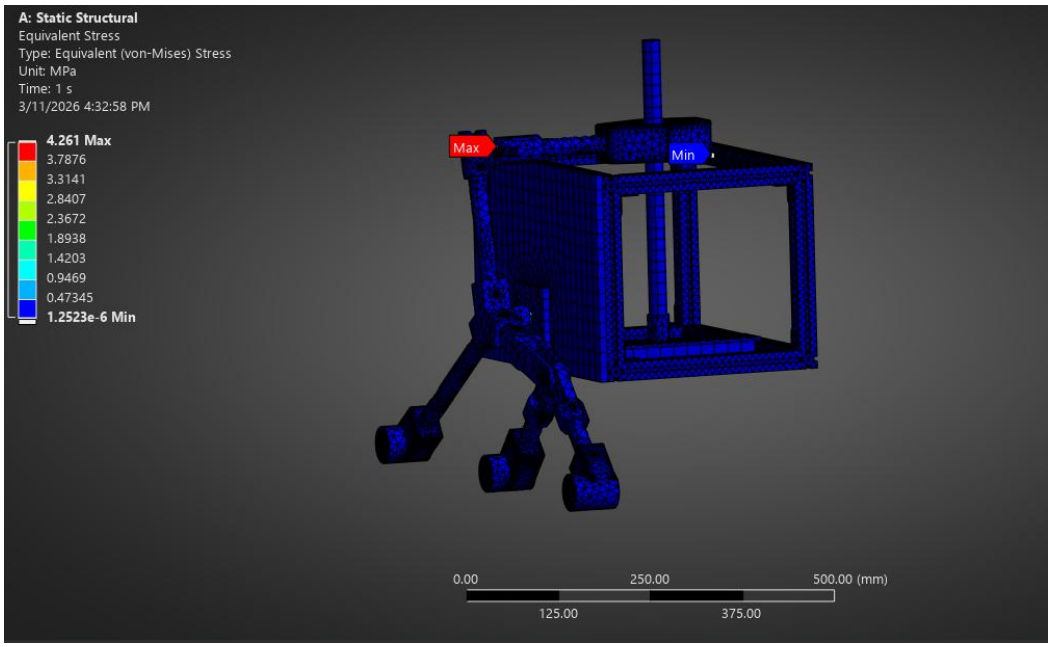

Figure 65: Half Body Simulation Equivalent Stress

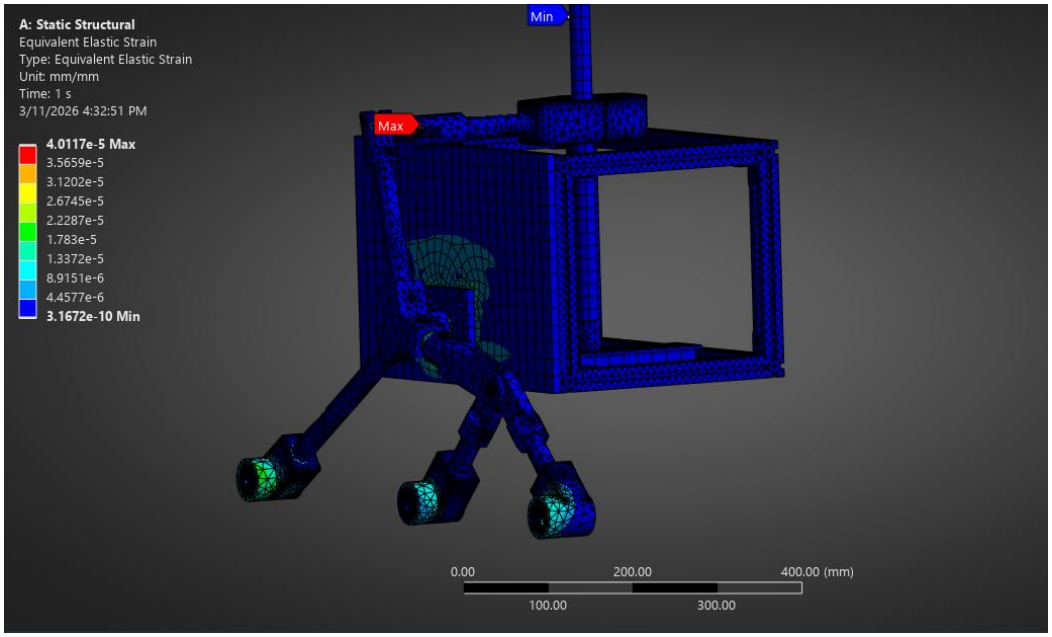

Figure 66: Half Body Simulation Equivalent Strain

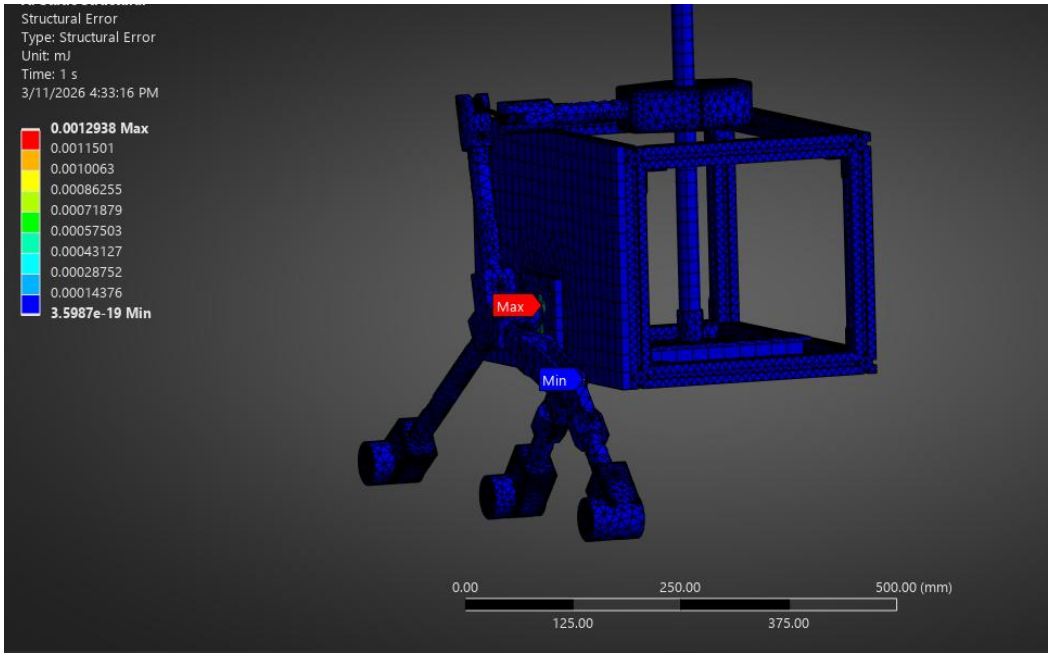

Figure 67: Half Body Simulation Structural Error

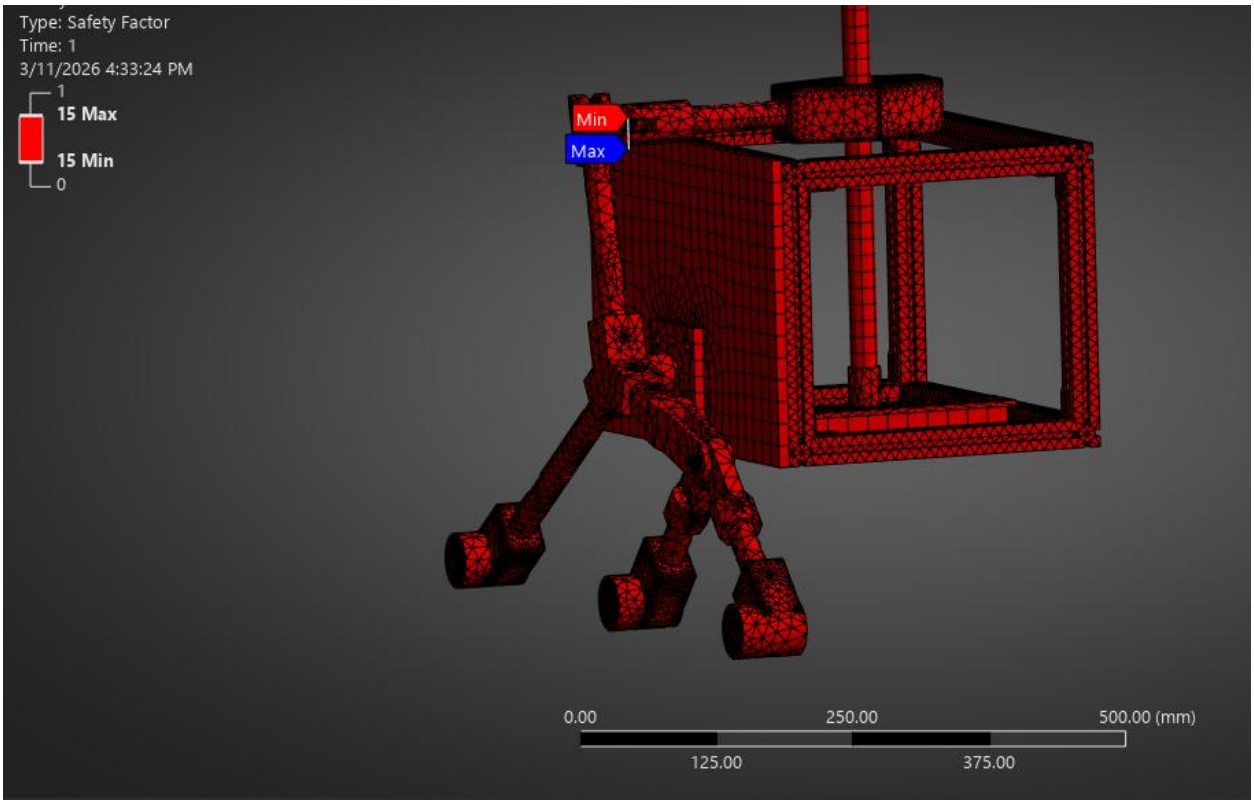

Figure 68: Half Body Simulation Factor of Safety

6. Electrical System Analysis

In order to determine the required strength of the servo motors, it is necessary to know the torques that are applied at each joint that the motors would be rotating about. This includes the torque generated by the mass of each part and their centers of gravity, as well as the masses of both the charger and the camera sensor.

Table 1: Torques on Each Link

Redacted due to Export Control/CUI requirements.

With the knowledge of the necessary torque required to move each segment of the arm, it is possible to select a motor that exceeds the required torques. Each of the motors which were selected exceeded the torques listed in the previous section, with the base arm T2 having the largest required torque, that link was chosen to have an ANNIMOS 160kg*cm 24V servo motor. For the base rotation motor and the second link motor, the 150kg*cm 12V motor from ANNIMOS was selected for extra redundancy.

Figure or Table containing sensitive information, or possible unauthorized copyright information has been removed.

*Figure 69: ANNIMOS 160kg*cm 24V Motor*

Listed below are the selected motor specifications with the red highlighted cell being the maximum total power draw. The numbers given were taken from the specification data sheet and the maximum power draw was calculated using the equation P=VI, where V is the operating voltage and I is the Stall Current of the motors. The arm is not expected to draw its maximum

power due to how the movement protocols work, however, the accessory electronics were chosen based on their ability to handle the maximum power draw.

Table 2: Maximum Power Draw based on Motor

Servo Type	Quantity	Operating Voltage (V)	Stall Current (A)	Maximum Power Draw of a Single Motor (W)	Total Power (W)
160kg	1	24	4.2	100.8	100.8
150kg	2	12	8	96	192
50kg	2	12	4.2	50.4	100.8
					393.6

Redacted due to Export Control/CUI requirements.

Figure 70: Station Wiring Diagram

As shown above, the station is plugged into 120VAC main power based on the assumption that the station will remain in one place, eliminating the need for onboard batteries. In between the main and the 120V standard outlets is a 10 Amp circuit breaker that will trip if the circuit as a whole attempts to draw more than 10A at one time. The outlet will provide power for both the

NVIDIA Jetson Nano and the WIBOTIC Induction Charger through their standard power cables, following the outlet will be the 120VAC to 24VDC converter that will be used to power the motors in the arm. In between the outlets and the power converter is a safety switch attached to the live AC wire, it is located here in order to cut power to the arm if necessary without having to unplug the entire system.

Figure or Table containing sensitive information, or possible unauthorized copyright information has been removed.

Figures 71 and 72: NVIDIA Jetson and Arduino UNO

The main function of the NVIDIA Jetson Nano is to be the main onboard computer handling all of the tasks regarding communication between the station and the rover, interpretation of the camera sensor data, and motor control. Connected to the Jetson is an Arduino Uno, which is a small microcontroller that is able to write commands easily to the larger motors in the arm to control them. The WIBOTIC TR-1000 converts standard wall power into a wireless power signal used for charging large batteries, like the one found on the rover. It is able to communicate with the Jetson Nano through its onboard ethernet cable and network API.

The motor which connects Links 1 and 2 of the charging arm is 160kgcm and operates at 24V, while the four other motors of the charging arm operate at 12V. It was necessary to include a 24V to 12V step down converter to supply the other four motors with their proper voltage. The converter shown in Figure X is rated for a maximum power output of 450W, and the calculated maximum power draw of all four motors is 393.6 W. This will provide adequate power supply to all four motors with a margin of safety. To increase the electrical safety of the motor power supply, two step down converters were used in the charging station.

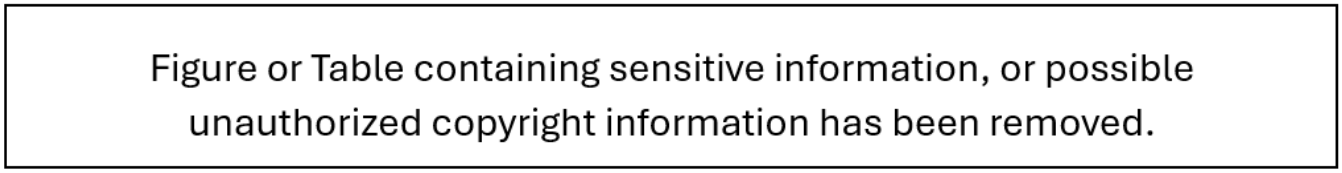

Figures 73 and 74: 24 Volt to 12 Volt Step Down Converter and Serial Servo Bus Adapters

At the end of the arm located above the induction pad of the WIBOTIC is the Intel RealSense D455 Webcam, a camera sensor that is used to detect the april tag that the software would use to determine the distance from the induction charger to the rover's induction receiver. It has a resolution of 1280x800 pixels giving it a very clear picture for discerning the unique pattern of the april tag and is connected to the Jetson via USB 3.1. This model was chosen because of its depth awareness accuracy, making it suitable for this application.

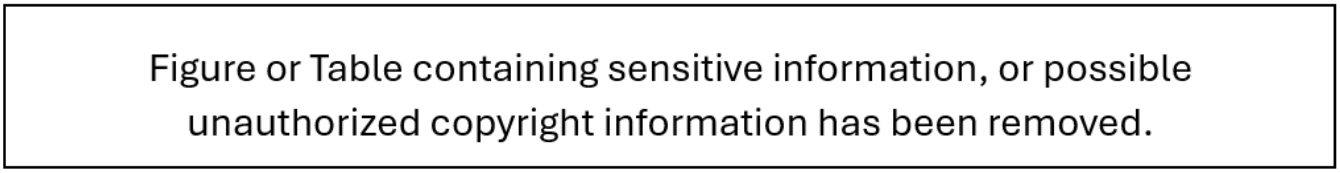

Figure 75: Intel RealSense Camera Sensor

The cytron duel channel 10A DC motor driver is used in the rover to control the front DC motors. It was necessary to receive speed data back from the motors to enable controls and can handle a speed control PWM frequency up to 20KHz. It can control up to two DC brushed motors and is rated for motors up to 10A and a voltage range of 5V to 30V. The device also has two activation buttons for each motor to allow for simple tests of the motors.

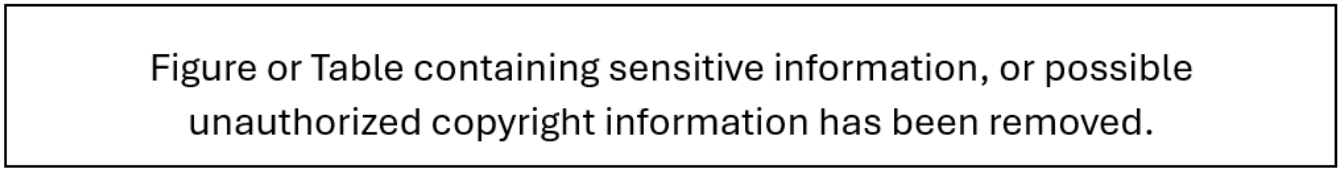

Figure 76: Cytron Dual Channel 10A DC Motor Driver MDD10A

The 9 DOF inertial measurement unit (IMU), specifically the Bosch BNO055 absolute orientation sensor, is located in the rover chassis and is integral for tracking the rover's position. This system-in-package IMU combines a 3-axis accelerometer, gyroscope, and magnetometer with an onboard microcontroller that performs internal sensor fusion. This component reduces computational overhead on the Jetson Nano and provides continuous data streams of heading, angular velocity, and linear acceleration, which form the basis for inertial odometry. The sensor outputs orientation in either Euler angles or quaternions, along with gravity-compensated linear acceleration.

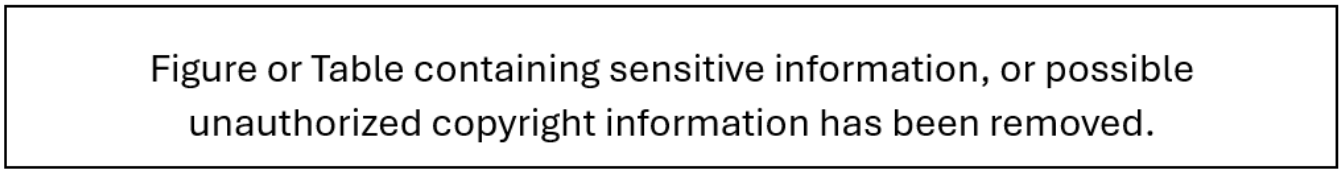

Figure 77: BNO055 9 DOF IMU Sensor

The 24V 10Ah lithium battery, as shown in Figure X, is located in the rover chassis and powers the rover while it performs activities. The battery is connected to both buck converters and is connected and charged by the WIBOTIC. The battery is rated for a maximum continuous discharge of 10A, however can peak at 20A for up to 5 seconds.

Figure or Table containing sensitive information, or possible unauthorized copyright information has been removed.

Figure 78: 24V 10Ah Lithium Iron-Phosphate Battery

The rover's power system incorporates a 30A 24 Volt to 12 Volt Step Down Converter to distribute electrical power to its supporting electronics. This buck converter efficiently steps down the 24V supplied by the main onboard lithium battery to a reliable 12V output. This stable 12V is then supplied to the rover's primary computing components: the NVIDIA Jetson Orin Nano and the Arduino microcontroller.

The rover has six wheels, three on each side, each with a continuous servo motor. All six motors are controlled by the NVIDIA Jetson via an onboard Arduino or Cytron controller. As shown below in Figure X, the rear bogie wheel and the rocker wheel are the driving wheels. This means that these four wheels output power to rotate in their mounts and move the rover forward. The front bogie wheel, which is in between the other two wheels, is the control wheel. The front bogie motor does not output power for propulsion, rather its encoder is connected to the onboard Arduino to transmit rotational speed data to control the four driving wheels. This motor control configuration aims to maximize motor driving and computational efficiency.

Figure 79: From left to right, rear bogie wheel, front bogie wheel, and rocker wheel

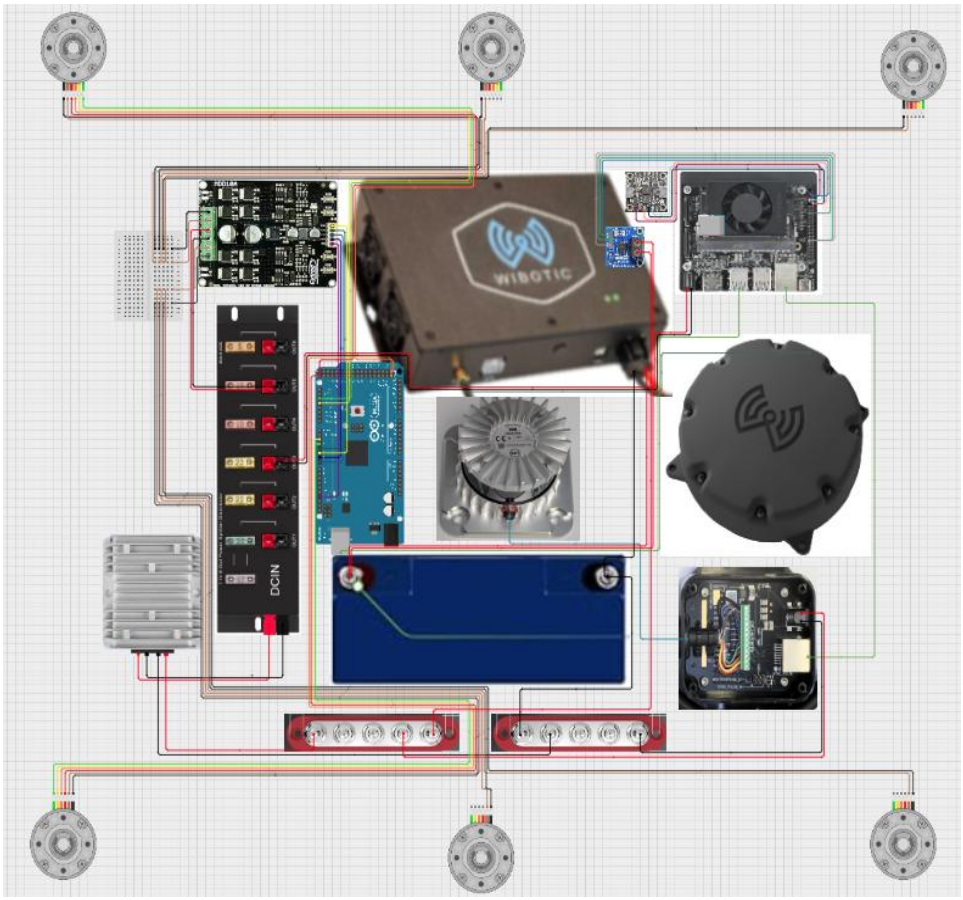

Figure 80: Rover complete wiring diagram

7. Programming Analysis

The following section details the functionality of all critical programs aboard the 2026 NASA X-Hab Station and Rover. Programs responsible for integrated functionality are covered first as the two serve no purpose without each other. Following this explanation, the rover's inner workings are discussed and then the station. For reader clarification, this section will mainly consist of pseudocode, system diagrams, and results, emphasizing end goal functionality. This decision has been made to maintain technical simplicity. Reference programs are available for reference in the Annex.

7.1 Combined System Architecture

The rover and station are intended to work as an integrated pair as one serves no purpose without the other. To accomplish this integration, the two are connected via programs that communicate data and commands via a Bluetooth Radio Frequency Communication (RFCOMM) protocol. As detailed in *Sections 6.2 and 6.5*, both systems are equipped with their own respective

Jetson Nano's. This is where all of the programming and processing occurs. Fig. 81 below illustrates the integrated system architecture and provides a general understanding of both systems' individual operations. Individual operations, particularly detailing program functionality, will be further described throughout the remainder of Section 7.

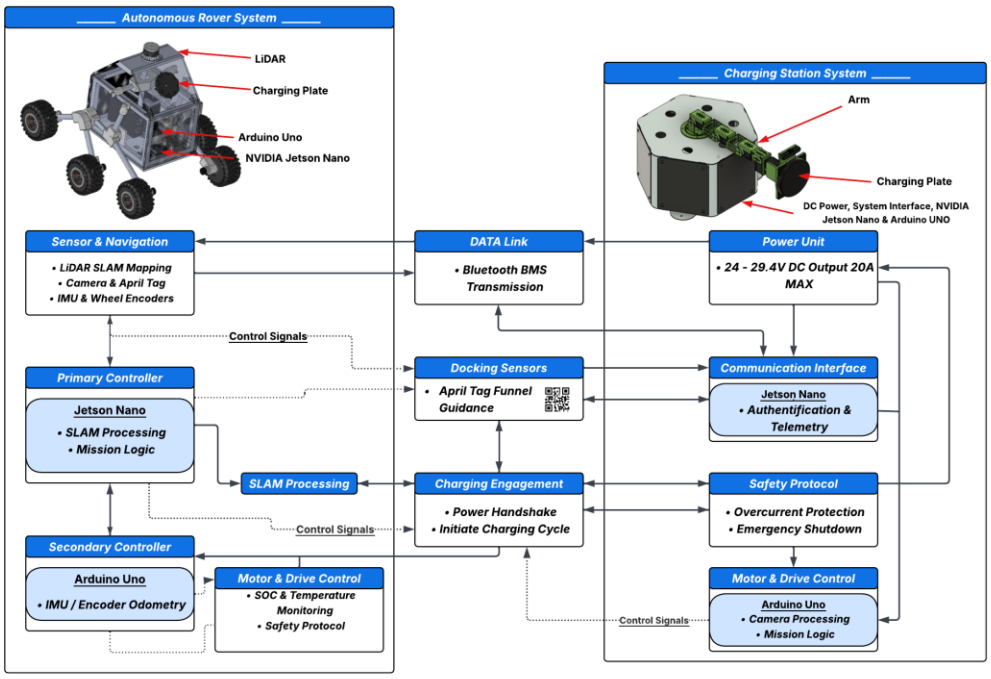

Figure 81. Autonomous Rover and Charging Station Interface Control Diagram

7.2 Communication Protocol (Bluetooth)

The most critical attribute for the rover-station dual-system architecture to function as intended is their ability to communicate. The communication is accomplished via Radio Frequency Communication (RFCOMM) Bluetooth protocol. RFCOMM is a stream-based Bluetooth communication structure which allows for multiple simultaneous communication channels to transmit constant data between the rover and station. This system allows the programs on board the subsystems to communicate as detailed below. Figure 82 displays the communication protocol between the station and rover, Figure 83 shows the station-specific communication protocol, and Figure 84 shows the rover-specific protocol.

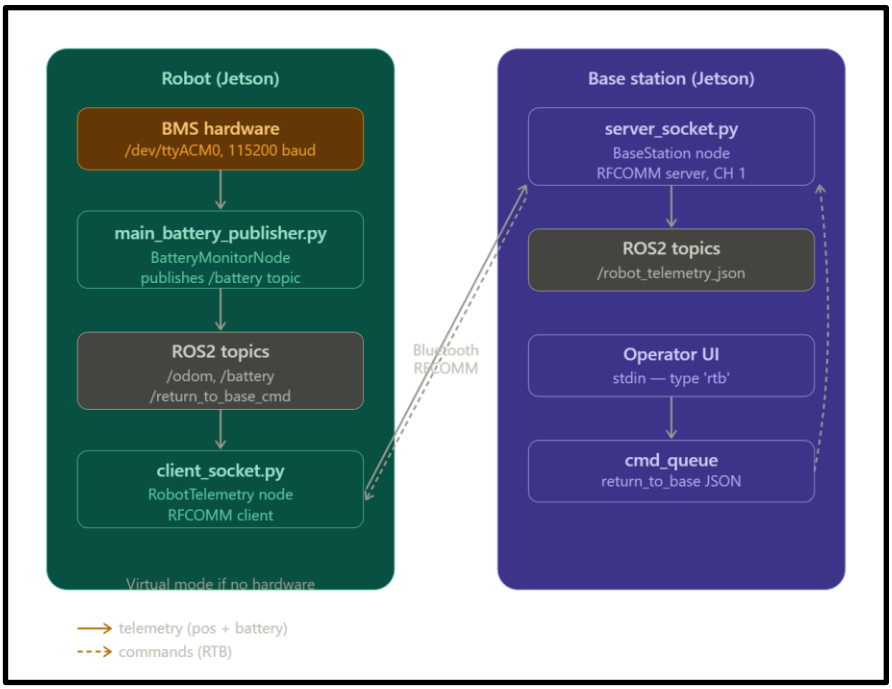

Figure 82. Integrated Rover and Station Communication Protocol

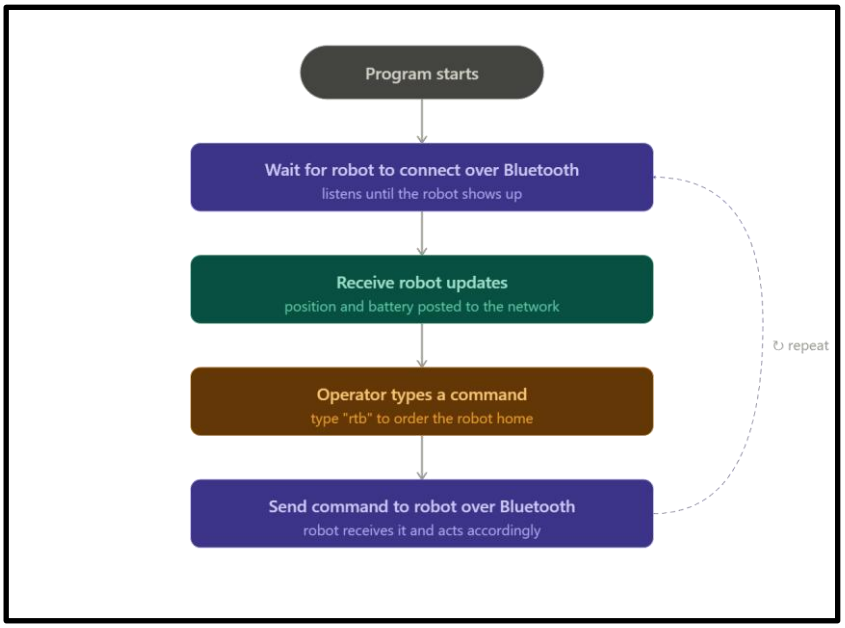

Figure 83. Station Bluetooth Protocol

Figure 85 below shows the preliminary testing of the station Bluetooth RFCOMM protocol; it shows the initialization of connection between the station and rover, as well as the Return To Base command option for operators.

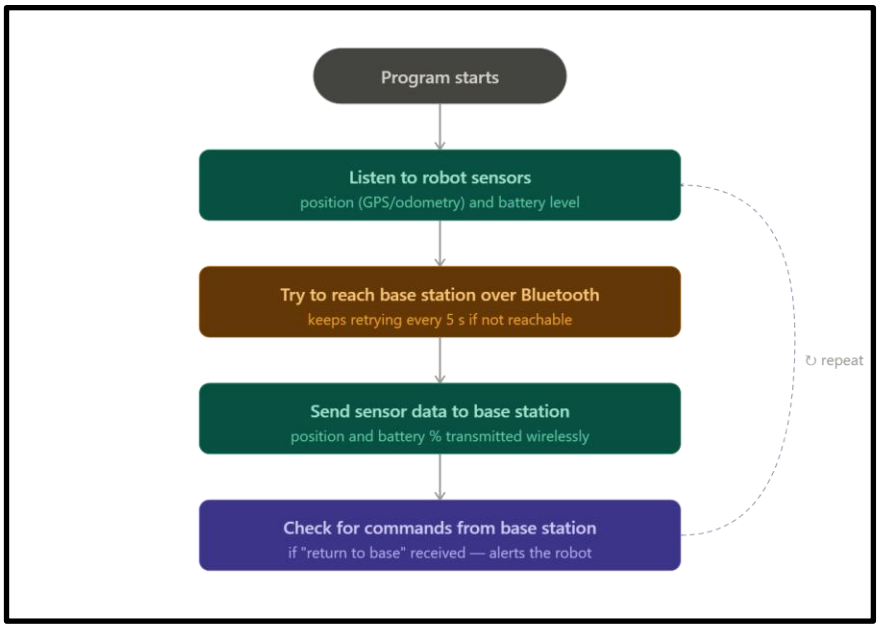

Figure 84. Rover Bluetooth Protocol

Figure or Table containing sensitive information, or possible unauthorized copyright information has been removed.

Figure 85. Station Bluetooth Connection Initialization w/ Redundancies

Figure 86 below shows the rover RCOMM protocol, showing the connection initialization to the charging station, labeled as Base Station in the protocol.

Figure or Table containing sensitive information, or possible unauthorized copyright information has been removed.

Figure 86. Rover Bluetooth Connection Initialization w/ Redundancies

7.3 Rover System Architecture

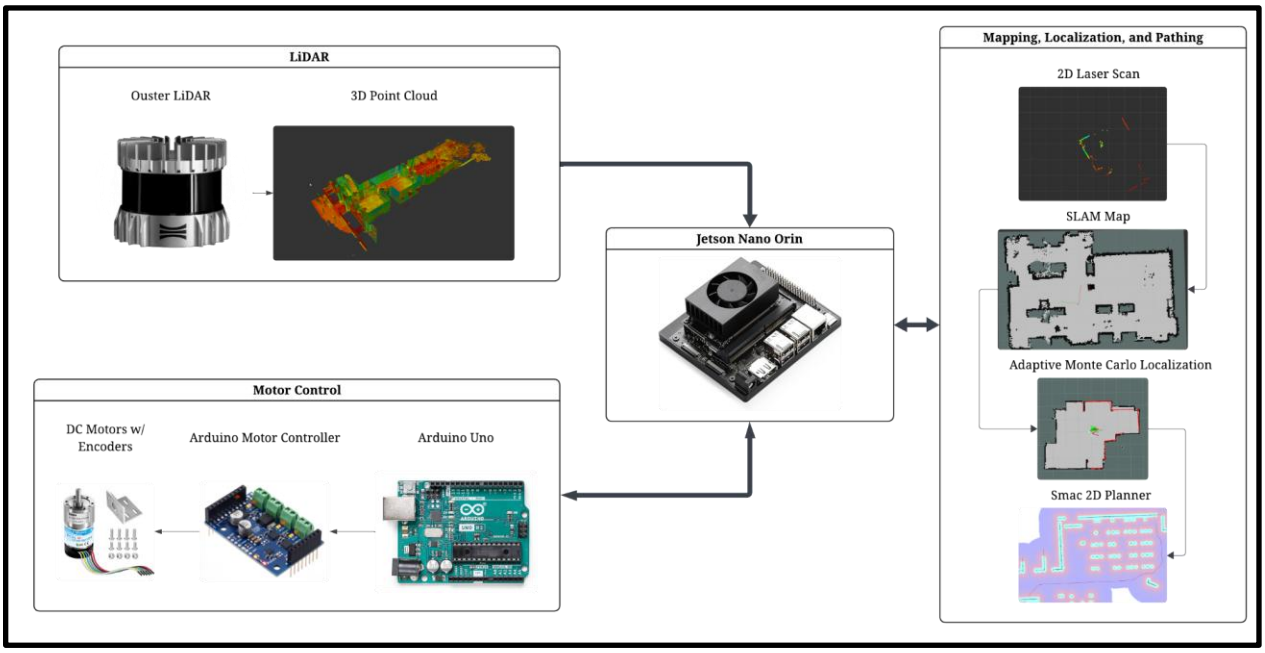

Figure 87. *Autonomous Rover Navigation Framework*

The autonomous rover relies on an Ouster OS0 3D LiDAR sensor as its primary perception device for navigation. The OS0 operates by emitting multiple laser beams across a wide field of view and measures the return time of each pulse to compute distances to surrounding objects. [6] This raw point cloud data is transmitted to the onboard NVIDIA Jetson Orin Nano, the 3D point cloud is filtered and projected into a 2D laser scan. Converting the data into 2D allows for greater computational efficiency and enables the Jetson to maintain real-time navigation performance. The 2D laser scan is passed into the SLAM subsystem, which constructs a SLAM map, as shown in Figure 88, while simultaneously estimating the rover's position within the local map. The SLAM map is combined with the Adaptive Monte Carlo Localization (AMCL) algorithm to create a global map of the environment which accounts for moving obstacles and filters noise.

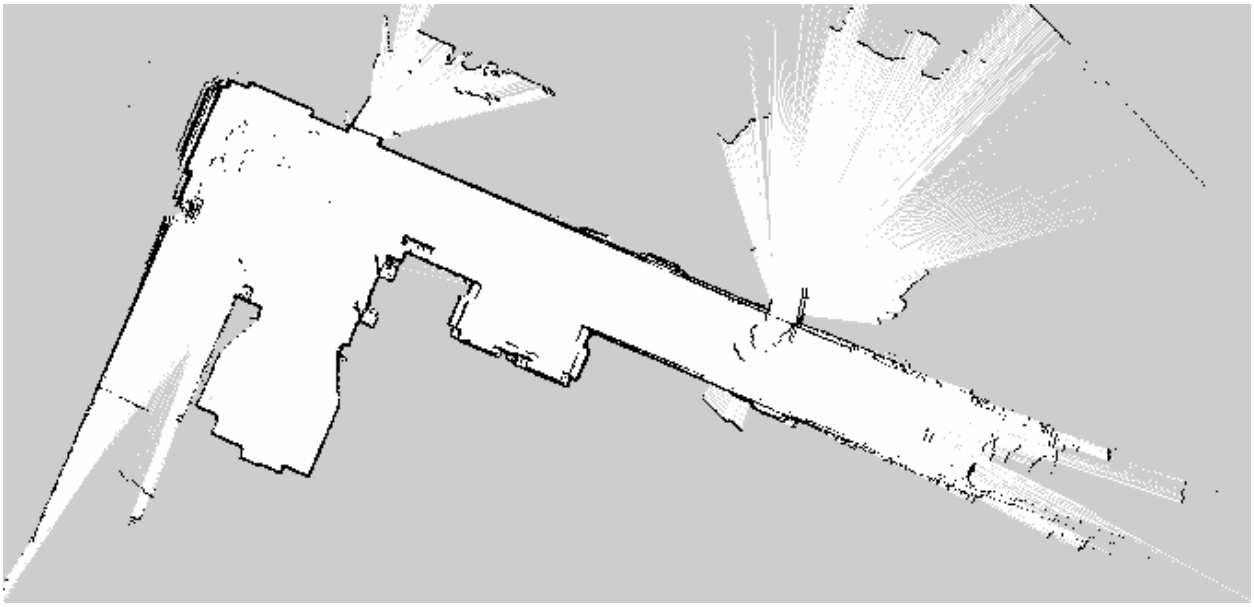

Figure 88. *SLAM Map from demonstration*

Once localization and mapping are fully initialized, the Smac 2D planner is activated to generate feasible paths through the mapped environment. The planner constructs a cost map, as shown in Figure 89, which integrates both static and dynamic obstacles, as well as a global path goal (as shown by the long green line shown in the left part of Figure 89) to calculate a desired path. The Smac planner computes many trajectories and sorts them into viable, non-ideal, and nonviable paths, as shown by the many green, red, and black lines in Figure 89. The trajectories are continuously updated with new LiDAR sensor data, allowing the rover to adapt to terrain changes while maintaining a smooth, ideal route to its destination.

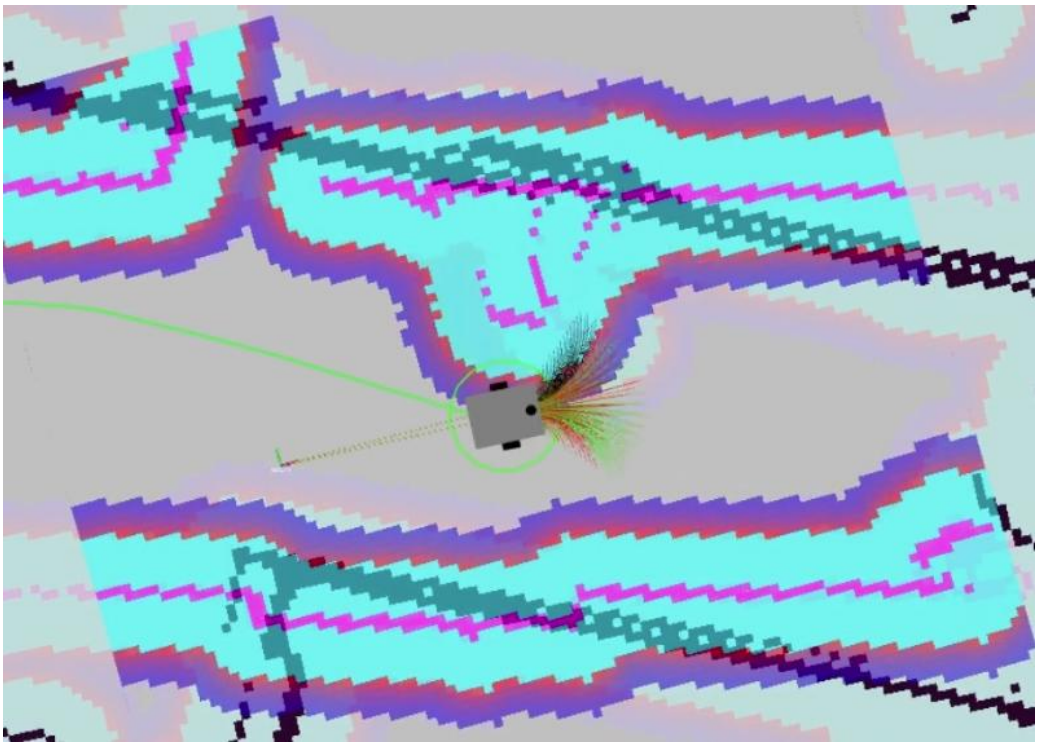

Figure 89: Cost map of rover navigating in a hallway

The implementation of a Bosch BNO055 absolute orientation sensor, shown below in Figure 90, on a Jetson Nano for autonomous rover navigation relies on integrating inertial sensing, coordinate transformations, and odometry-based trajectory reconstruction into a cohesive software pipeline. The BNO055 is a system-in-package inertial measurement unit (IMU) that combines a 3-axis accelerometer, gyroscope, and magnetometer with an onboard microcontroller that performs sensor fusion internally, outputting orientation in Euler angles or quaternions along with gravity-compensated linear acceleration. This significantly reduces computational overhead on the Jetson Nano, allowing Python-based applications to directly access fused orientation data via I2C using libraries such as Adafruit's CircuitPython driver. Once initialized over the Jetson Nano's I2C bus, the sensor provides continuous streams of heading, angular velocity, and linear acceleration, which form the basis for inertial odometry.

Figure or Table containing sensitive information, or possible unauthorized copyright information has been removed.

Figure 90: Bosch BNO055 orientation sensor [5]

To estimate the rover's pose, the system defines two coordinate frames: the body frame, fixed to the rover, and the world frame, representing the navigation environment. The BNO055 outputs acceleration in the body frame, which must be transformed into the world frame using a rotation matrix derived from the sensor's orientation (preferably expressed as quaternions to avoid singularities such as gimbal lock). This transformation allows acceleration vectors to be aligned with the global reference frame. The rover's velocity is then computed by integrating the transformed acceleration over time, and position is obtained through a second integration step. This process, known as dead reckoning, is implemented in Python using a time-stepped loop that reads sensor data, computes the time delta between iterations, and incrementally updates velocity and position vectors. However, because this involves double integration of noisy IMU signals, the resulting position estimate is highly susceptible to drift, with errors growing rapidly over time due to sensor bias and noise.

To address these limitations, the system typically incorporates a state estimation framework such as a Kalman filter or Extended Kalman filter (EKF). In this formulation, the rover's state vector includes position, velocity, and orientation, and the filter fuses IMU measurements with optional additional inputs such as wheel encoder data. The prediction step propagates the state forward using a motion model driven by measured acceleration and angular velocity, while the update step corrects the estimate based on observed measurements and their associated uncertainties. Although the BNO055 already performs internal fusion to provide stable orientation estimates, external filtering is still necessary for reliable position tracking. This layered fusion approach improves robustness and reduces the impact of noise and bias on the odometry solution.

During operation, the rover records its estimated trajectory as a sequence of timestamped poses, typically stored in a structured format such as JSON or CSV. Each entry contains position coordinates and orientation, enabling the reconstruction of the path traversed during exploration. To retrace the path, the recorded trajectory is reversed, and the rover follows the sequence of waypoints using a control algorithm such as pure pursuit or proportional–integral–derivative (PID)

control. The controller computes steering commands based on the difference between the rover's current orientation and the desired heading toward the next waypoint, while forward velocity is modulated according to the distance to the target. This enables the rover to approximate its original path, although accumulated odometry errors may lead to deviations, particularly over longer distances or in environments with significant sensor interference.

Despite its advantages, the use of a low-cost IMU such as the BNO055 for standalone position tracking is fundamentally constrained by drift, bias instability, and sensitivity to environmental disturbances, particularly in the magnetometer. Consequently, practical implementations often augment the system with additional sensing modalities, such as wheel encoders for relative motion constraints or visual odometry and simultaneous localization and mapping (SLAM) techniques for global correction. These hybrid approaches significantly enhance localization accuracy and make reliable path retracing feasible in real-world autonomous navigation scenarios.

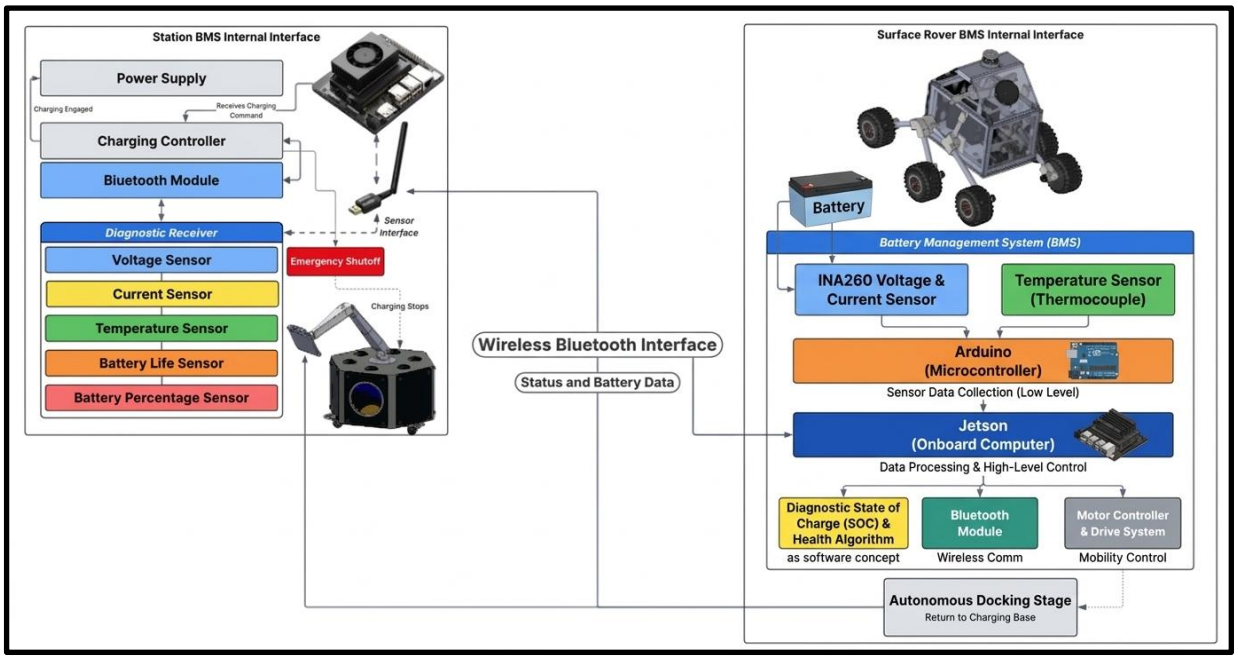

Figure 91. BMS-Bluetooth System Architecture

The Battery Management System (BMS) communication process is designed to continuously monitor the rover's battery condition and relay critical information to the station to enable safe and autonomous operation. The system begins with the INA260 sensor measuring voltage, current, and power directly from the rover's battery system. This data is read by the Arduino, transmitted to the Jetson for processing, and then relayed to the station via Bluetooth communication. The overall process operates in a continuous loop, allowing near real-time monitoring of the rover's battery state and enabling timely responses to changing conditions.

Battery data is transmitted at an approximately real-time rate, with updates occurring at about 1 Hz (once per second). Each transmission includes voltage, current, power, State of Charge

(SOC), system status, warning level, fault condition, and a recommended action. SOC represents the estimated percentage of remaining battery capacity and is derived from the measured voltage using predefined mappings appropriate for the battery type. Voltage and current provide direct insight into battery performance and load conditions, while SOC offers a simplified indicator of remaining operational capacity. The status field identifies whether the battery is idle, charging, or discharging, and the warning and fault indicators flag abnormal or unsafe conditions. The recommended action field summarizes the system's decision based on the evaluated data.

On the rover side, the BMS processes incoming sensor data to determine the battery state and evaluate operational thresholds. A warning threshold is defined at 15% SOC, at which point the rover initiates a return-to-station sequence. This ensures that sufficient energy remains for safe navigation back to the charging station. If more severe conditions occur, such as critically low voltage or abnormal current levels, the system escalates its response through fault detection and appropriate recommended actions. The rover continuously evaluates these conditions within its control loop, allowing it to make autonomous decisions without requiring external intervention.

On the station side, incoming BMS data is continuously monitored to track the rover's battery condition and operational state. When the rover reaches the station, the system initiates the charging sequence. Charging continues until the battery reaches approximately 90% SOC, at which point the station stops charging to prevent overcharging and preserve battery health. After charging is complete, the robotic arm disengages, and the rover backs away from the station, making the system ready for the next operational cycle. This coordinated behavior ensures efficient energy management and smooth interaction between rover and station.

The use of continuous communication and defined thresholds improves both the safety and reliability of the system. By transmitting data at a steady rate and evaluating clear SOC and voltage limits, the BMS ensures that the rover avoids deep discharge conditions and maintains sufficient energy for critical operations. The selected thresholds, such as the 15% SOC return trigger and 90% charging cutoff, are chosen to balance operational efficiency with battery longevity. Overall, this approach enables a robust and autonomous energy management system capable of supporting extended rover missions with minimal human intervention.

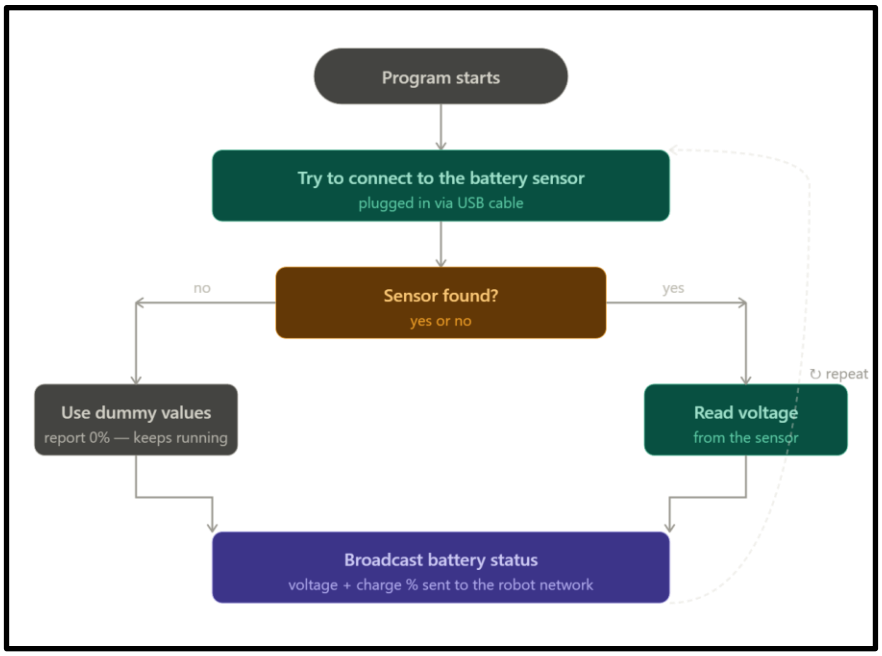

Figure 92. BMS System Pseudocode Diagram

Figure or Table containing sensitive information, or possible unauthorized copyright information has been removed.

Figure 93. BMS Code Initialization

Figure or Table containing sensitive information, or possible unauthorized copyright information has been removed.

Figure 94. BMS Code Output (virgin demonstration)

Lastly, the Mission Manager is the rover's central brain — it coordinates everything from the moment the program starts to the moment the rover parks safely at home. When the rover first powers on, it waits until it has a confirmed GPS position, saves that spot as its home base, and then sets off to explore. While out in the field, it constantly monitors two things: its remaining battery level and any commands arriving wirelessly from the operator at the base station. If the battery drops below 20%, the rover makes the decision to head home on its own, without needing to be told. If the operator decides the mission is complete and sends a "return home" command over

Bluetooth, the rover responds immediately. In either case, the onboard autopilot takes over and navigates the rover back to the exact spot where it started. If it arrives successfully, the mission ends cleanly; if something goes wrong during the journey home, the system flags an error so the operator knows to intervene.

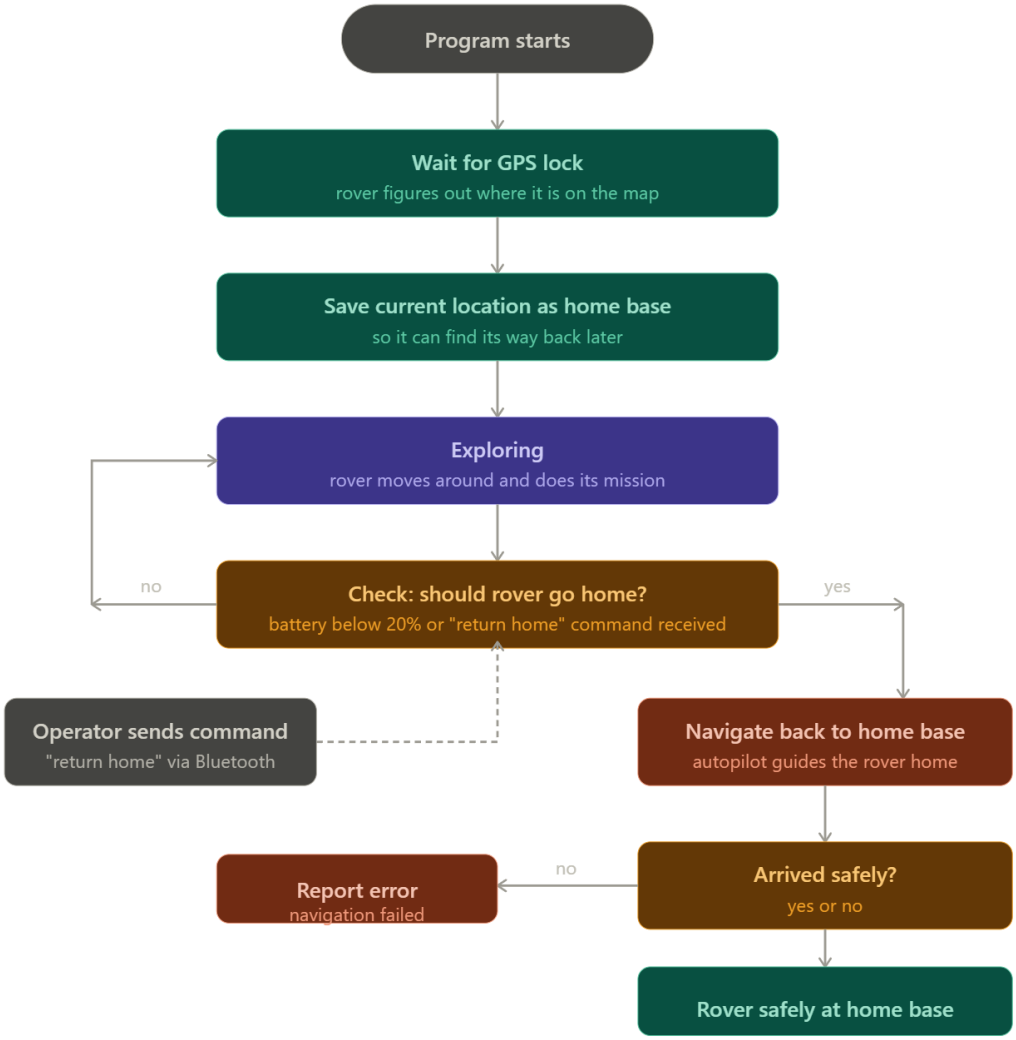

Figure 95: Mission Manager Pseudocode

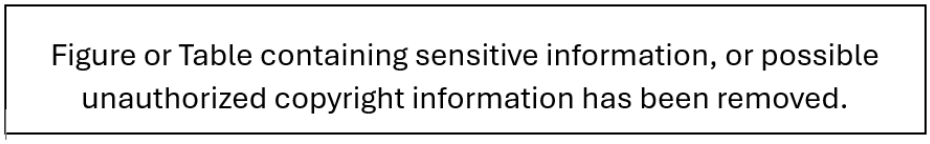

Figure 96: Mission Manager verification output

7.4 Station System Architecture

The robotic arm of the charging station utilizes five ANNIMOS servo motors that operate simultaneously to achieve smooth and synchronized motion of the arm as a whole. The servo motors are directly driven by an Arduino microcontroller, which is responsible for generating pulse-width modulation (PWM) signals for each motor, as well as setting rotational safety limits to prevent component damage. The Arduino is connected to the NVIDIA Jetson, which serves as the high-level motion planning based on the data received from the Intel RealSense camera tracking. While the Jetson is capable of direct motor controlling, it was necessary to add an Arduino as a motor controller to achieve slower, smoother, and safer charging arm movement.

The original charging arm motors were FEETECH 50kgcm and 30kgcm motors, and these were replaced with ANNIMOS 160kgcm and 150kgcm motors to support the weight of the induction charger transceiver coil. The motors initially moved to the final positions as quickly as possible, resulting in high jerk and component damage. A significant amount of development time was devoted to tuning the movement speed of the servo motors, especially for slowing down the rotational speed of the servos. To mitigate this, step size adjustments were implemented in the control programming which effectively slowed the movement of the charging arm. PWM ramping was also investigated to try to slow down and smooth the motion of the charging arm.

Inverse Kinematics (IK) was studied to further improve the motion of the charging arm. Specifically, a Forward And Backward Reaching Inverse Kinematics (FABRIK) algorithm was explored and tested with the charging arm. FABRIK is an iterative IK solver that computes joint positions based upon desired end effector location without the need for rotational angles or matrices, thus streamlining computational processes and producing smoother, faster, and more accurate robotic arm motion. [7] This algorithm was tested but not fully implemented onto the charging station arm.

The utilization of AprilTags provided a robust visual system to provide the "eyes" for the robotic arm. Unlike traditional color-tracking methods, AprilTags utilize high contrast black and white patterns that remain detectable under varying lighting conditions and shadows. The tag family used was tag25h9, where the specific pattern allows for built-in error correction and unique identification. This ensures that the system can isolate a specific target while ignoring background noise or visual clutter which is a critical advantage for autonomous reliability. The detection process works by identifying the four sided shapes within the camera frame and decoding the bit pattern inside. Once a tag is identified, the system changes the camera geometry from 2D pixel data into 3D spatial coordinates. The camera uses these coordinates and the comparison of the tag's measured size in pixels against its known physical dimensions, to calculate real-time distance using the camera’s focal length. This allows the robot to determine exactly how far it is from the Apriltag without the need for additional sensors.

Figure 97: AprilTag

The Battery Monitoring System (BMS) is achieved via the WiBotic Induction charger transmitter control panel located inside of the station. The control panel is accessed via an ethernet cable connected to the station’s Jetson or an external laptop and the transmitter. The WiBotic control panel interface provides live monitoring on the performance of the WiBotic system as well

as many necessary battery specifications such as the voltage, charge current, power levels, and cycle data.

8. Final Manufacturing

To realize the new charging station and rover designs, significant time was spent machining components, as well as 3D printing and assembling components. Milling and CNC machining were used extensively on the rover structural additions, which successfully repaired the rover suspension and enabled zero-point turn functionality. 3D printing using ABS was primarily used on the new charging station arm, but was also used to prototype the rover suspension redesign.

8.1 Rover Structural Modifications

The rover was assessed for structural integrity, and several areas of concern were identified. First, the rover suspension system exhibited a high angle of camber. The aluminum pipes of the rocker-bogie suspension, which were supposed to be vertical, were angled away from the rover body at approximately 10 degrees, as shown in Figure 98. Most of the camber originated from the bogie-to-rocker joint design, and the loose fitting at the rocker-to-body joint. This presented a serious potential failure point, and negatively impacted the maneuverability of the rover. Several modifications were made to eliminate the camber of the suspension system, and the results can be seen in Figure 99.

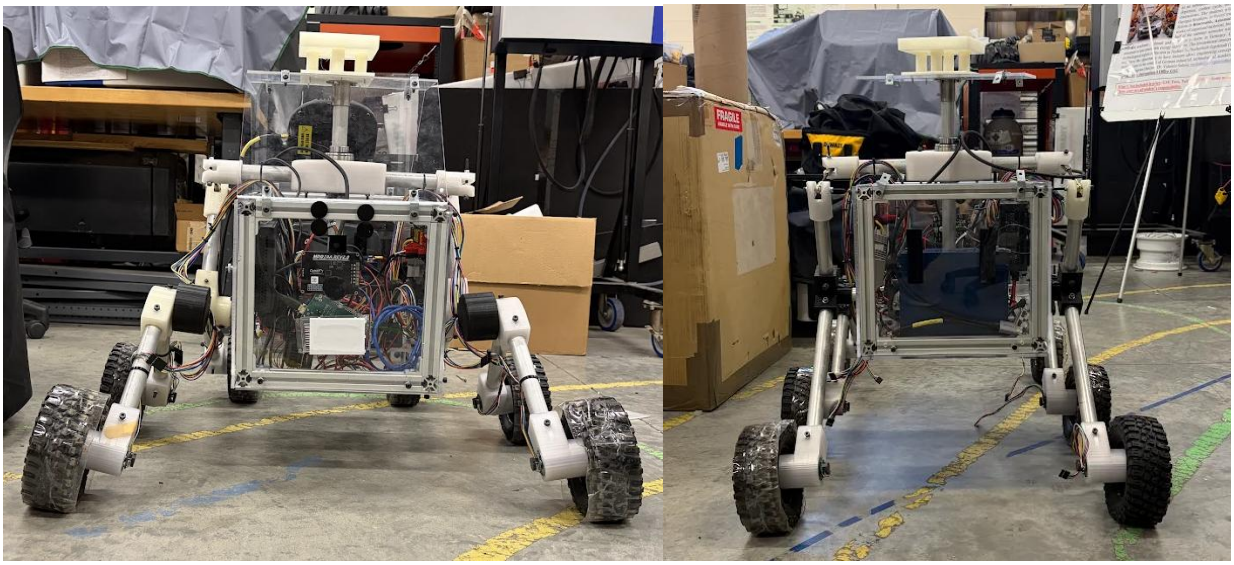

Figures 98 and 99: Existing rover showing excessive camber in suspension, and rebuilt rover with ABS prototyping joints showing camber issue resolved

The bogie-to-rocker joint was redesigned as a knuckle joint, effectively eliminating the torque previously applied to this joint in the suspension system. The rocker-to-body joint was modified and made more secure with additional hardware. The screws connecting this joint were not secured in place and could easily be pulled out of their fittings, and the new screws are secured in place with lock nuts and securely tightened. Figure 100 shows the structural modifications to the rover suspension system, and it can be seen that the camber in the updated suspension system is effectively zero.

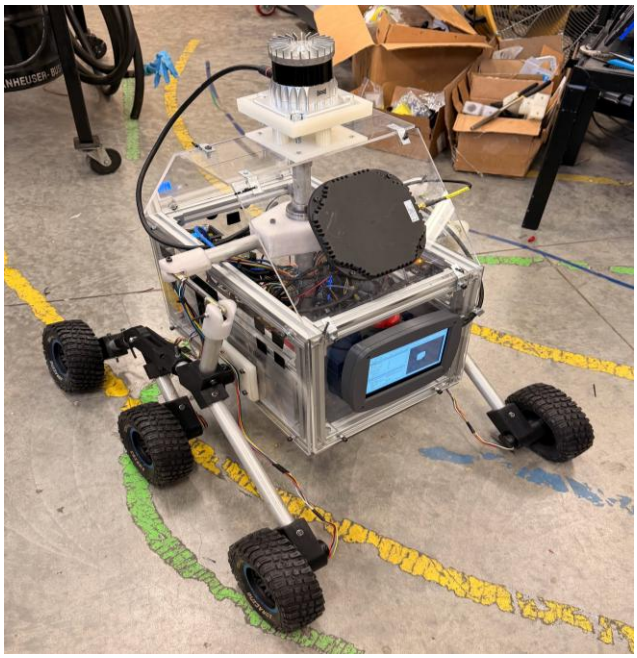

Figure 100: Existing rover with ABS prototyping joints

The existing rocker-to-body joint was secured directly to the plexiglass rover body via the bearing housing and four screws. This caused significant strain on the plexiglass, and led to cracking at multiple locations on the plexiglass. Considering the extreme cold temperatures of the moon environment, using plexiglass as a structural component is not advised because it becomes very brittle in the cold. Structural improvements were added to this joint by adding a ¼" thick aluminum plate behind the plexiglass and securing it with additional t-slodded aluminum rail. The t-slotted rail was secured to the main frame of the rover body using l-bracket hardware. Figure 101 shows the reinforcement plate, and the bearing plate secured through the plexiglass to the aluminum plate behind it. This significantly reduces the strain on the plexiglass, and creates a more durable suspension-body connection.

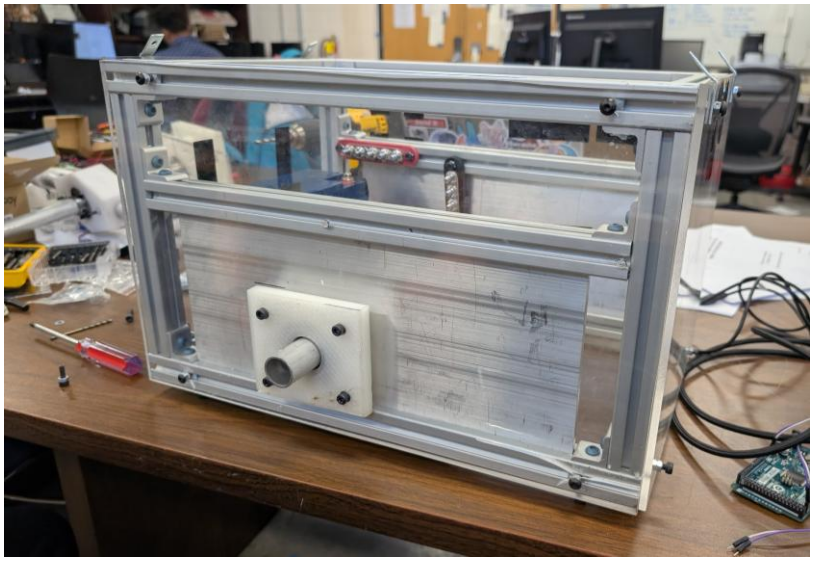

Figure 101: Rover body-leg joint reinforcement plate

Lastly, the previous differential support was similarly secured to plexiglass inside the rover. The previous differential support was secured to a sheet of plexiglass screwed into a singular t-slotted rail at the base of the rover body. This support was easily deflected from its intended upright position when turning the rover, causing significant strain in the plexiglass. In Figure 102, the modified differential support plate of the rebuilt rover is seen. This support plate was created with a ¼" thick aluminum plate and secured to the main rover body frame using two additional t-slotted rails spanning the width of the rover main body, as shown in Figure 103.

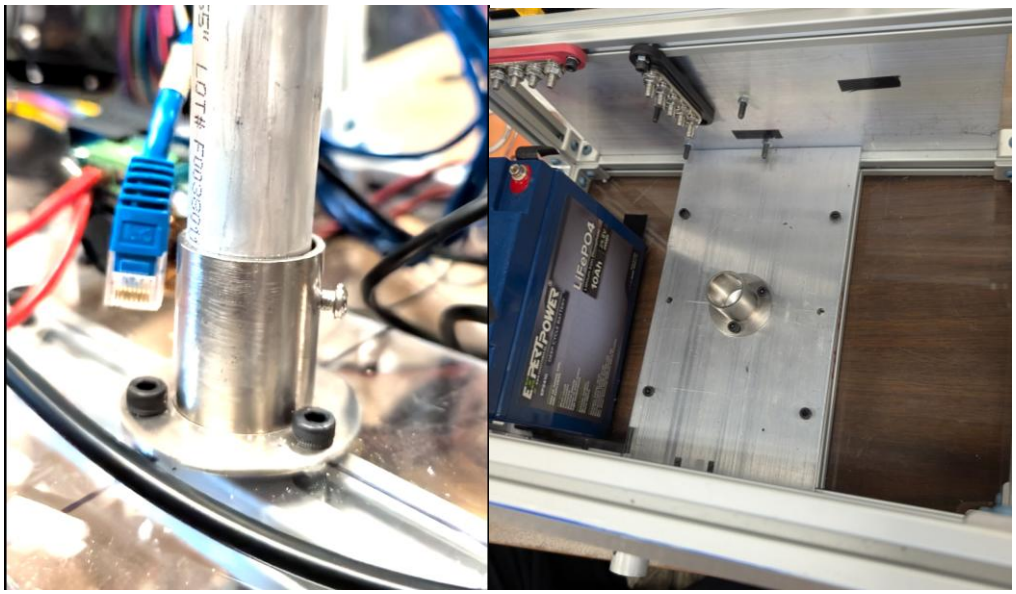

Figures 102 and 103: Gen. 1 differential support, and Gen. 2 differential support plate

It was necessary to further reinforce the rover suspension system with the addition of aluminum joints to replace the prototyping ABS joints. The ABS joints served the purpose of verifying the new knuckle joint design and modified main rover joint, but were determined insufficient to support the rover for long-term usage. The aluminum joints were made using a CNC machine, and underwent additional machining to drill holes for support screws and file down all sharp corners. Significant time was taken to smooth the sharp corners, as this was a matter of safety for all team members.

Figure 104: Aluminum rover joints

Additional testing was performed with the aluminum joints installed to assess the zero-point turn capability and structural integrity. It was determined the aluminum joints exceed the structural stability needs of the rover for long-term usage.

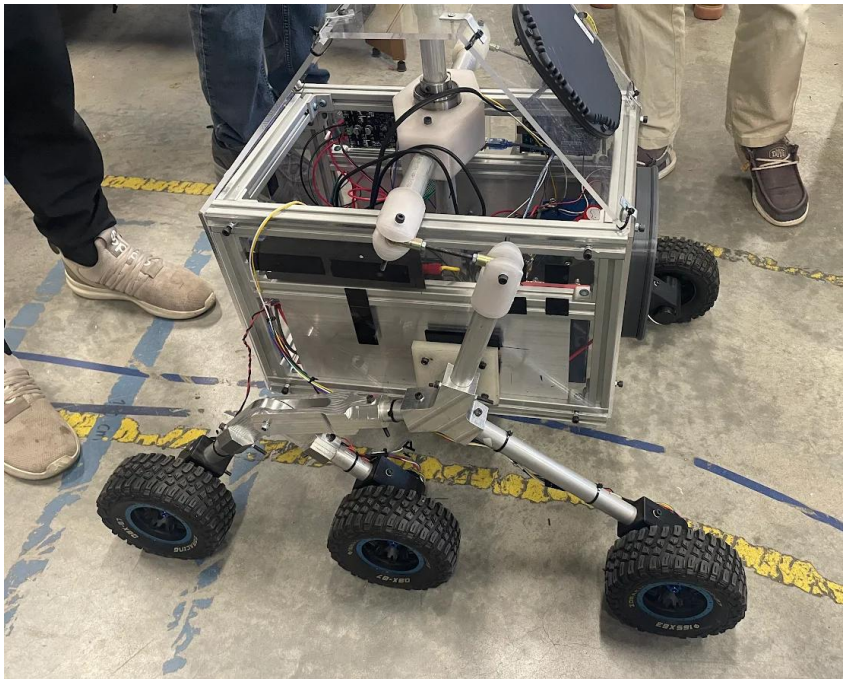

Figure 105: Rover with aluminum joints

8.2 Station Arm Rebuild

The charging station robotic arm was completely redesigned. This redesign added approximately 20” of additional length to the arm. Additional length was required to accommodate imperfect rover docking in the presence of terrain. Figure 106 shows the Gen. 1 charging station arm, and Figure 107 shows the redesigned and rebuilt Gen. 2 charging station arm. The links of the redesigned arm are hollow, reducing weight and allowing for internal wire management. The induction charging mount, Link 5, is redesigned to reduce thickness and weight while fully supporting the 1.5 lb charging plate. Each of the main links of the charging station arm were designed with thicker motor mount connection points, and longer screws were purchased to accommodate for this. Additionally, Link 1 inside the charging station base was redesigned to provide substantially more support to Motor 1, the motor which facilitates arm rotation during scanning.

Figure 106 and 107: Gen. 1 charging station arm, and Gen. 2 charging station arm

9. Final Product Verification

The Battery Monitoring System (BMS) was successfully verified through real-time data acquisition and processing during rover operation. Bluetooth connection between the rover and station was verified. The INA260 sensor successfully measured battery voltage, current, and power, which were transmitted through the Arduino to the Jetson for processing. As shown in Figure 108, the system consistently reported voltage values near 26.3 V and current values ranging between approximately 0.35 A and 0.45 A, resulting in power outputs between 9 W and 11 W. These values are consistent with expected power consumption under light operational load, confirming that the sensor readings are accurate and stable.

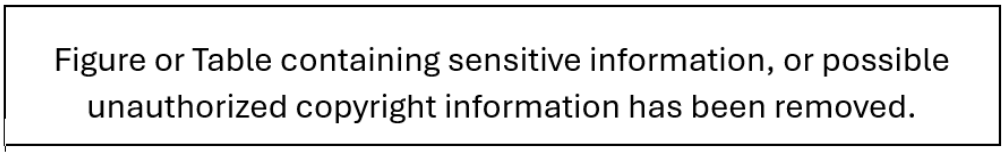

Figure 108: BMS data transmission from rover to station

The continuous data stream demonstrates that the communication pipeline between the INA260 sensor, Arduino, and Jetson is functioning correctly. Additionally, the system was able to maintain a steady update rate, supporting near real-time monitoring of battery conditions. This verifies that the BMS is capable of reliably collecting and transmitting battery data, forming a valid foundation for higher-level battery state estimation, warning detection, and autonomous decision-making such as return-to-station behavior.

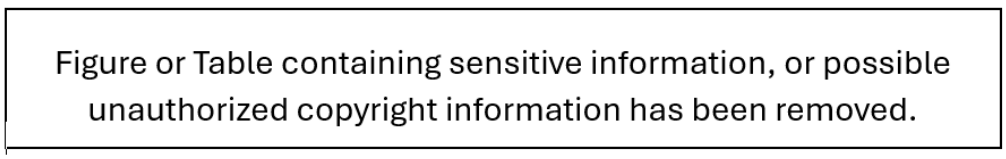

Figure 109: Battery value data stream from rover to station

The results presented confirm that the Battery Monitoring System is capable of providing consistent and reliable battery data during rover operation. The successful acquisition and transmission of voltage, current, and power values demonstrate that the hardware and communication pipeline between the sensor, Arduino, and Jetson are functioning as intended. This establishes a dependable foundation for higher-level battery management processes, including State of Charge estimation, warning detection, and autonomous decision-making.

While full validation of advanced features such as precise SOC estimation and fault handling requires further testing under varying load conditions, the current results verify the core functionality of the BMS. The system is therefore capable of supporting the rover's autonomous energy management strategy, particularly enabling safe operation and future implementation of return-to-station behavior based on battery conditions.

The charging station arm was tested for payload capacity by repeating a full arm deployment five times successively. The arm successfully completed the payload demonstration test, proving that it reliably supports the 1.5 lb induction charging coil. The deployed position is shown below in Figure 110. In addition, the induction charging system successfully transmits power to the onboard rover battery.

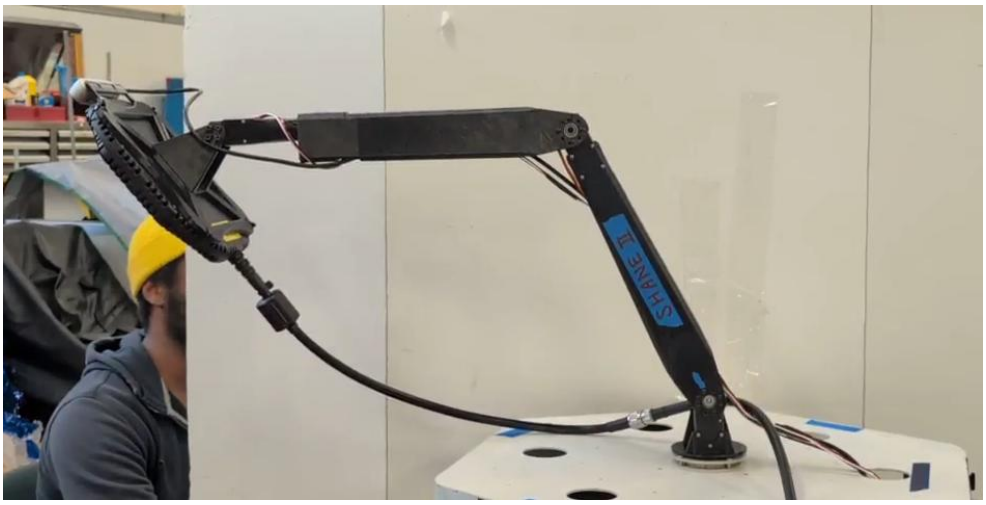

Figure 110: Payload demo test charging deployment position

Testing of the rebuilt rover suspension was tested by performing multiple successive zero-point turns, both clockwise and counterclockwise. The aluminum joints performed as expected, and prevented any pulling or dislocation of the rover legs during maneuvering. Additionally, structural stability was verified by traversing over small obstacles, and it was determined that the improved suspension system and new motors give the rover increased terrain traversal capabilities. The characteristic flexing of the rocker-bogie suspension system was observed, and all six wheels remained in contact with the floor at all times during obstacle traversal. Camber has been successfully eliminated via implementation of the aluminum joints, and the rover possesses increased capabilities to maneuver and traverse obstacles and rough terrain.

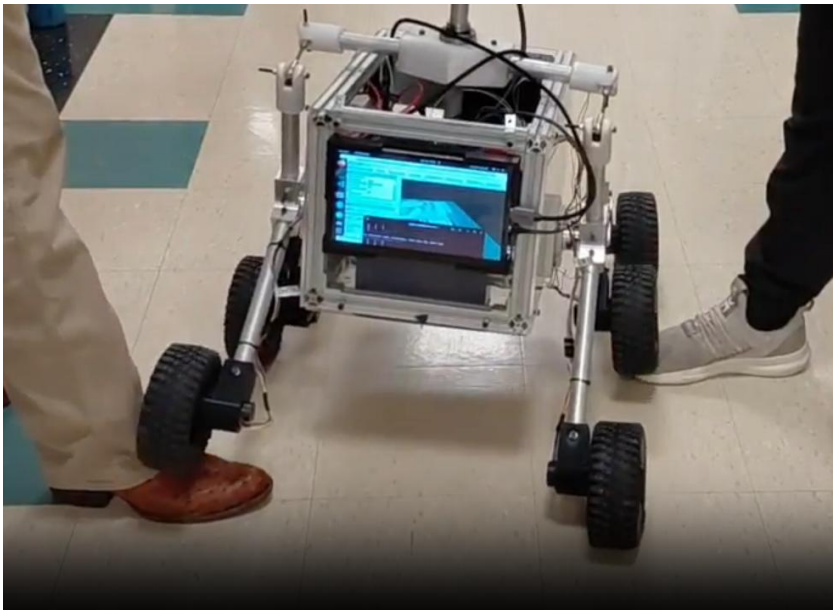

Figure 111: Rover small obstacle traversal testing

10. Bill of Materials

Figure or Table containing sensitive information, or possible unauthorized copyright information has been removed.

Table 3: Charging Station 2025 Bill of Materials

Figure or Table containing sensitive information, or possible unauthorized copyright information has been removed.

Table 4: Rover 2025 Bill of Materials

Figure or Table containing sensitive information, or possible unauthorized copyright information has been removed.

Table 5: Charging Station 2026 Bill of Materials

Figure or Table containing sensitive information, or possible unauthorized copyright information has been removed.

Table 6: Rover 2026 Bill of Materials

11. References

[1] U.S. Department of Labor, Occupational Safety and Health Administration, “29 CFR Part 1910, Subpart S—Electrical,” Code of Federal Regulations. Accessed: Apr. 24, 2026 [Online]. Available: https://www.law.cornell.edu/cfr/text/29/part-1910/subpart-S

[2] B. Ingram, D. Jones, A. Lewis, M. Richards, C. Rich and L. Schachterle, "A code of ethics for robotics engineers," 2010 5th ACM/IEEE International Conference on Human-Robot Interaction (HRI), Osaka, Japan, 2010, pp. 103-104, doi: 10.1109/HRI.2010.5453245.

[3] Ingram, B., Jones, D., Lewis, A., and Richards, M., 2010, “A Code of Ethics for Robotics Engineers,” Interactive Qualifying Project Report, Worcester Polytechnic Institute, Worcester, MA, Mar. 6.

[4] American Society of Mechanical Engineers (ASME), 2024, “Code of Ethics of Engineers,” Society Policy P-15.7, ASME, New York, NY, Oct. 1.

[5] K. Townsend and E. Herrada, Adafruit BNO055 Absolute Orientation Sensor, Adafruit Learning System, New York, NY, Apr. 22, 2015, last modified May 16, 2025. [Online]. Available: https://learn.adafruit.com/adafruit-bno055-absolute-orientation-sensor/overview. Accessed: Apr. 29, 2026.

[6] Ouster, Inc., 2023, “Guide to Evaluating SLAM,” Ouster Insights Blog. Available at: https://ouster.com/insights/blog/guide-to-evaluating-slam (accessed April 22, 2026).

[7] *C. A. Miller, S. A. Rosen, and M. L. Beeson, 2011, “A Review of Human Factors in Handheld Device Use,” Journal of Children and Media*, **5**(2), pp. 113–129, DOI: 10.1016/j.jchb.2011.02.001.

12. Annex

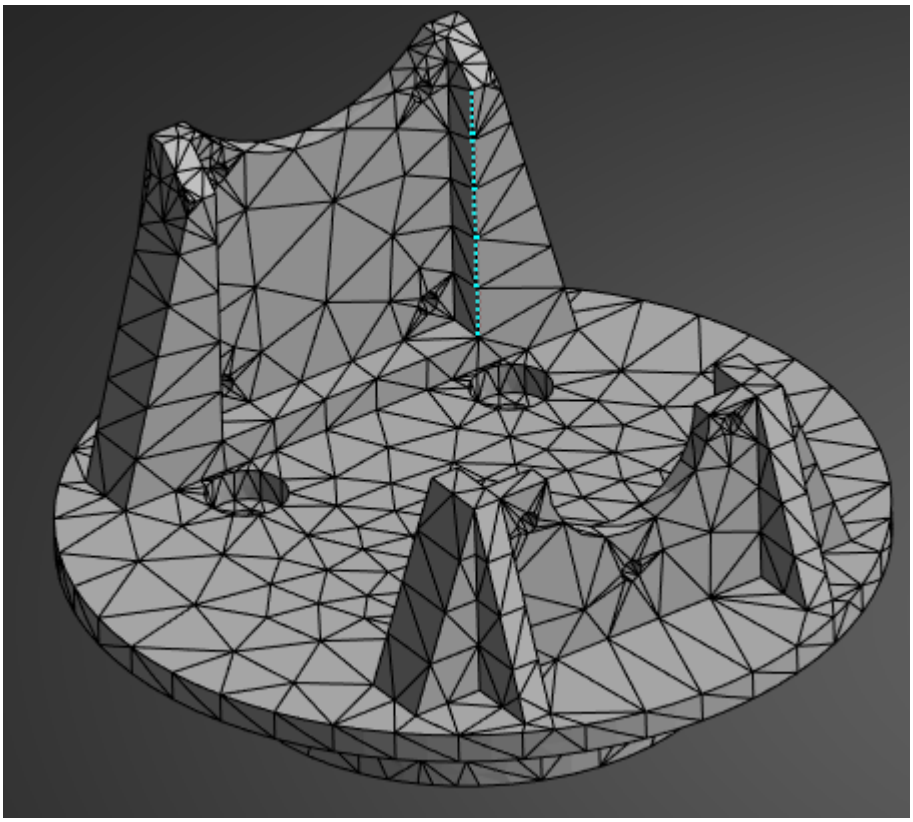

Fig #. Concept 2 Link 1 Mesh

Redacted due to Export Control/CUI requirements.

Fig #. Concept 2 Link 1 Dimensioned Part Drawing

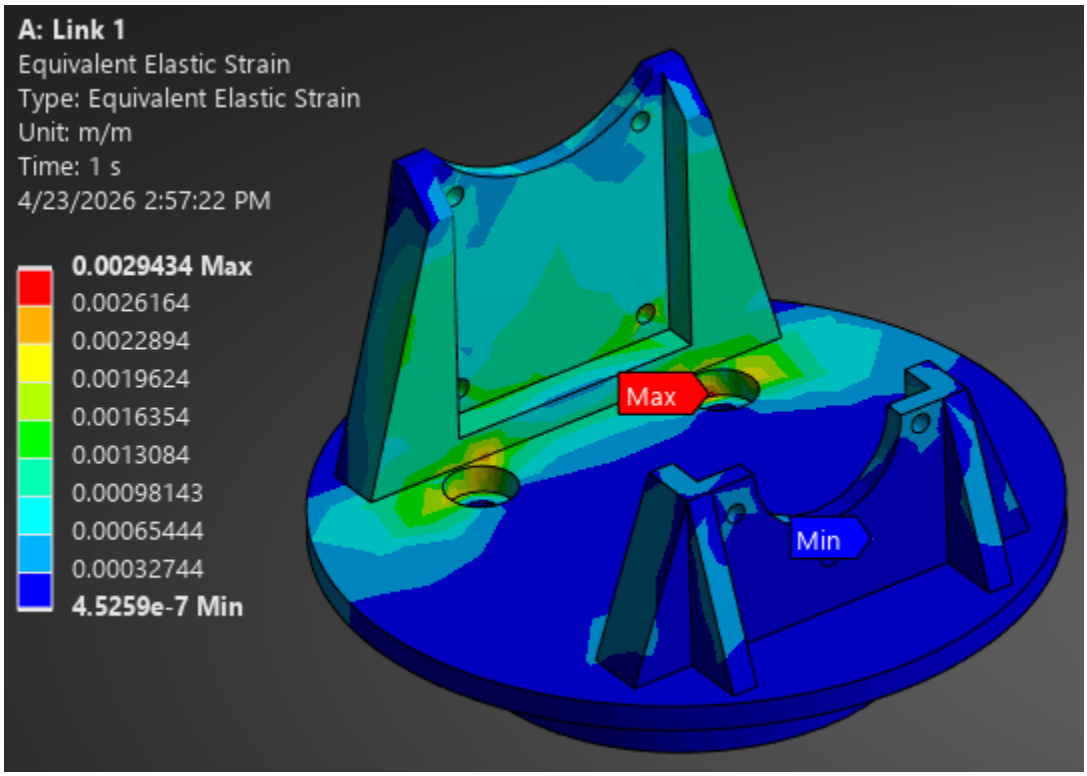

Fig #. Concept 2 Link 1 FEA Results for Equivalent Elastic Strain

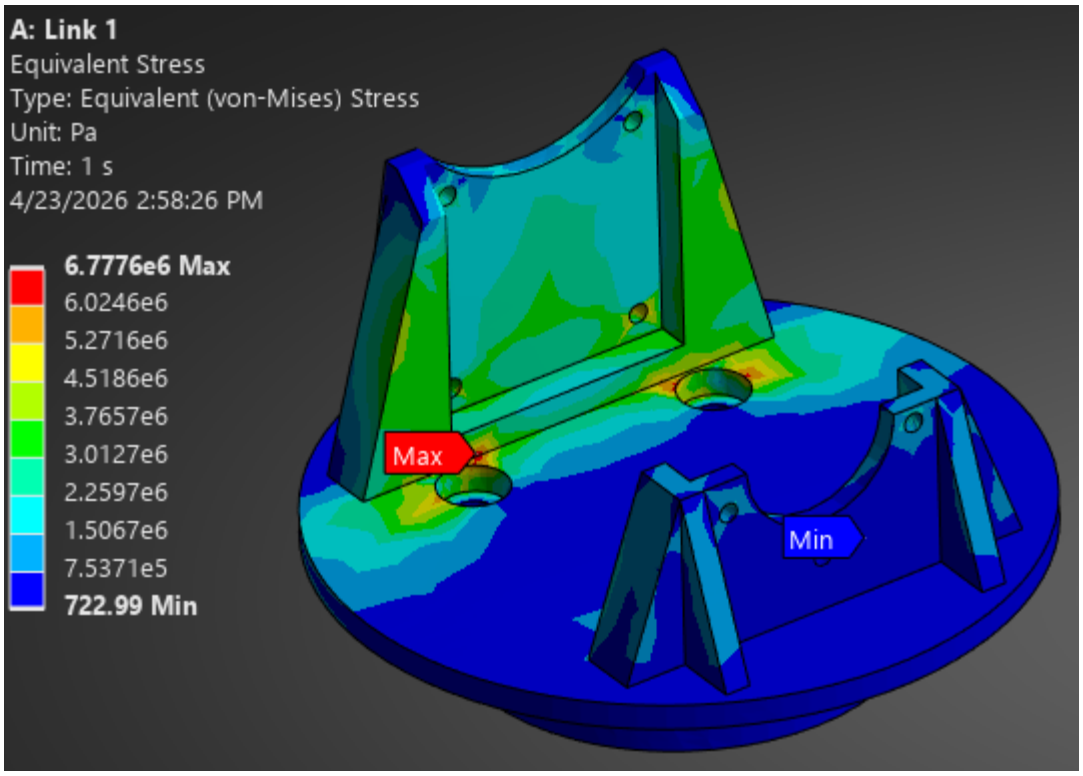

Fig #. Concept 2 Link 1 FEA Results for Von-Mises Stress

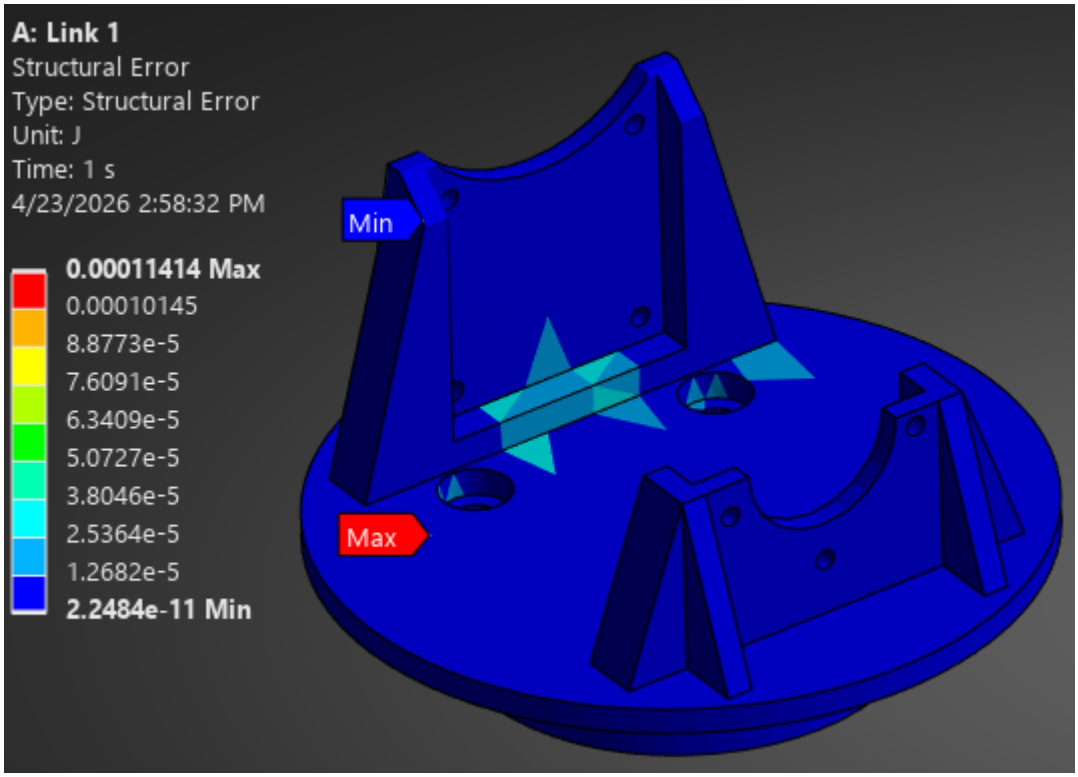

Fig #. Concept 2 Link 1 FEA Results for Structural Error

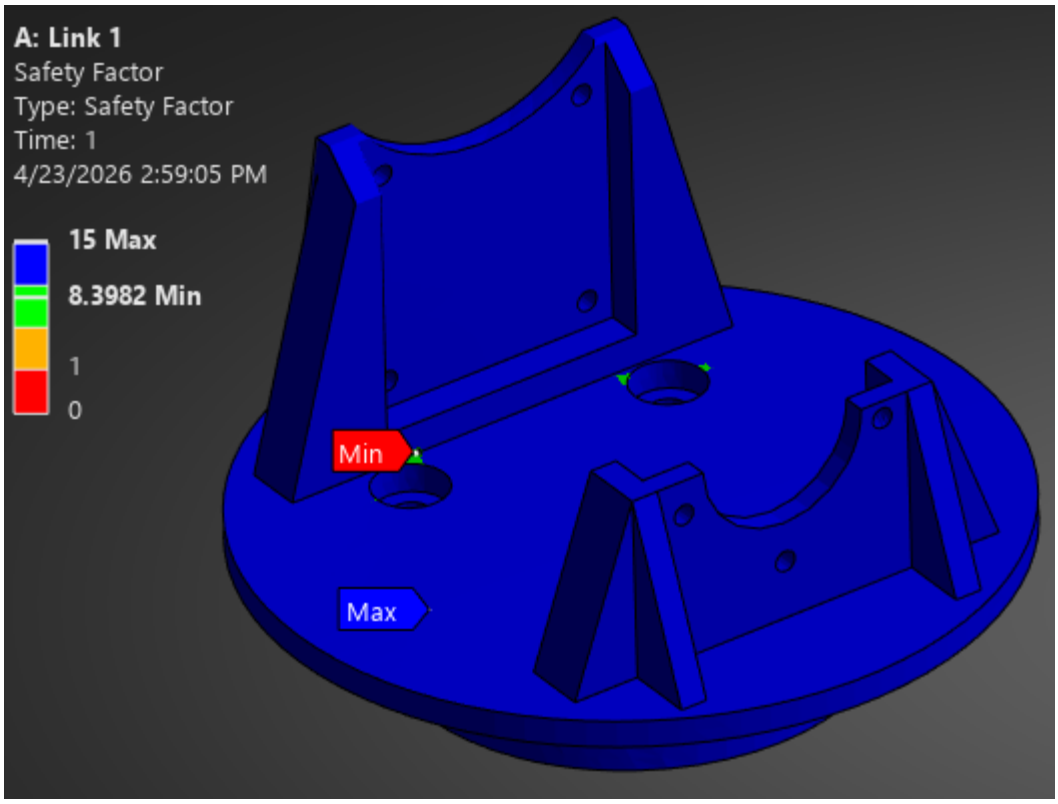

Fig #. Concept 2 Link 1 FEA Results for Safety Factor

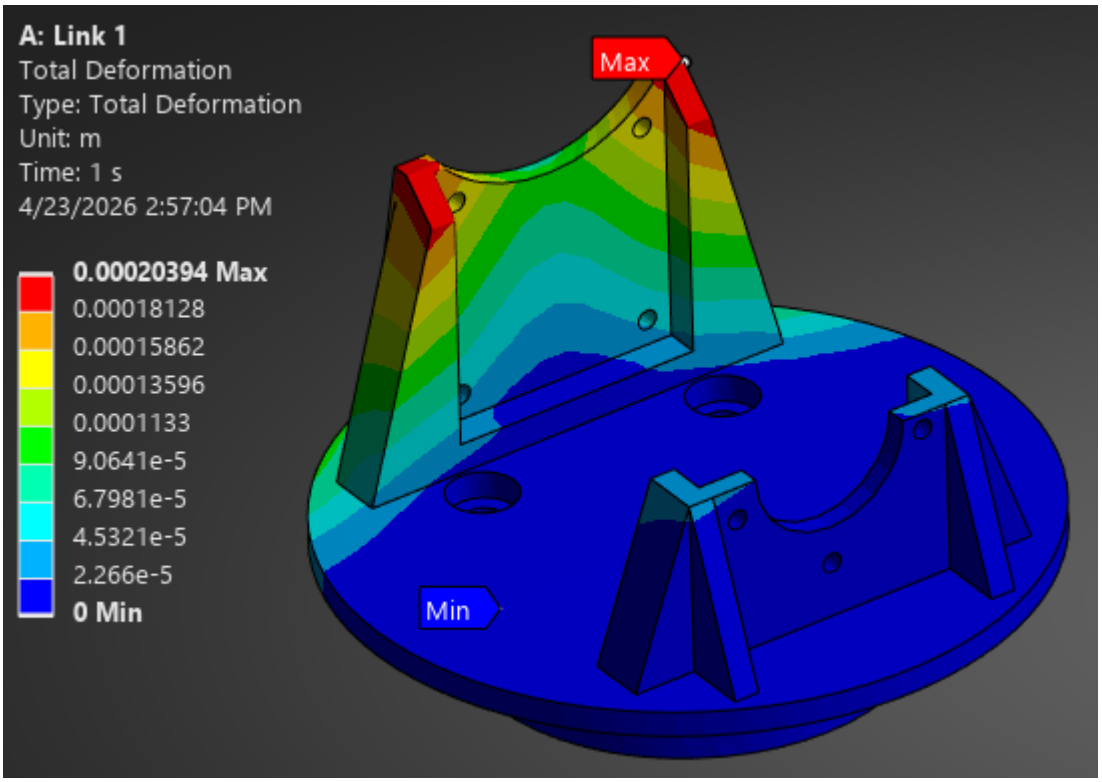

Fig #. Concept 2 Link 1 FEA Results for Total Deformation

Redacted due to Export Control/CUI requirements.

Figure #: Concept 2 Link 3 Dimensioned Part Drawing

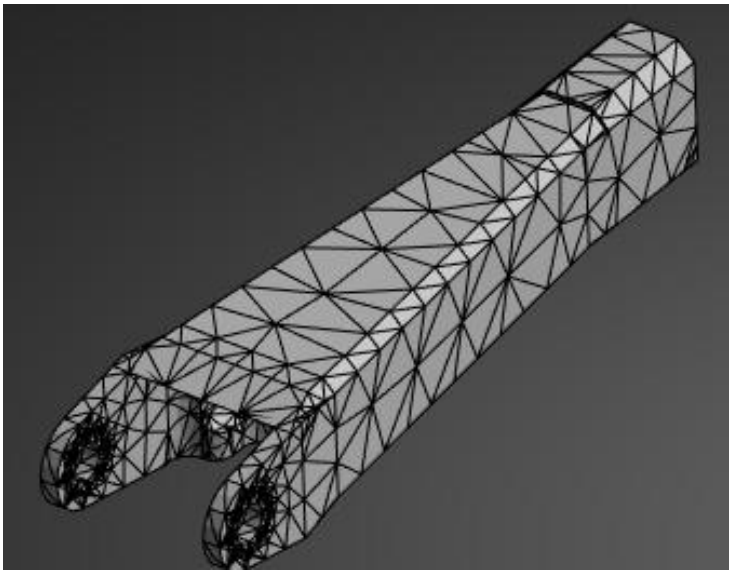

Figure #: Concept 2 Link 3 Mesh

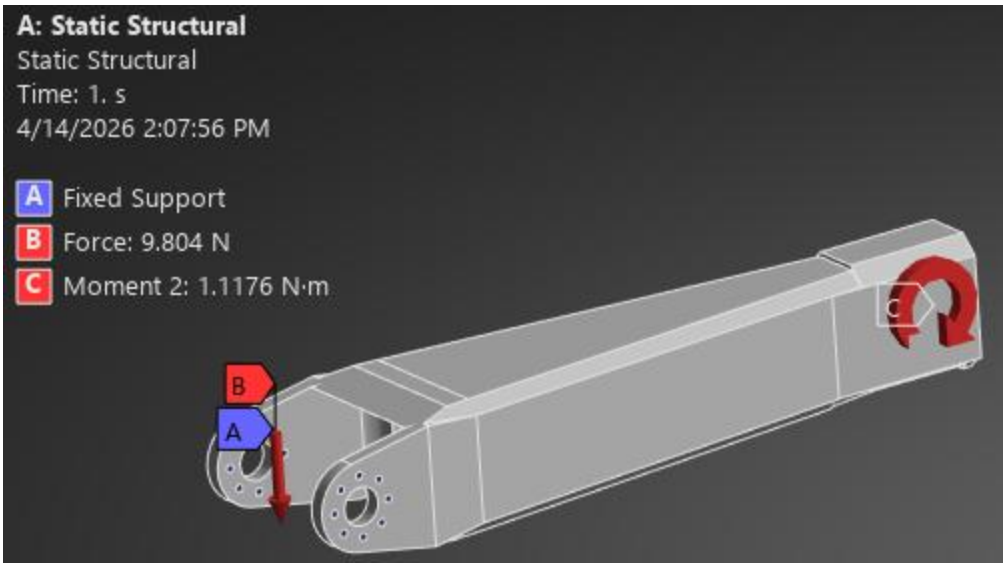

Figure #: Concept 2 Link 3 Applied Forces and Fixed Support

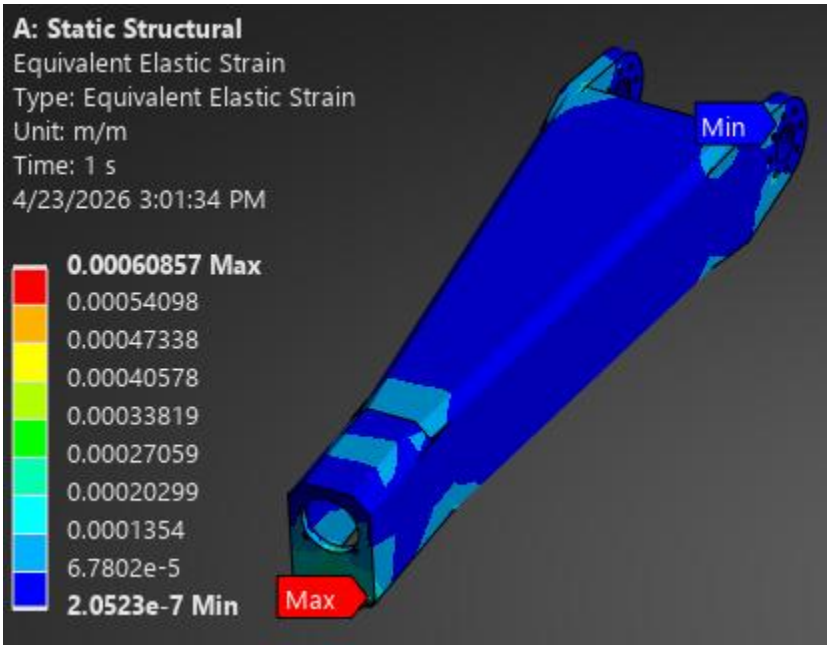

Figure #: Concept 2 Link 3 FEA Results of Equivalent Elastic Strain

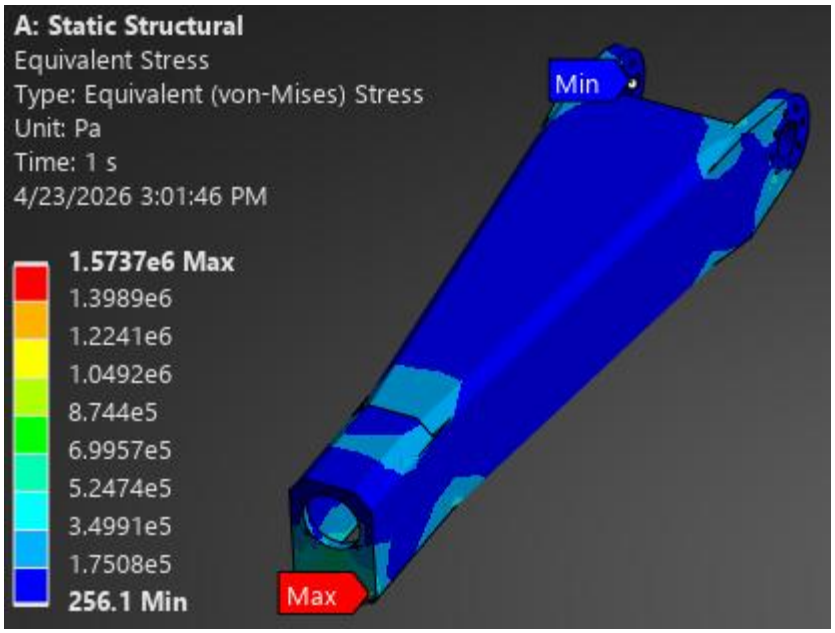

Figure #: Concept 2 Link 3 FEA Results of Equivalent Elastic Stress

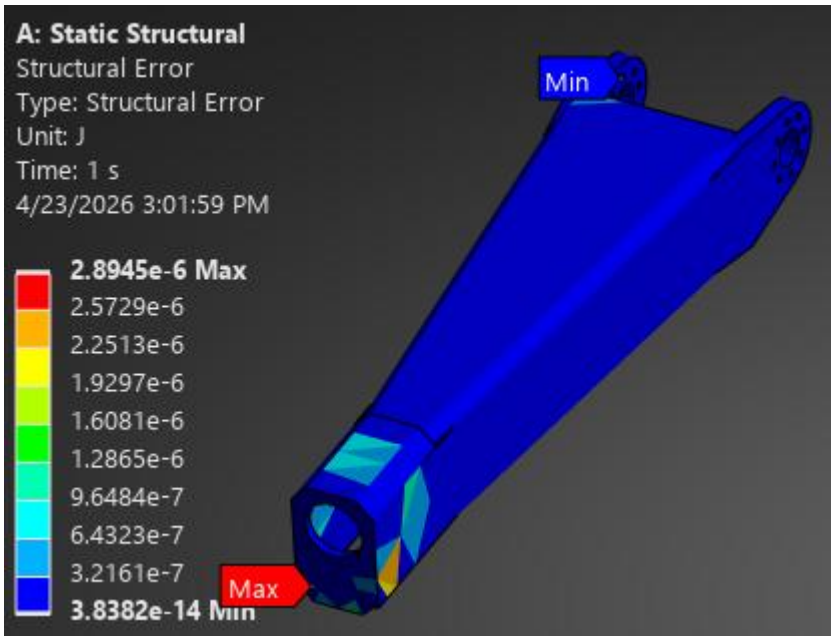

Figure #: Concept 2 Link 3 FEA Results for Structural Error

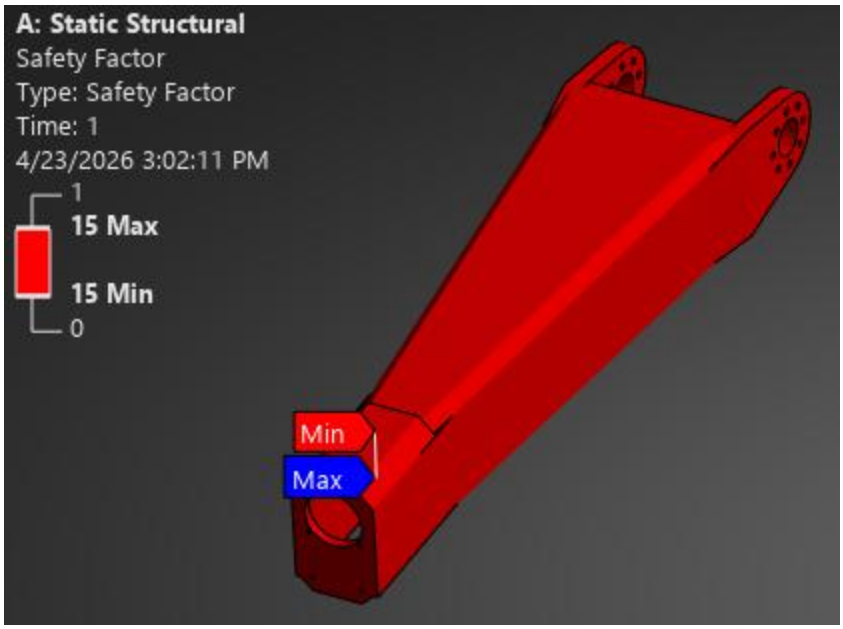

Figure #: Concept 2 Link 3 FEA Results for Factor of Safety

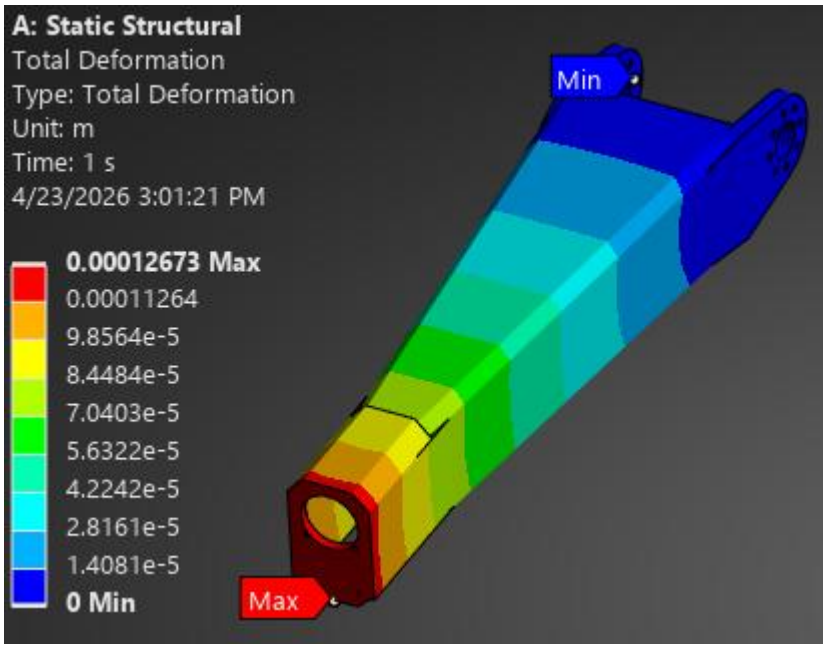

Figure #: Concept 2 Link 3 FEA Results for Total Deformation

Redacted due to Export Control/CUI requirements.

Figure #: Concept 2 Link 4 Dimensioned Part Drawing

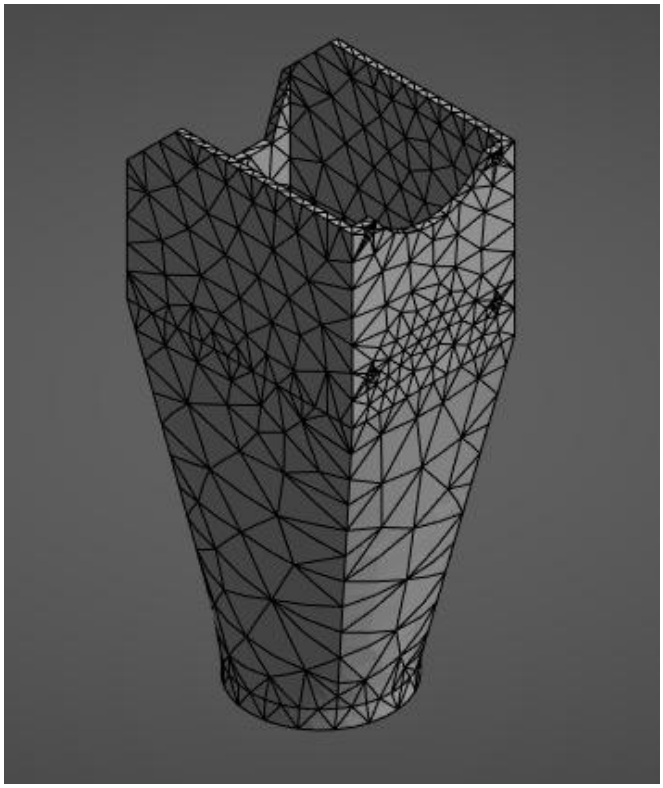

Figure #: Concept 2 Link 4 Mesh

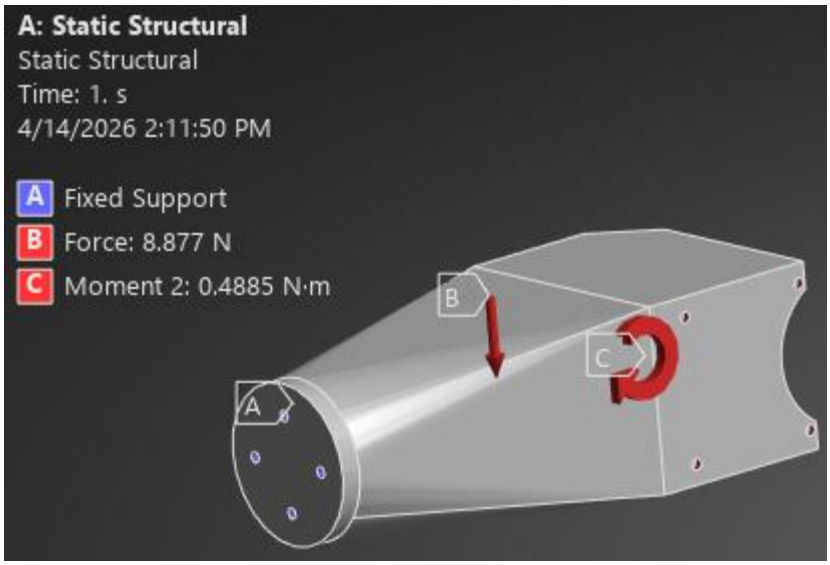

Figure #: Concept 2 Link 4 Applied Forces and Fixed Support

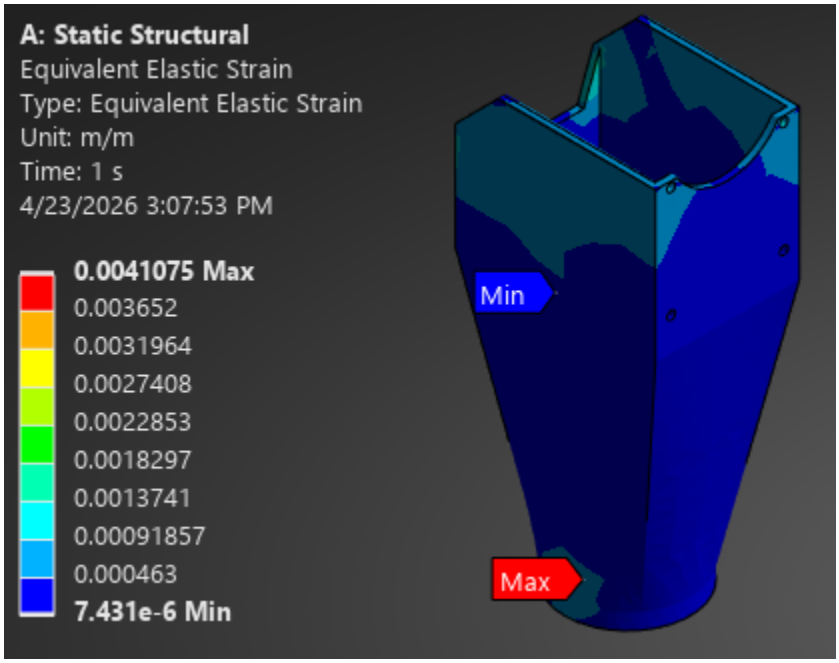

Figure #: Concept 2 Link 4 FEA Results of Equivalent Elastic Strain

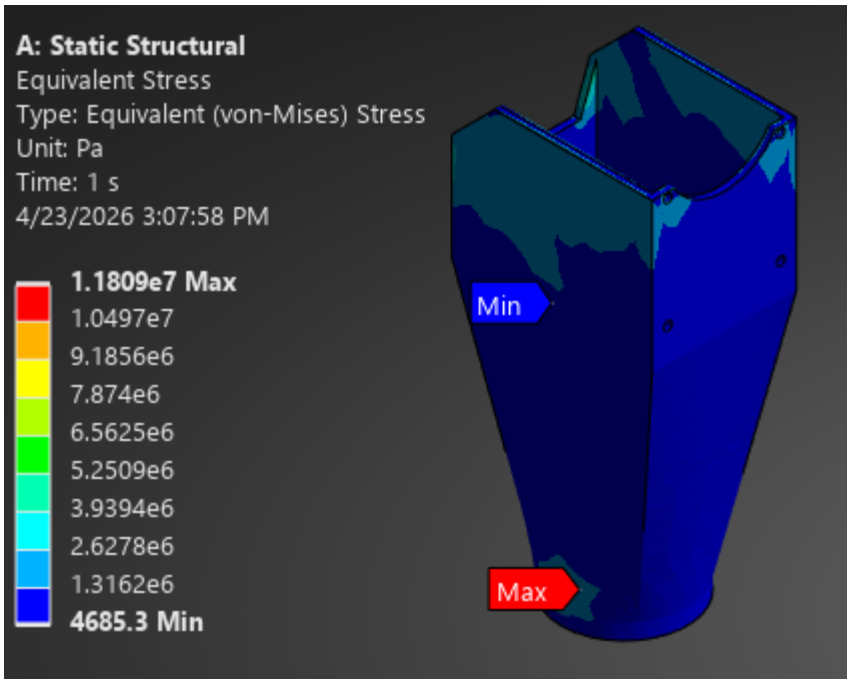

Figure #: Concept 2 Link 4 FEA Results of Equivalent Elastic Stress

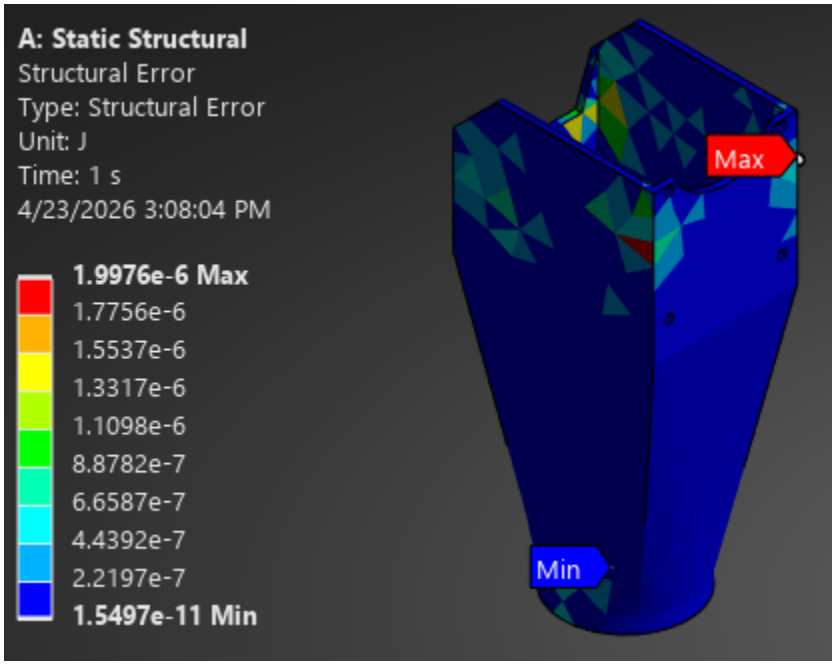

Figure #: Concept 2 Link 4 FEA Results for Structural Error

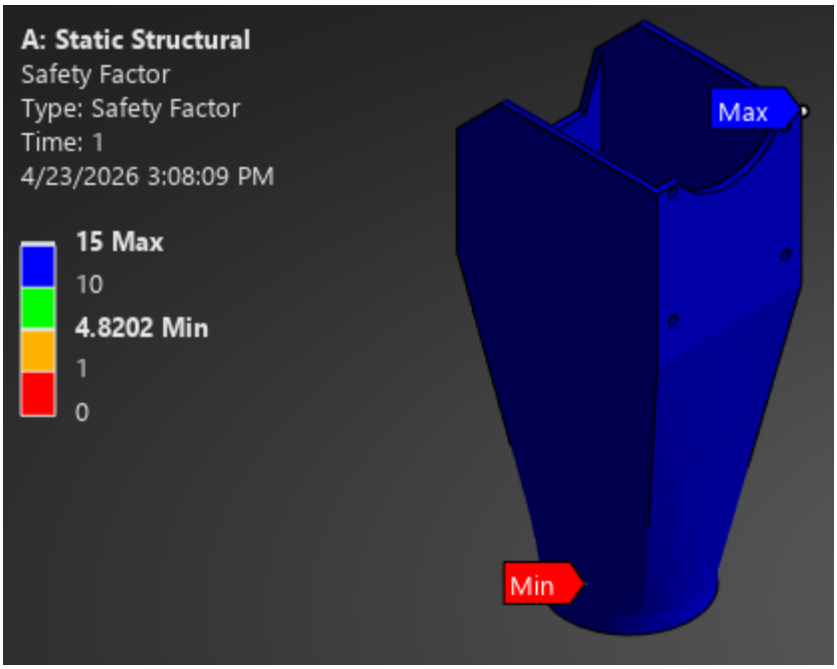

Figure #: Concept 2 Link 4 FEA Results for Factor of Safety

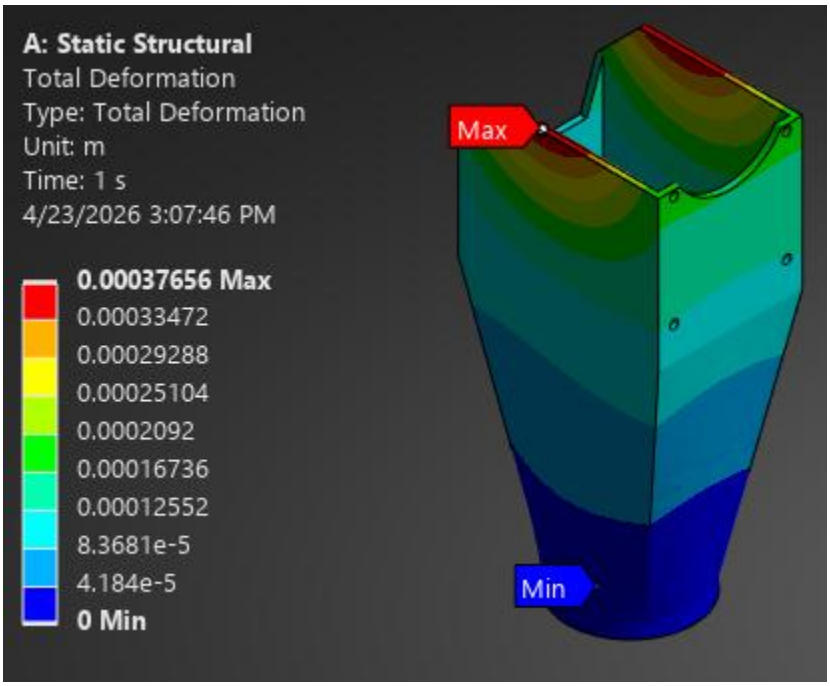

Figure #: Concept 2 Link 4 FEA Results for Total Deformation

Redacted due to Export Control/CUI requirements.

Figure #: Concept 2 Link 5 Dimensioned Part Drawing

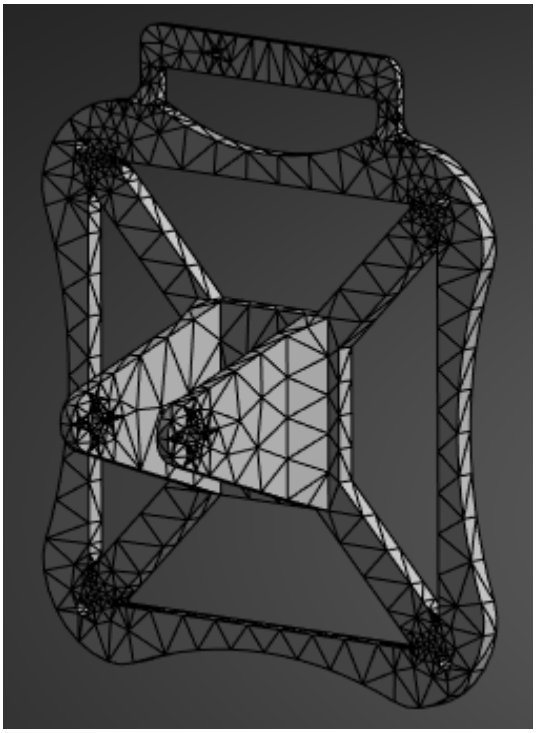

Figure #: Concept 2 Link 5 Mesh

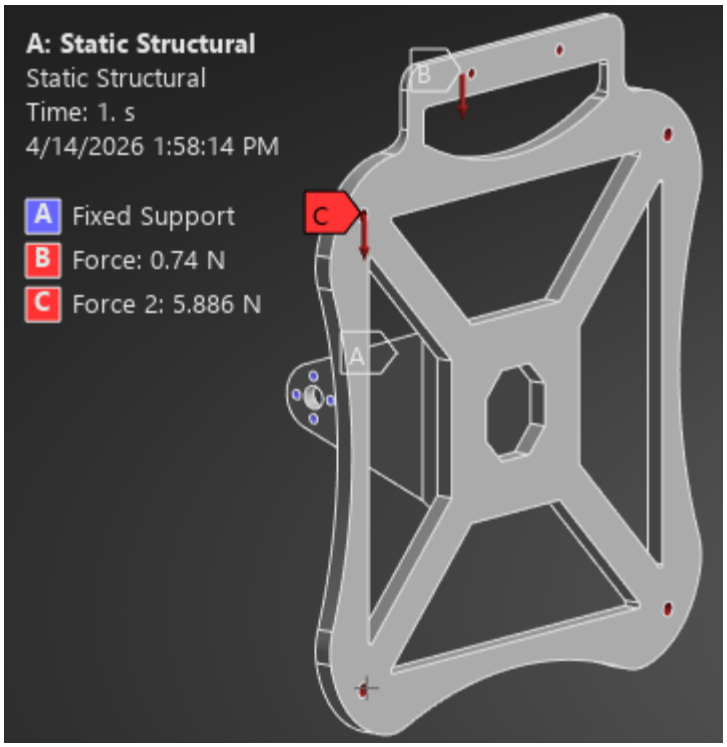

Figure #: Concept 2 Link 5 Applied Forces and Fixed Support

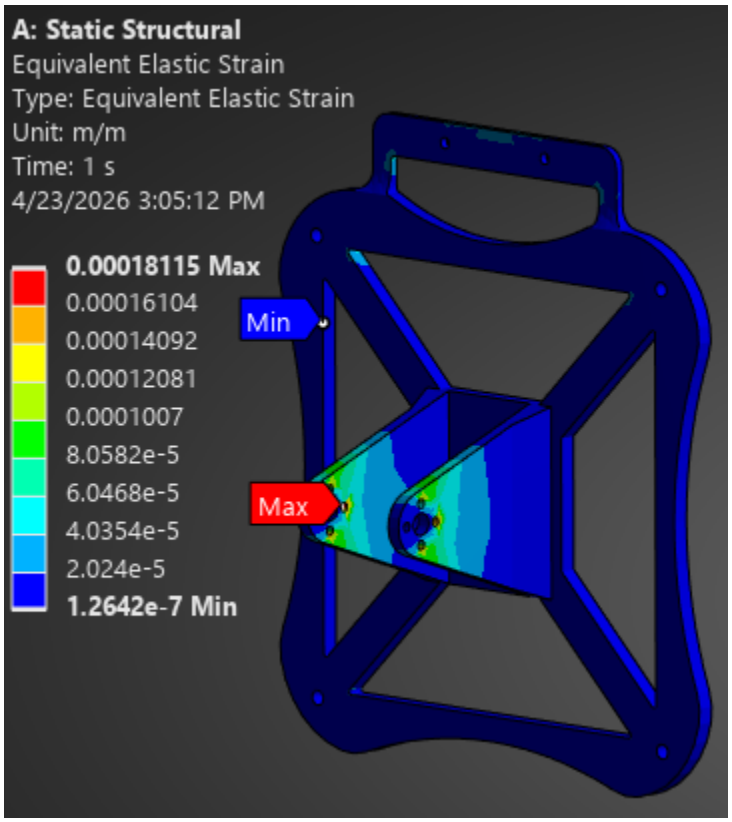

Figure #: Concept 2 Link 5 FEA Results of Equivalent Elastic Strain

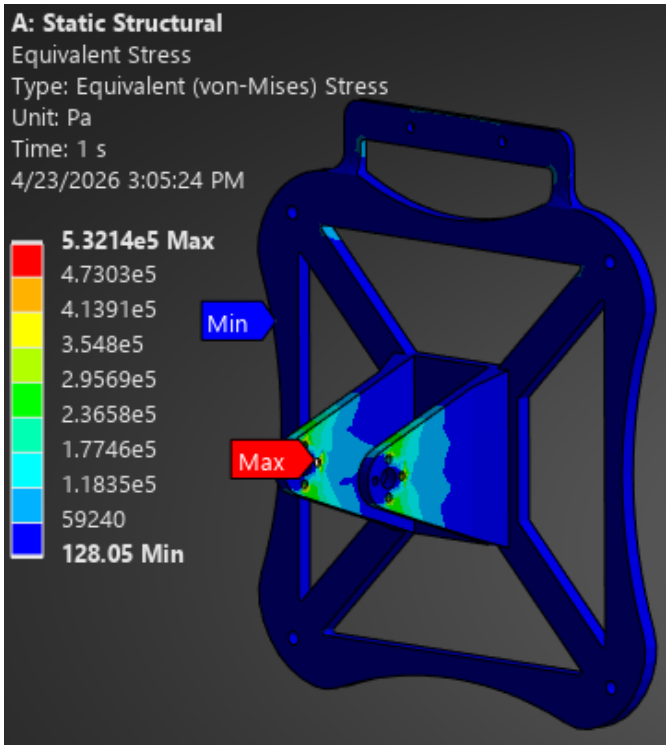

Figure #: Concept 2 Link 5 FEA Results of Equivalent Elastic Stress

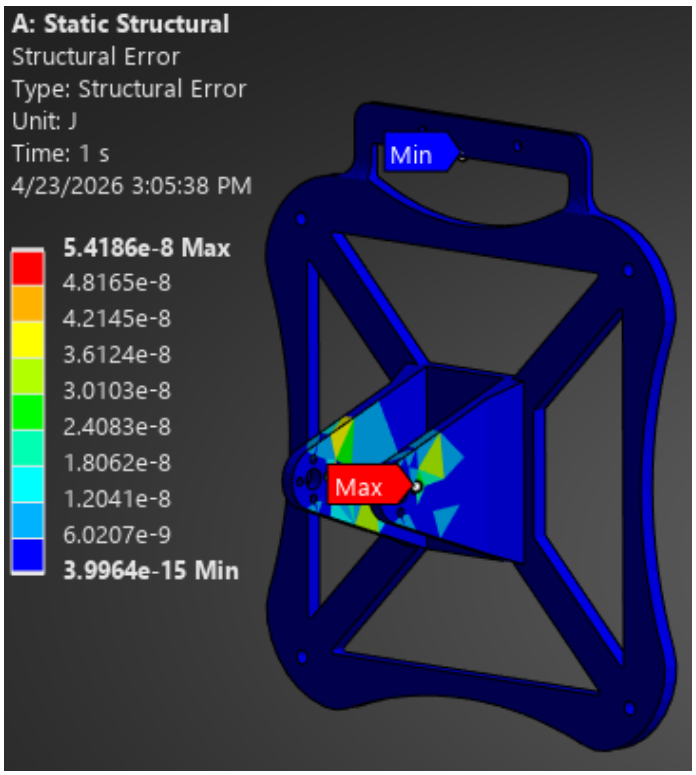

Figure #: Concept 2 Link 5 FEA Results for Structural Error

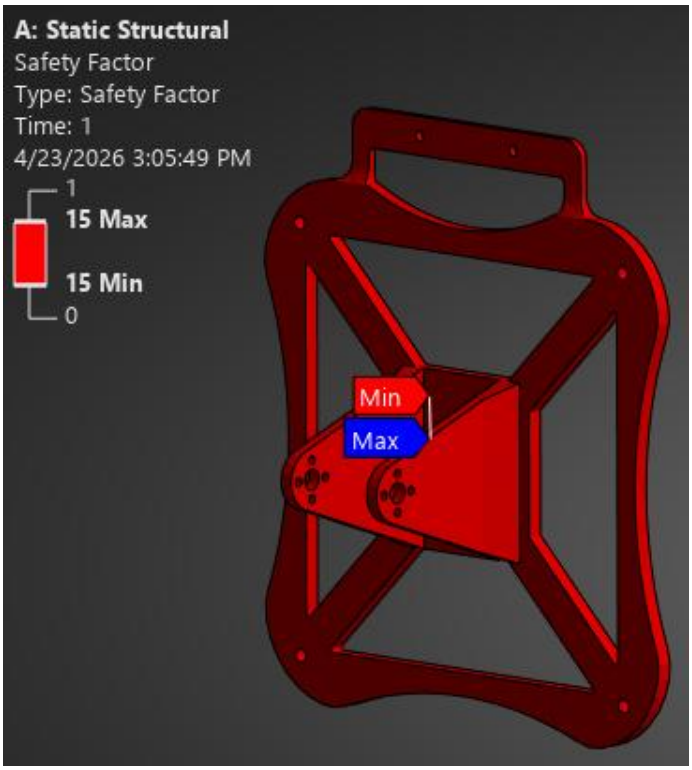

Figure #: Concept 2 Link 5 FEA Results for Factor of Safety

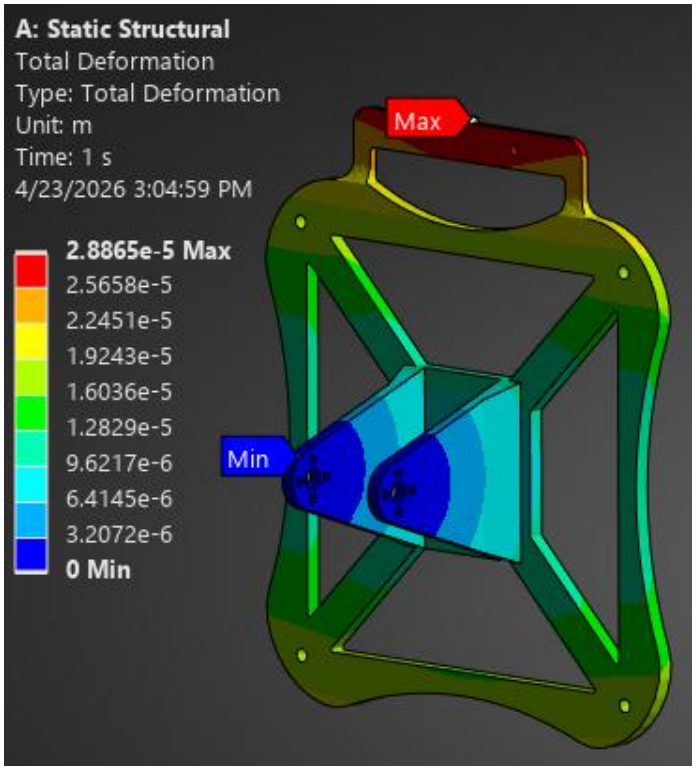

Figure #: Concept 2 Link 5 FEA Results for Total Deformation

Redacted due to Export Control/CUI requirements.

Figure X: Outer Knuckle Dimensioned Drawing

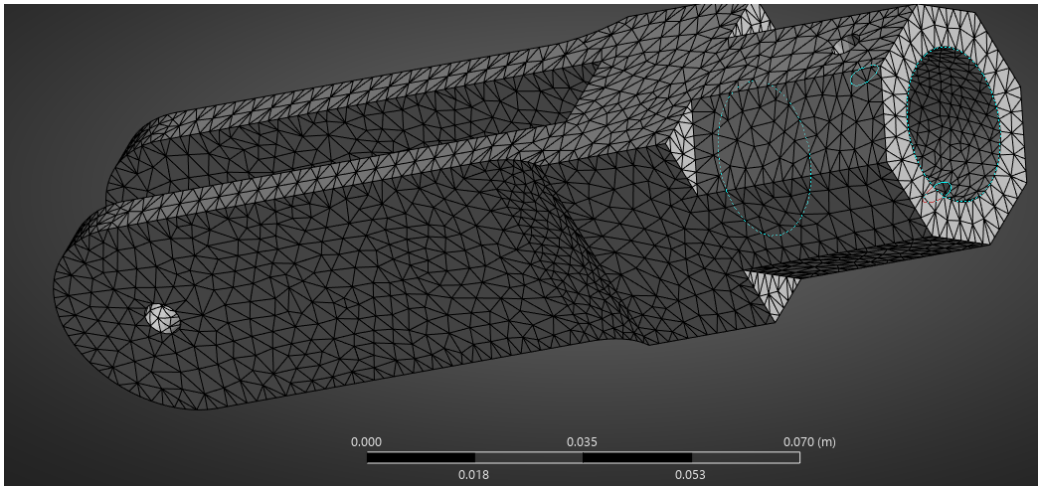

Figure X: Outer Knuckle Mesh

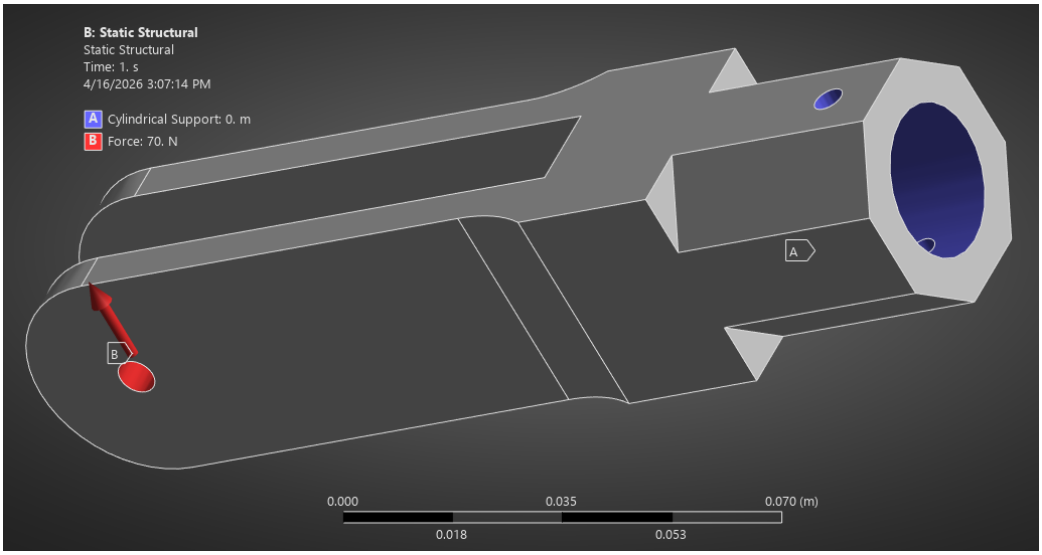

Figure X: Outer Knuckle Forces and Supports

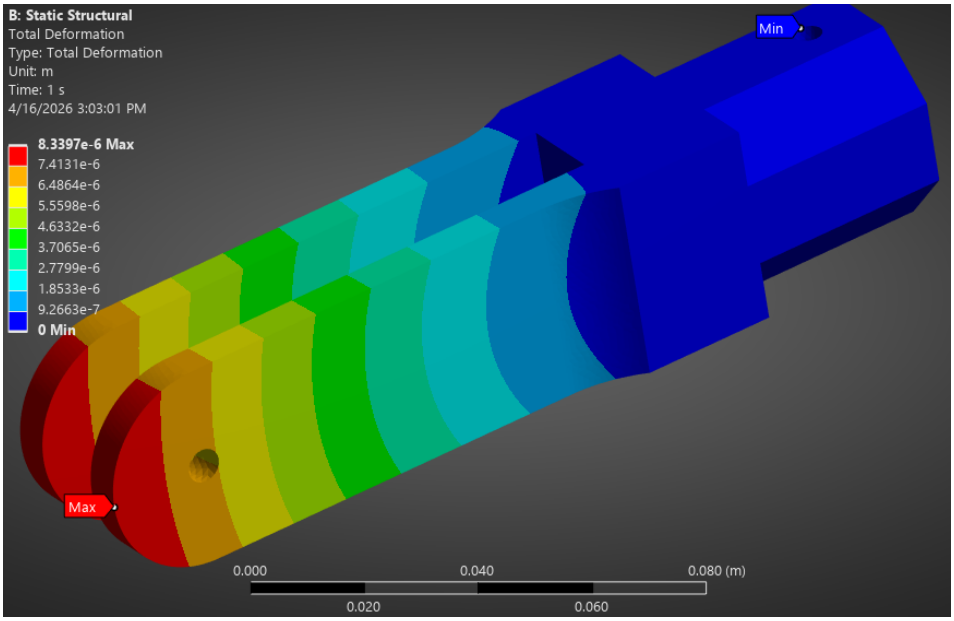

Figure X: Outer Knuckle Total Deformation

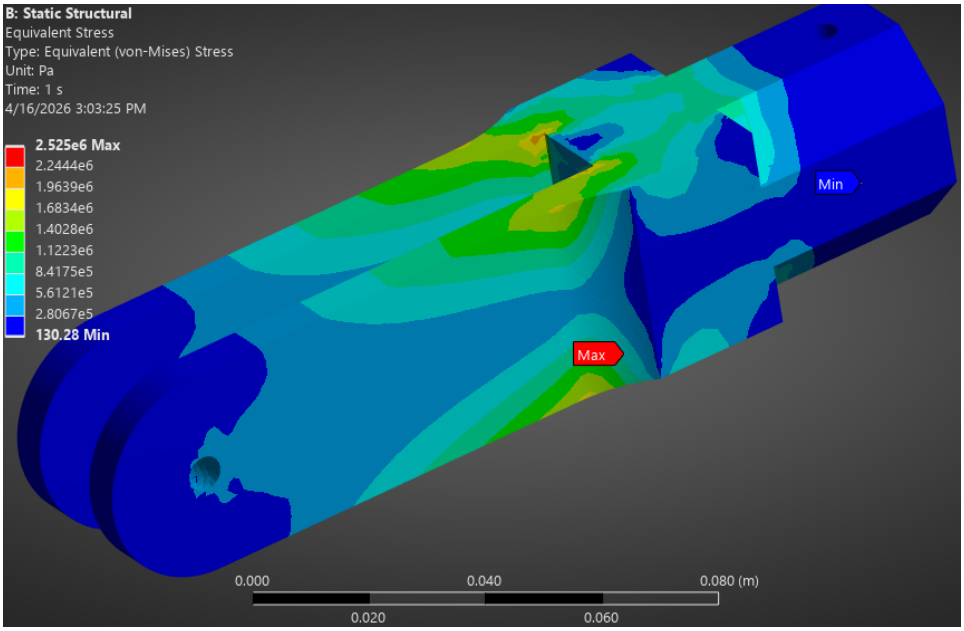

Figure X: Outer Knuckle Equivalent Stress

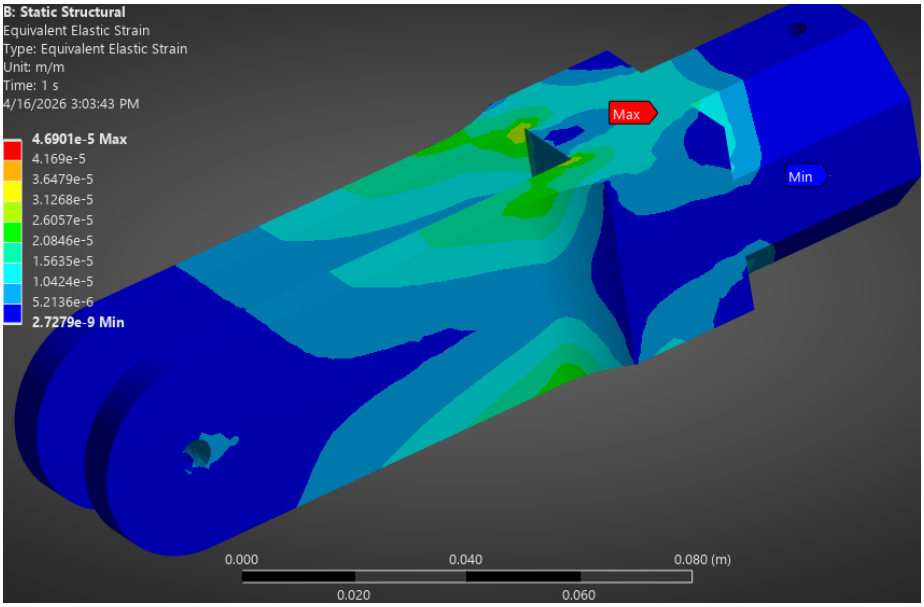

Figure X: Outer Knuckle Equivalent Strain

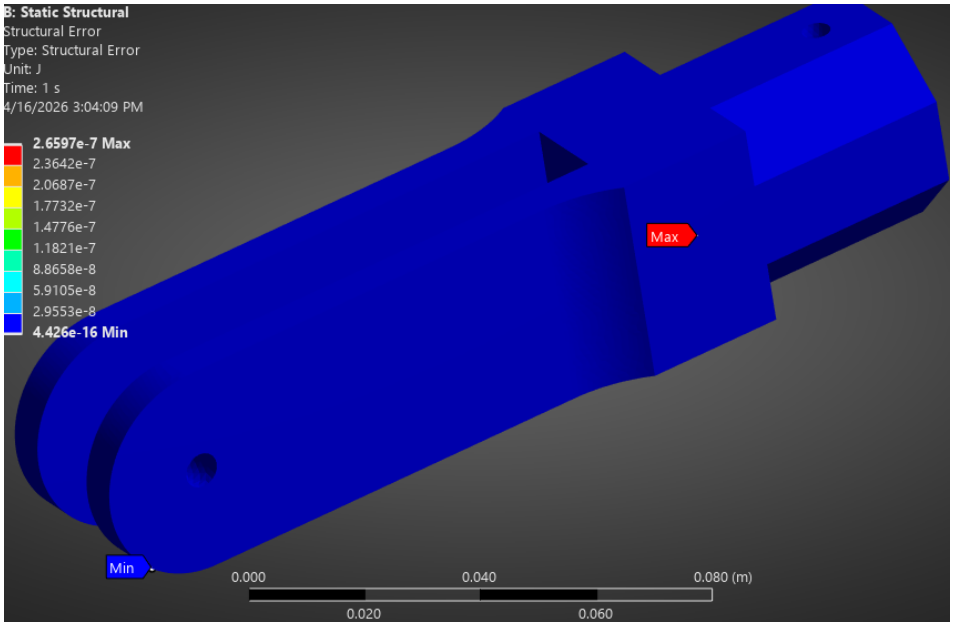

Figure X: Outer Knuckle Structural Error

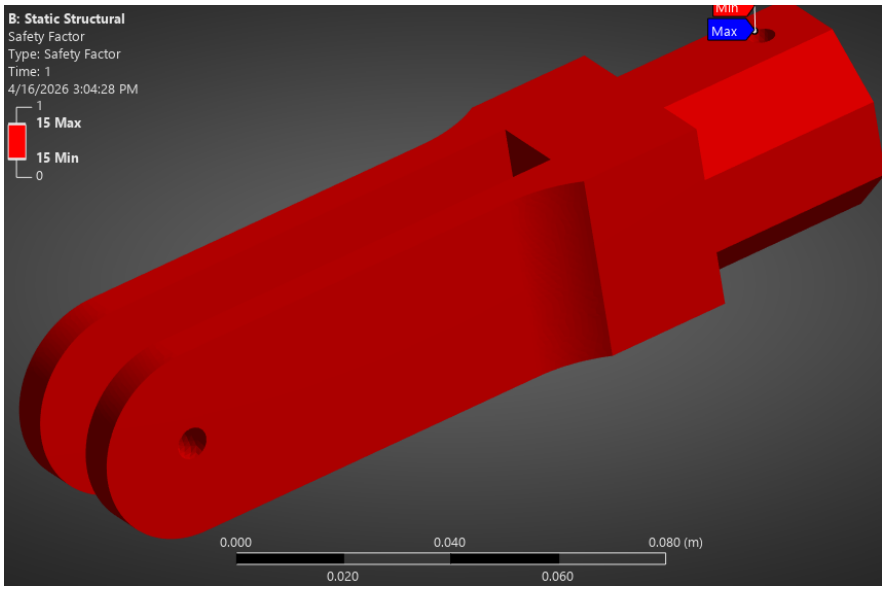

Figure X: Outer Knuckle Factor of Safety

Redacted due to Export Control/CUI requirements.

Figure X: Motor Mounts Dimensioned Drawing

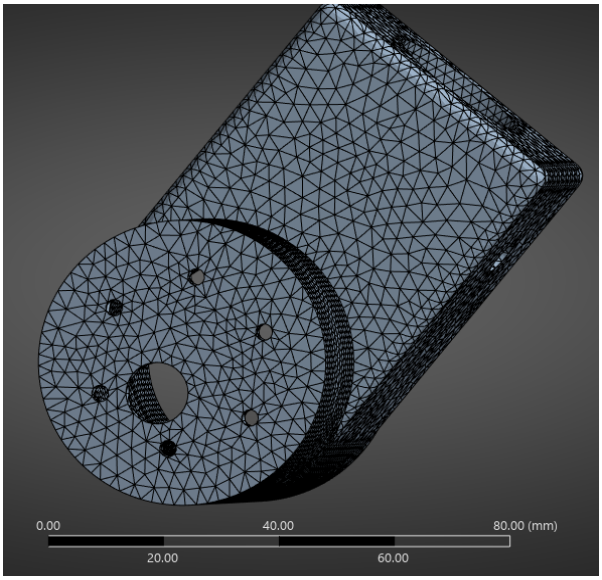

Figure X: Motor Mounts Mesh

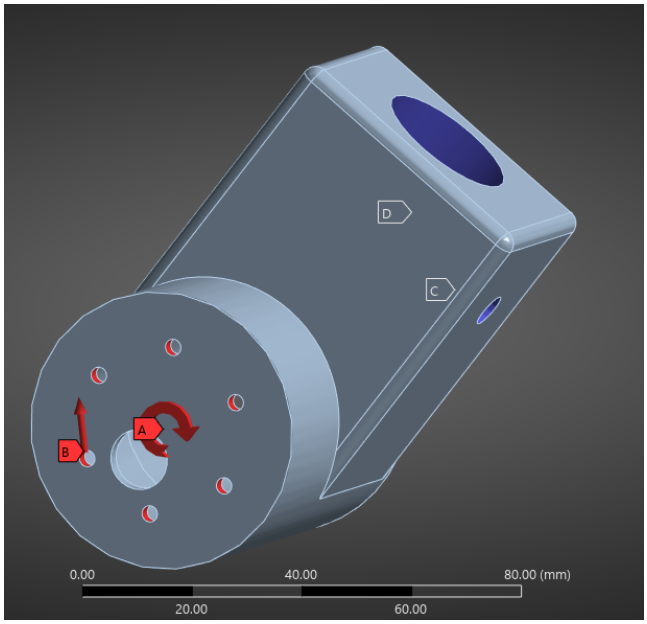

Figure X: Motor Mounts Forces and Supports

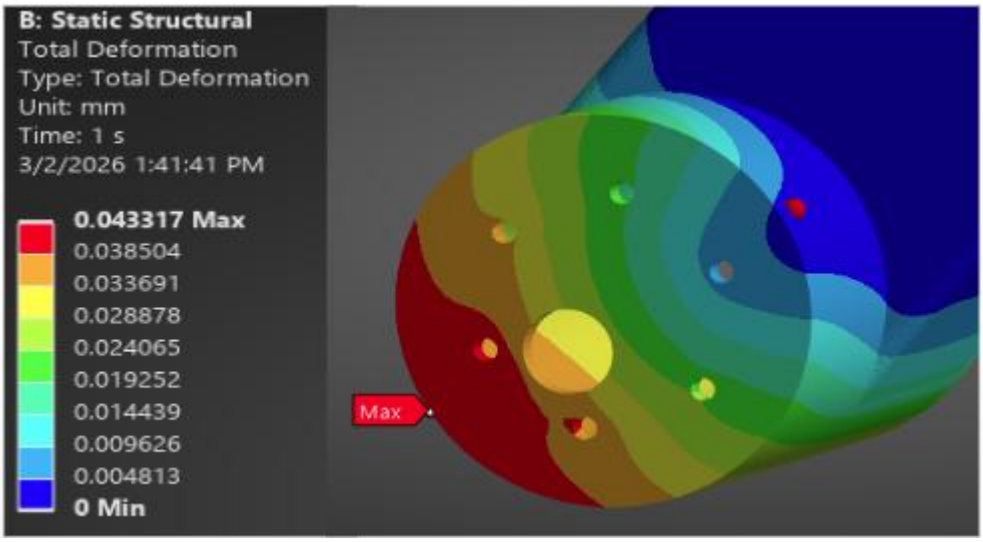

Figure X: Motor Mounts Total Deformation

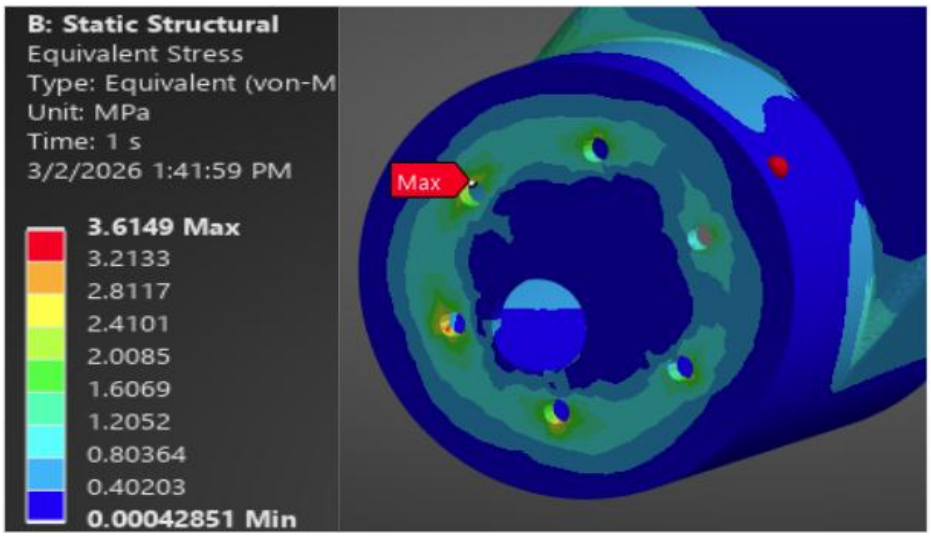

Figure X: Motor Mounts Equivalent Stress

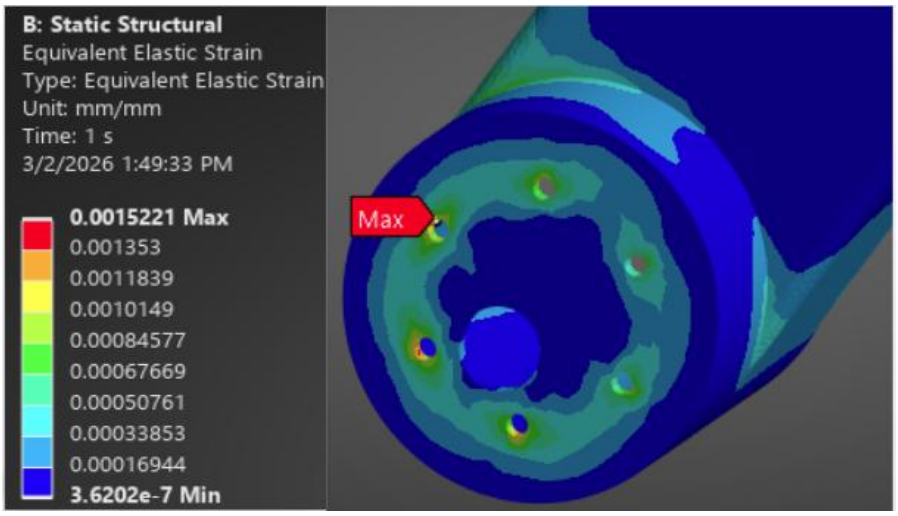

Figure X: Motor Mounts Equivalent Strain

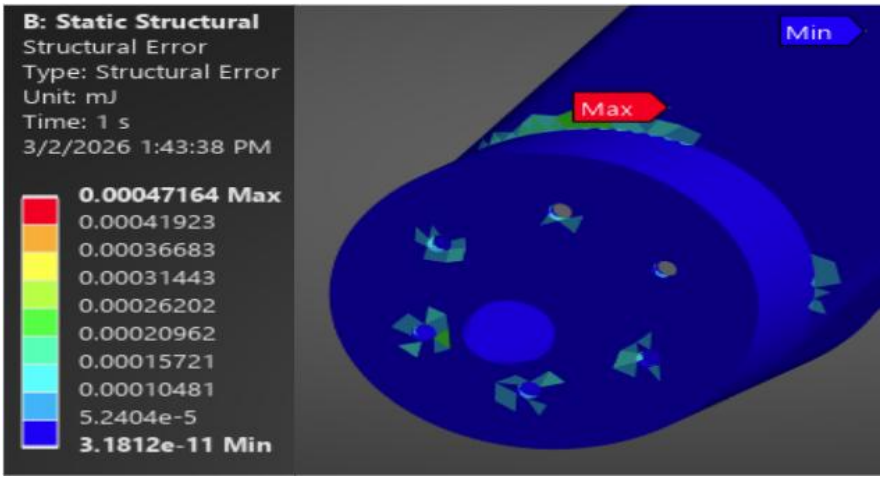

Figure X: Motor Mounts Structural Error

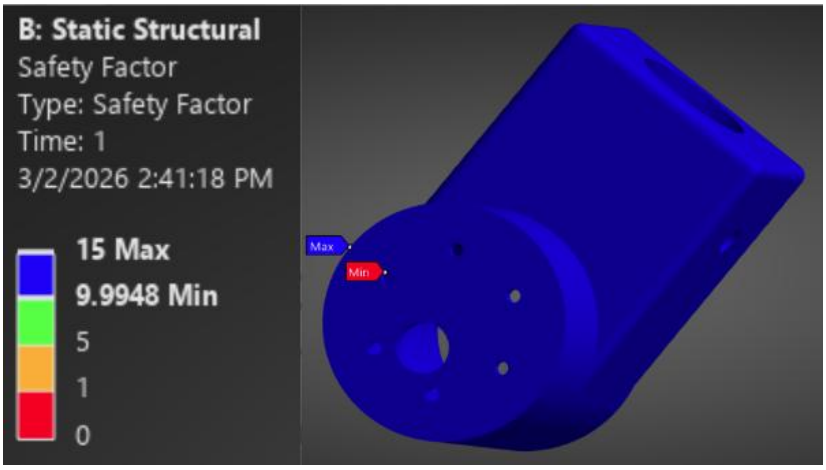

Figure X: Motor Mounts Factor of Safety

Redacted due to Export Control/CUI requirements.

Figure X: Bearing Housing Dimensioned Drawing

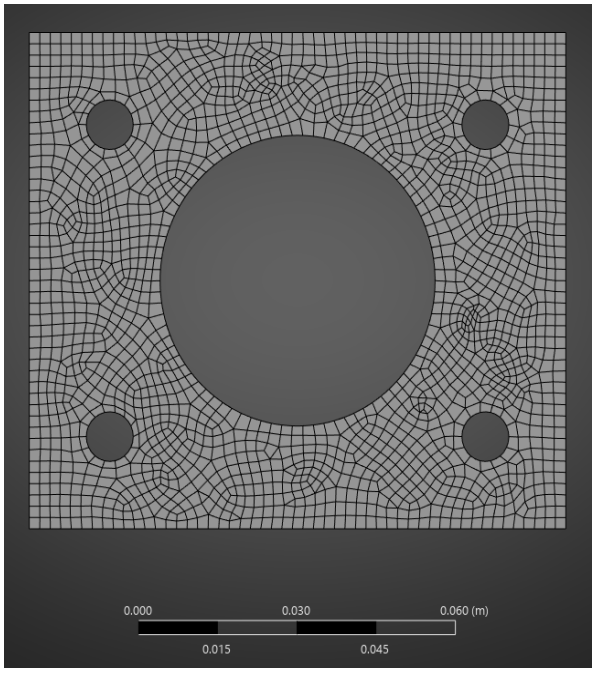

Figure X: Bearing Housing Mesh

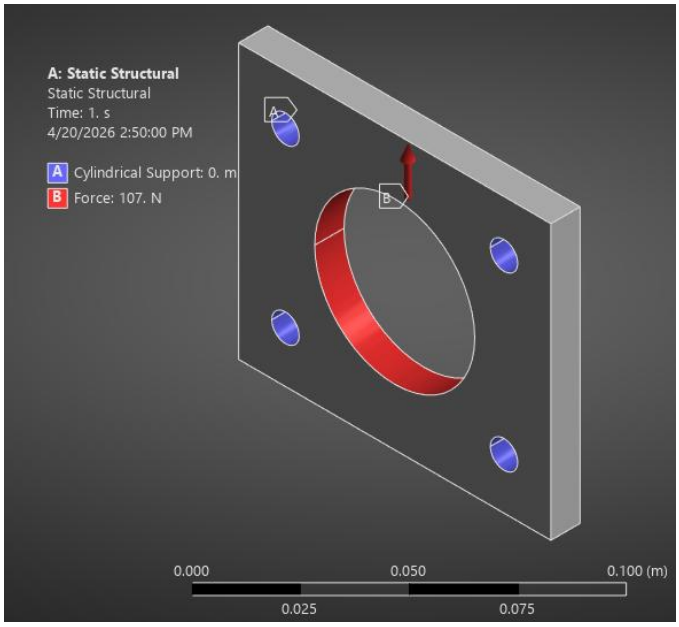

Figure X: Bearing Housing Forces and Supports

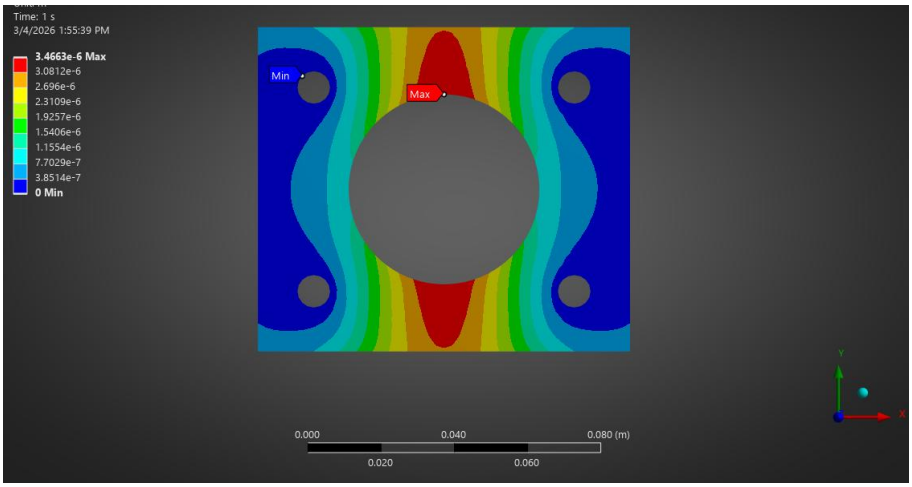

Figure X: Bearing Housing Total Deformation

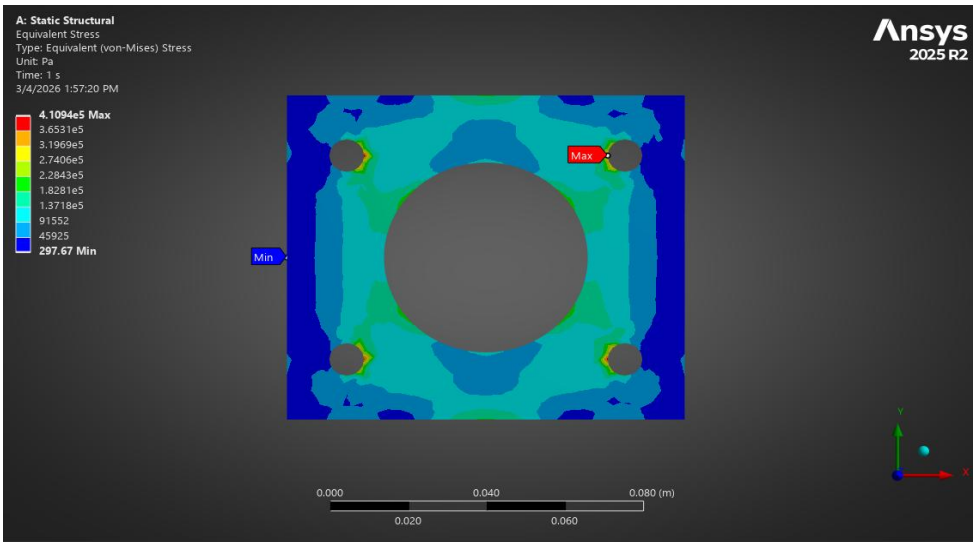

Figure X: Bearing Housing Equivalent Stress

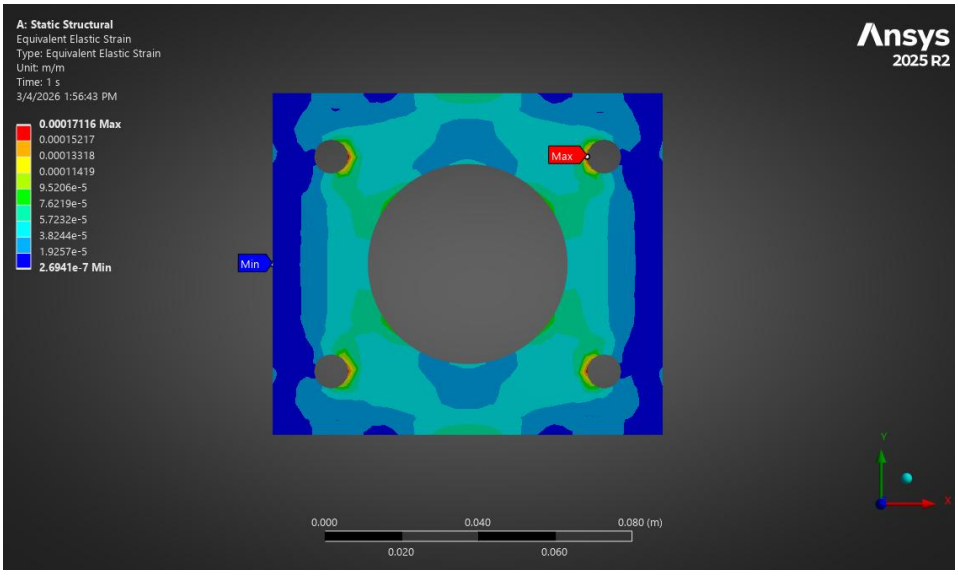

Figure X: Bearing Housing Equivalent Strain

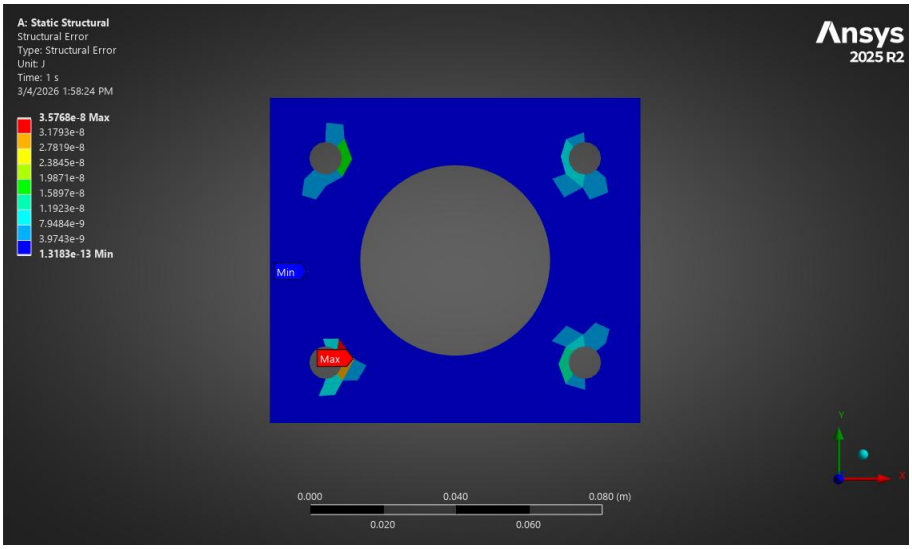

Figure X: Bearing Housing Structural error

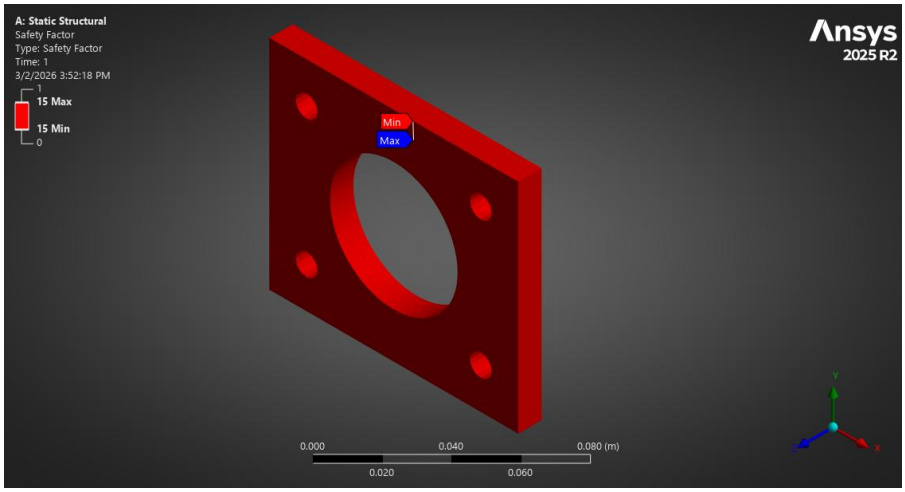

Figure X: Bearing Housing Factor of Safety

Redacted due to Export Control/CUI requirements.

Figure X: Main Leg Joint Dimensioned Drawing

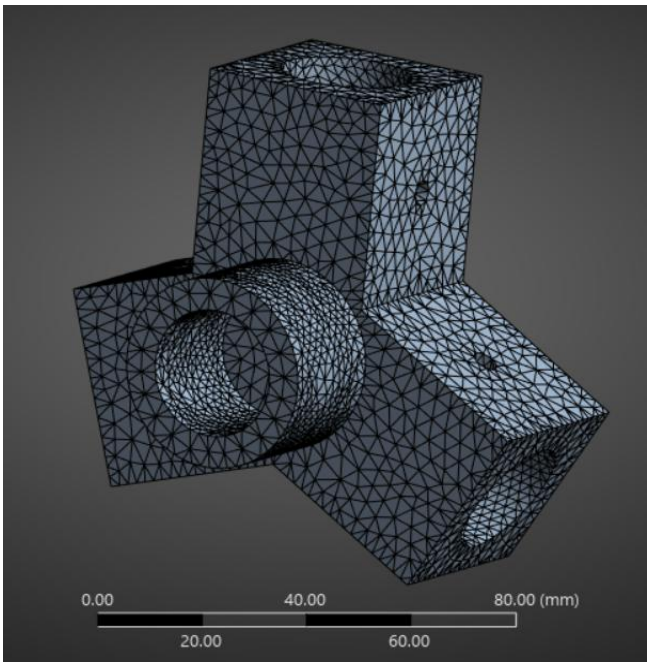

Figure X: Main Leg Joint Mesh

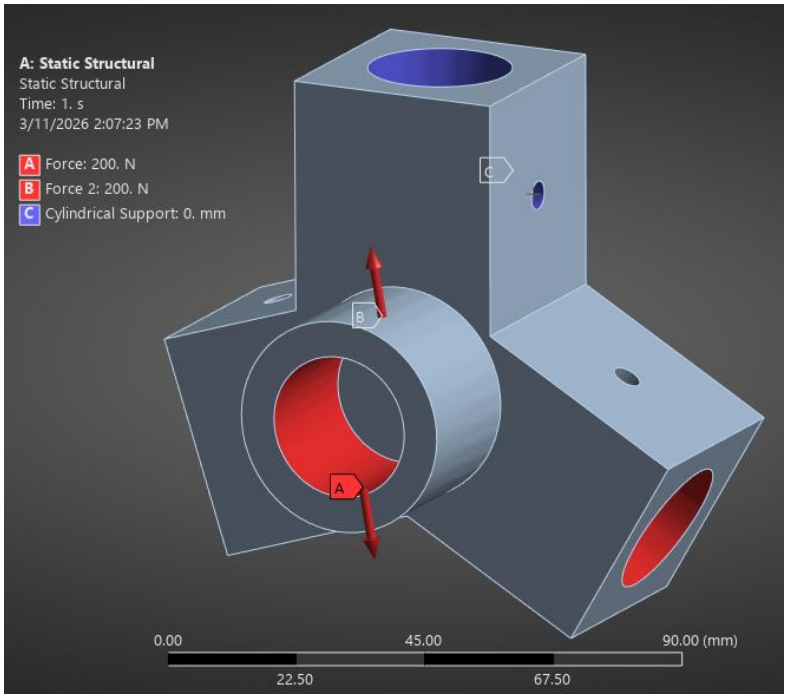

Figure X: Main Leg Joint Forces and Supports

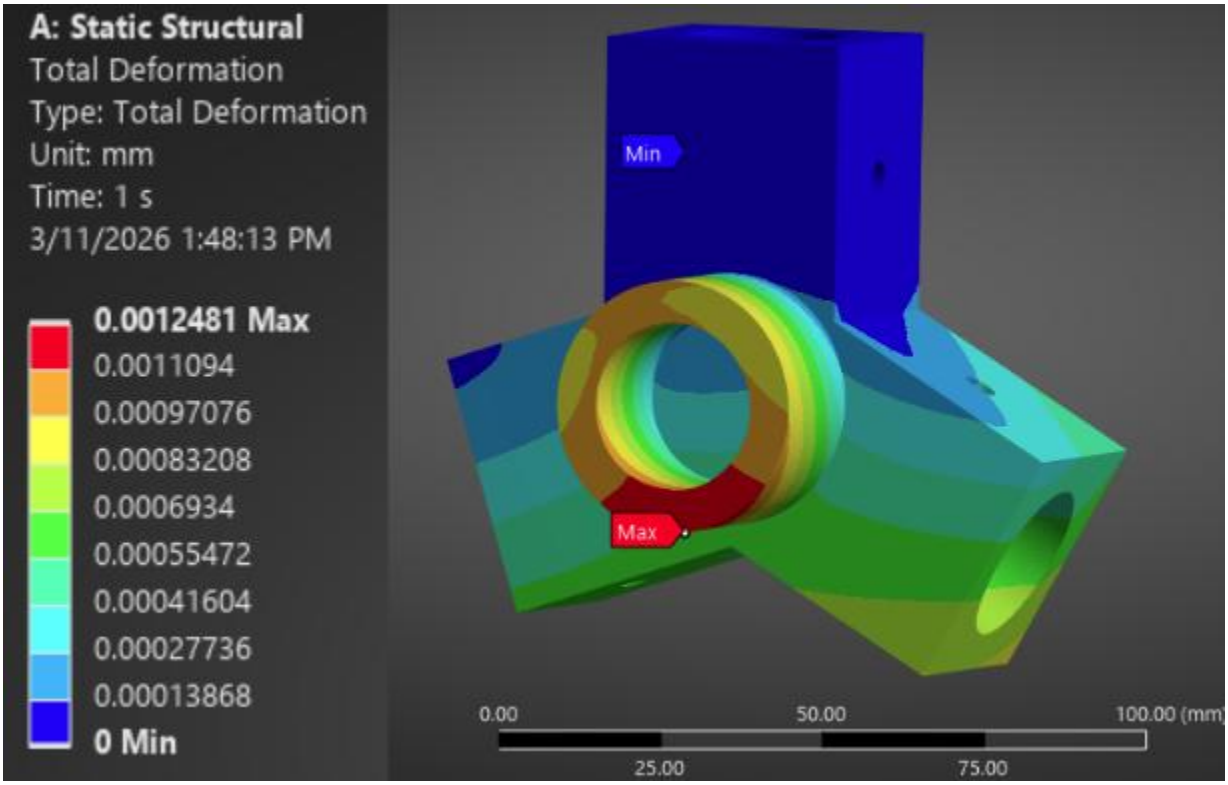

Figure X: Main Leg Joint Total Deformation

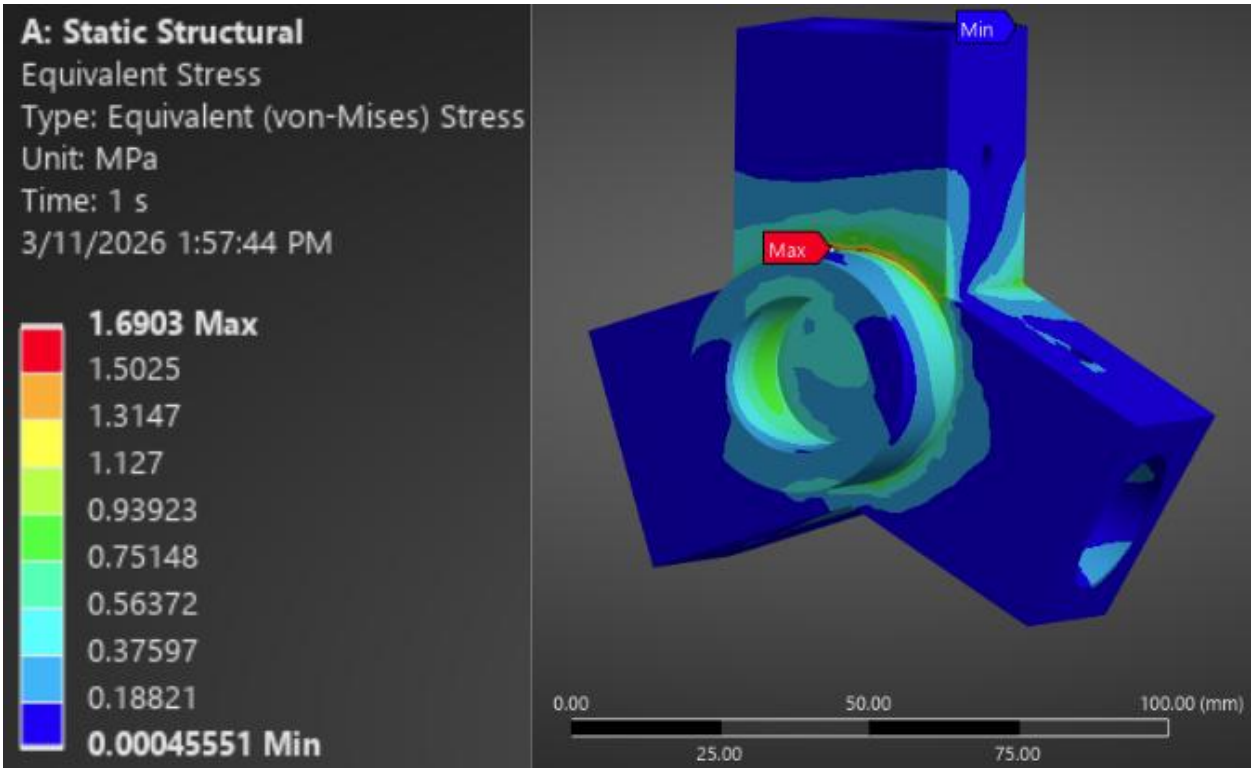

Figure X: Main Leg Joint Equivalent Stress

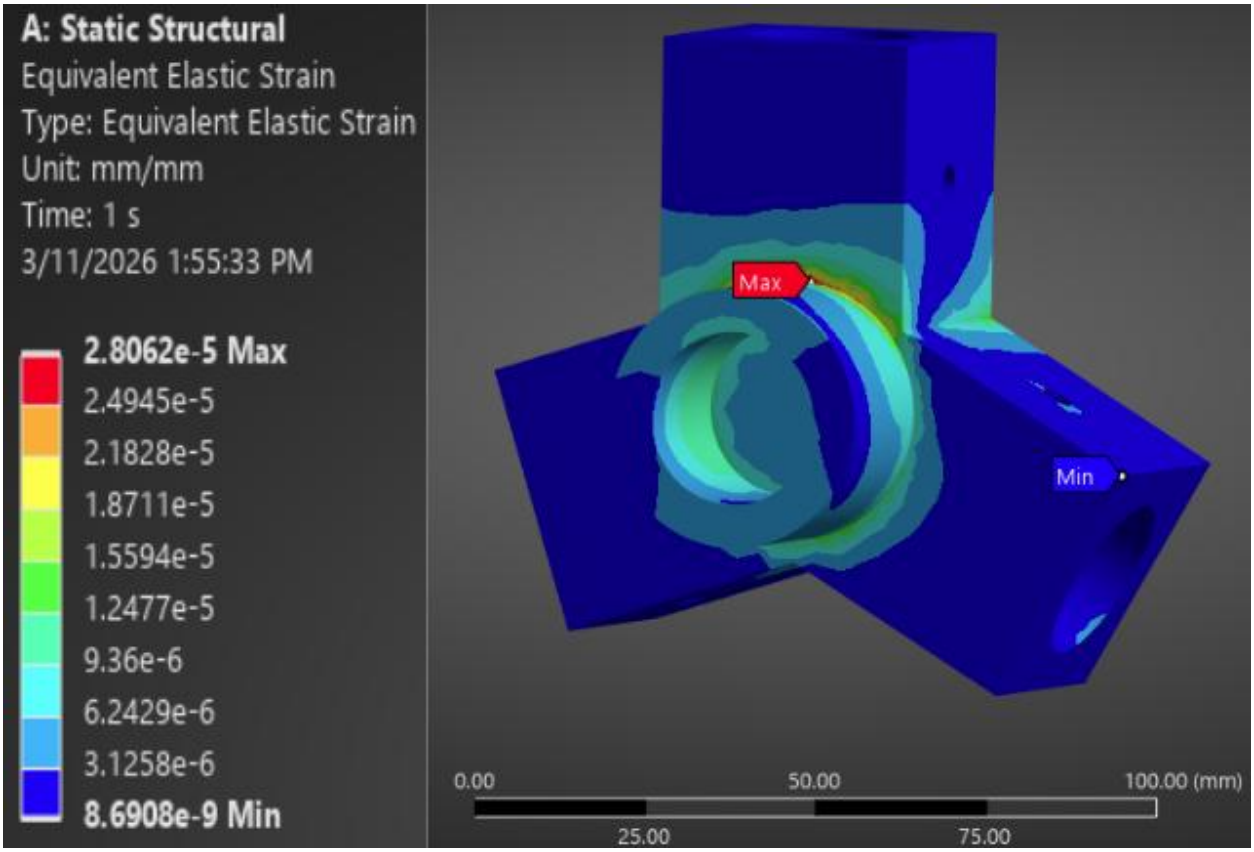

Figure X: Main Leg Joint Equivalent Strain

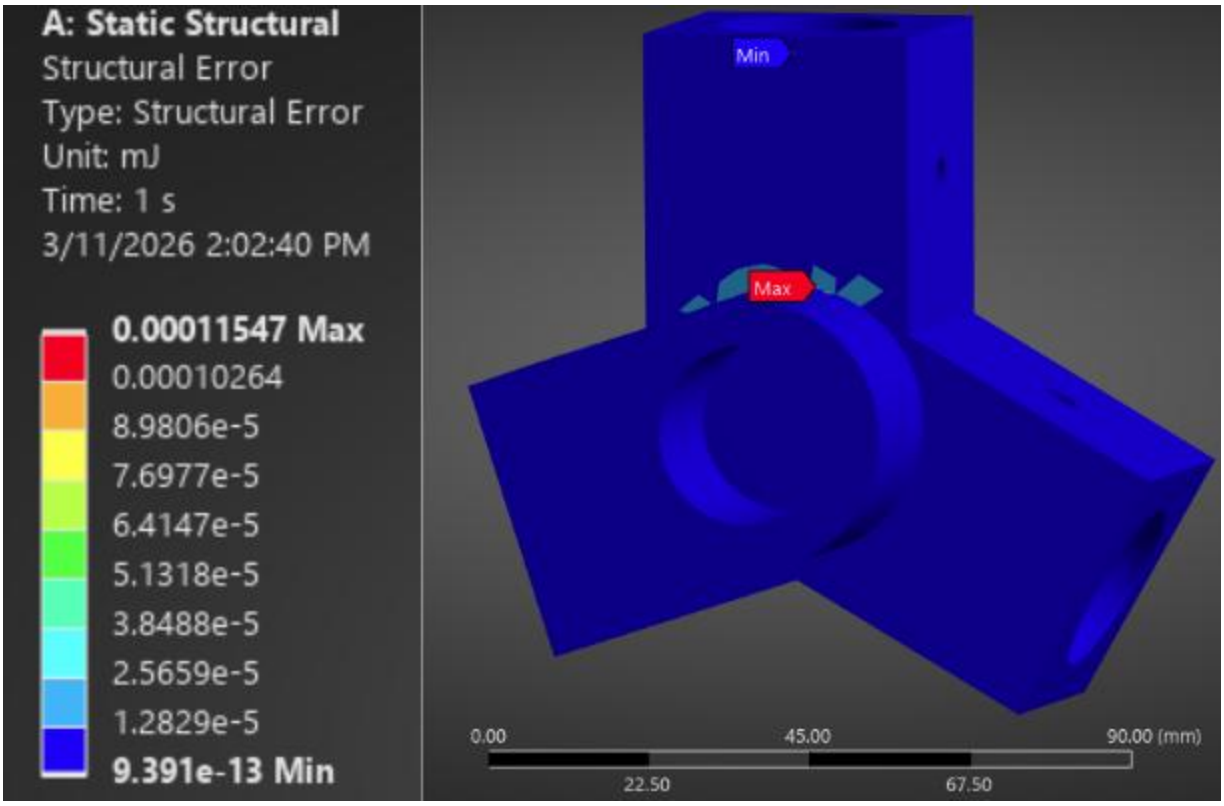

Figure X: Main Leg Joint Structural Error

Figure X: Main Leg Joint Factor of Safety

Redacted due to Export Control/CUI requirements.

Figure X: Differential Bracket Dimensioned Drawing

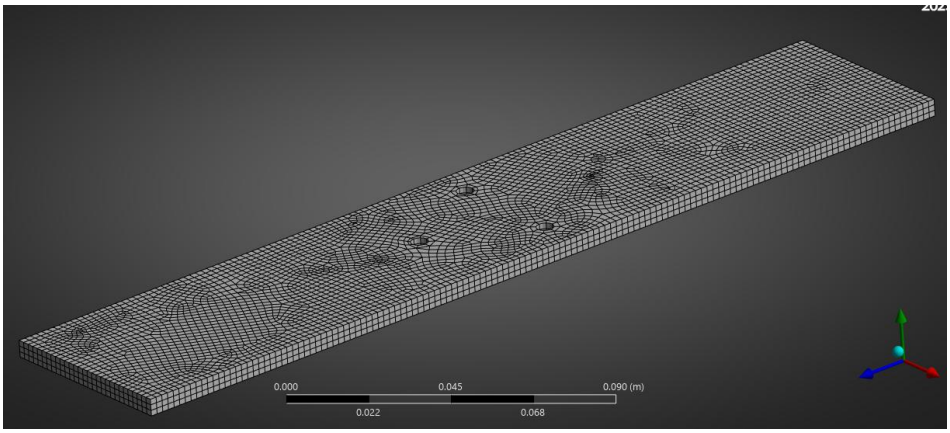

Figure X: Differential Bracket Mesh

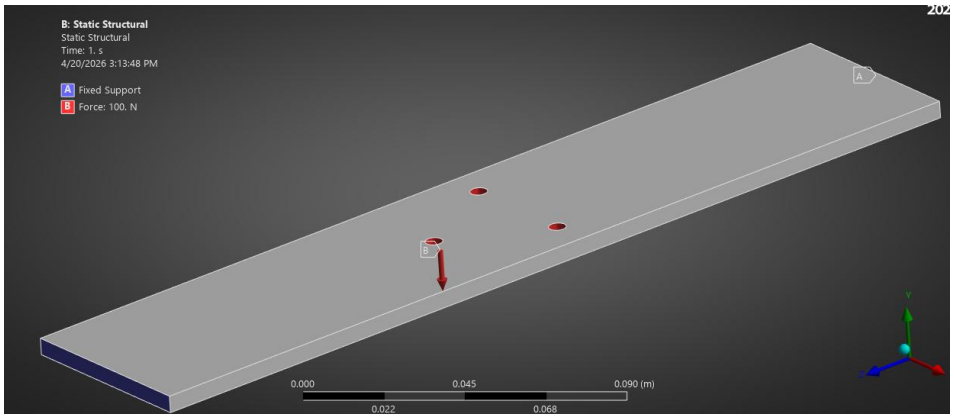

Figure X: Differential Bracket Forces and Supports

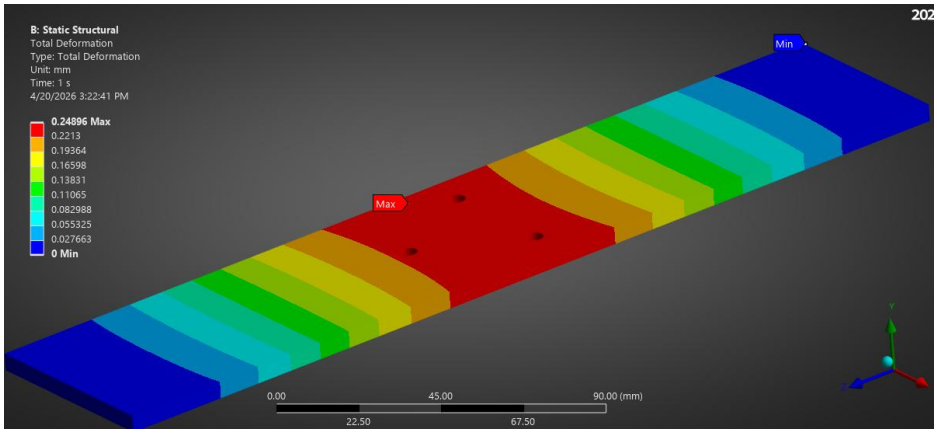

Figure X: Differential Bracket Total Deformation

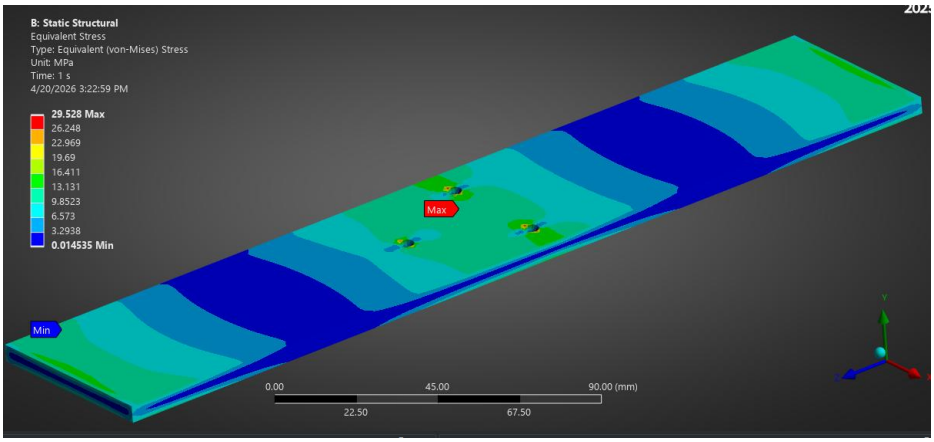

Figure X: Differential Bracket Equivalent Stress

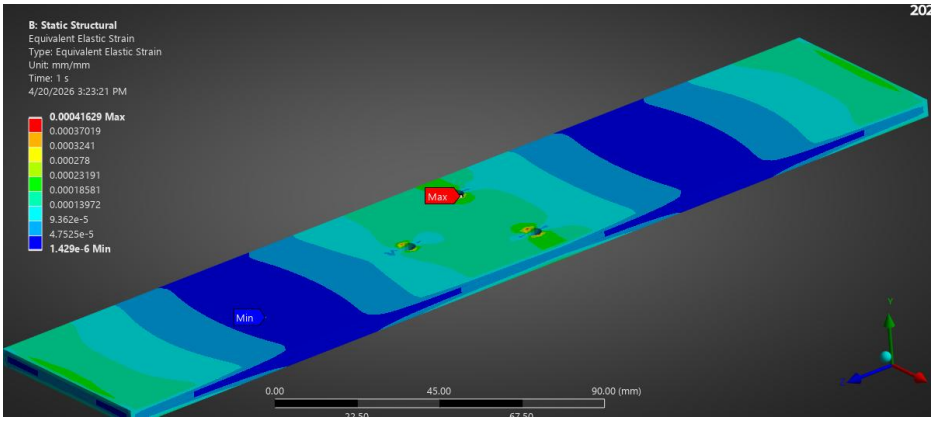

Figure X: Differential Bracket Equivalent Strain

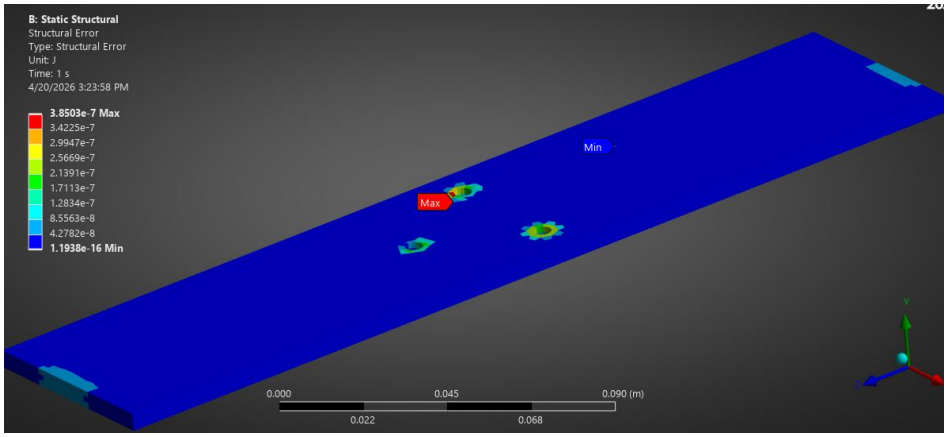

Figure X: Differential Bracket Structural Error

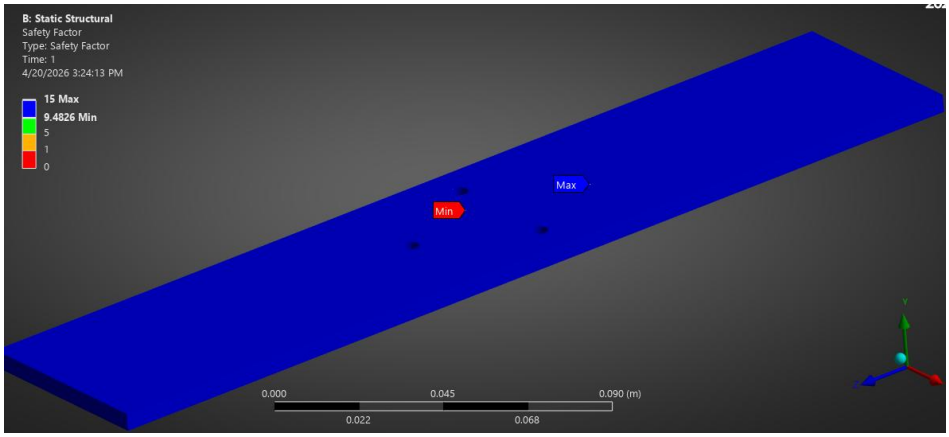

Figure X: Differential Bracket Factor of Safety

Redacted due to Export Control/CUI requirements.

Figure X: Differential Support Bar Dimensioned Drawing

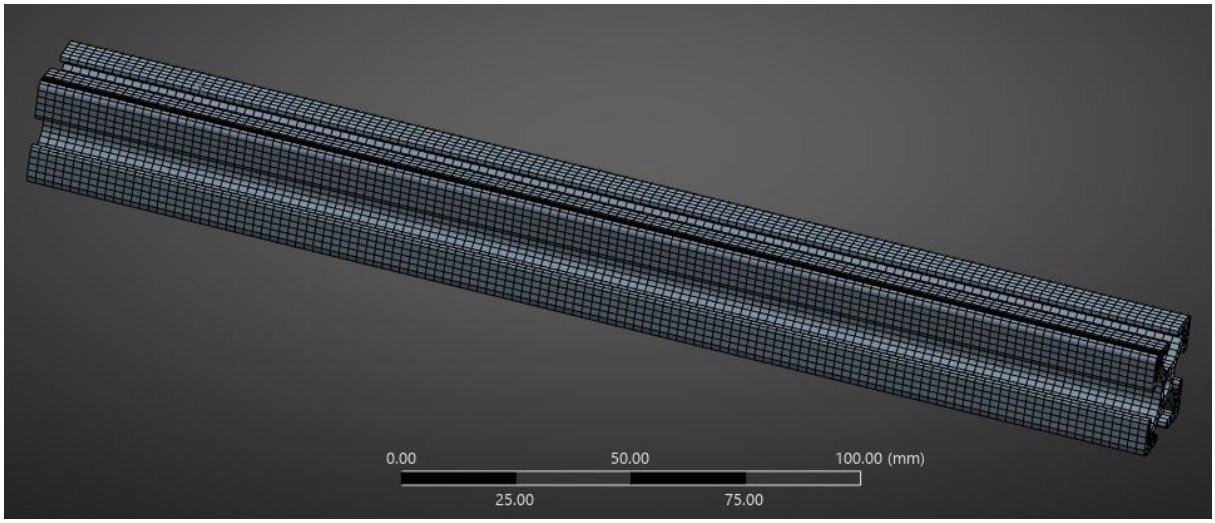

Figure X: Differential Support Bar Mesh

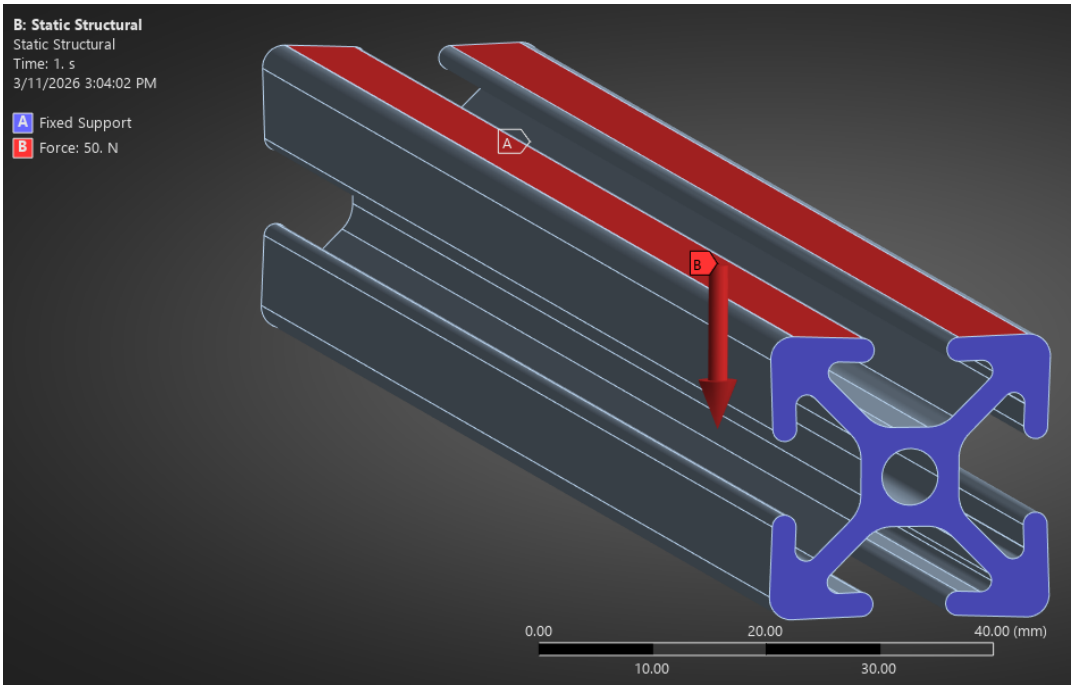

Figure X: Differential Support Bar Forces and Supports

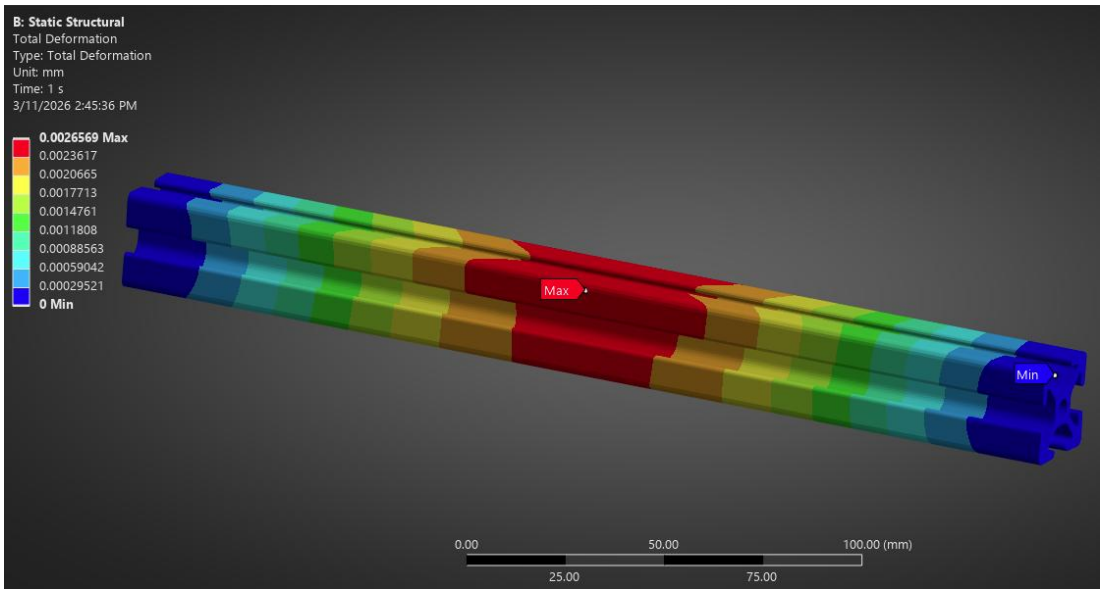

Figure X: Differential Support Bar Total Deformation

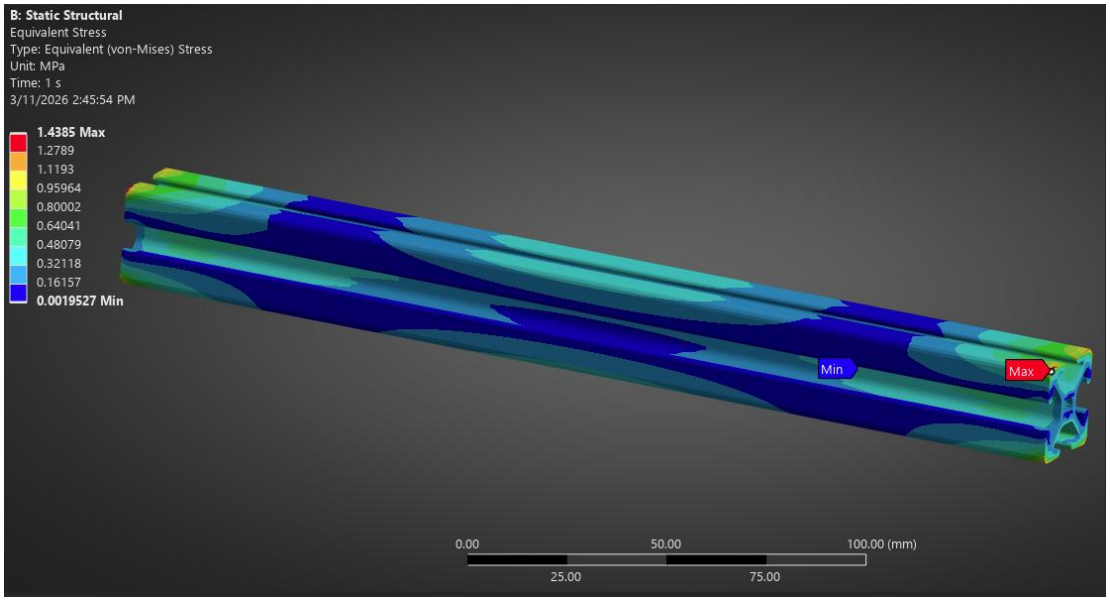

Figure X: Differential Support Bar Equivalent Stress

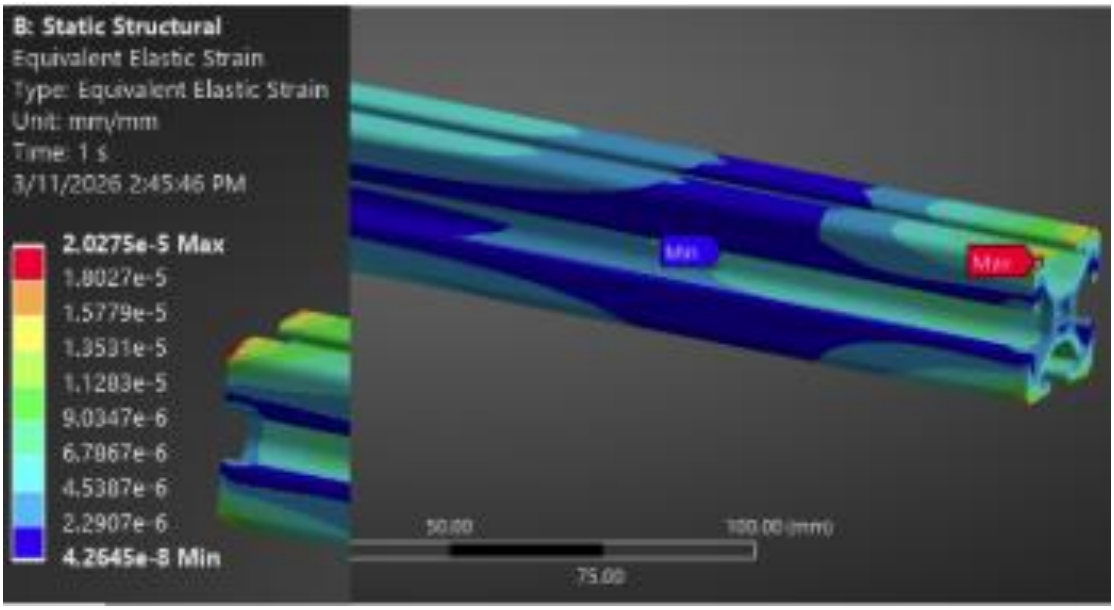

Figure X: Differential Support Bar Equivalent Strain

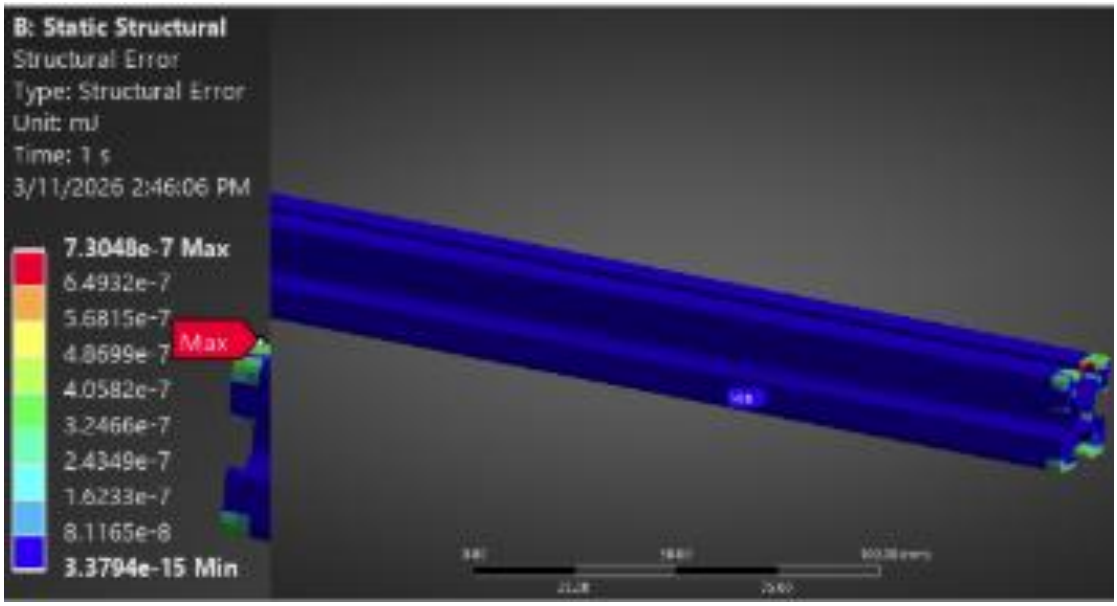

Figure X: Differential Support Bar Structural Error

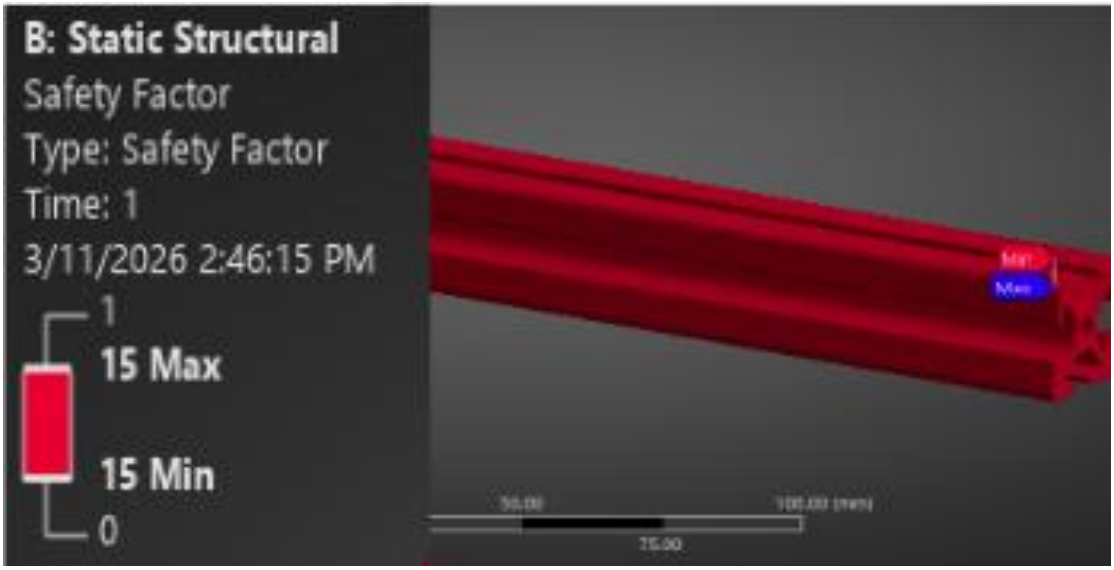

Figure X: Differential Support Bar Factor of Safety

Figure X: Differential Tube Fitting Dimensioned Drawing

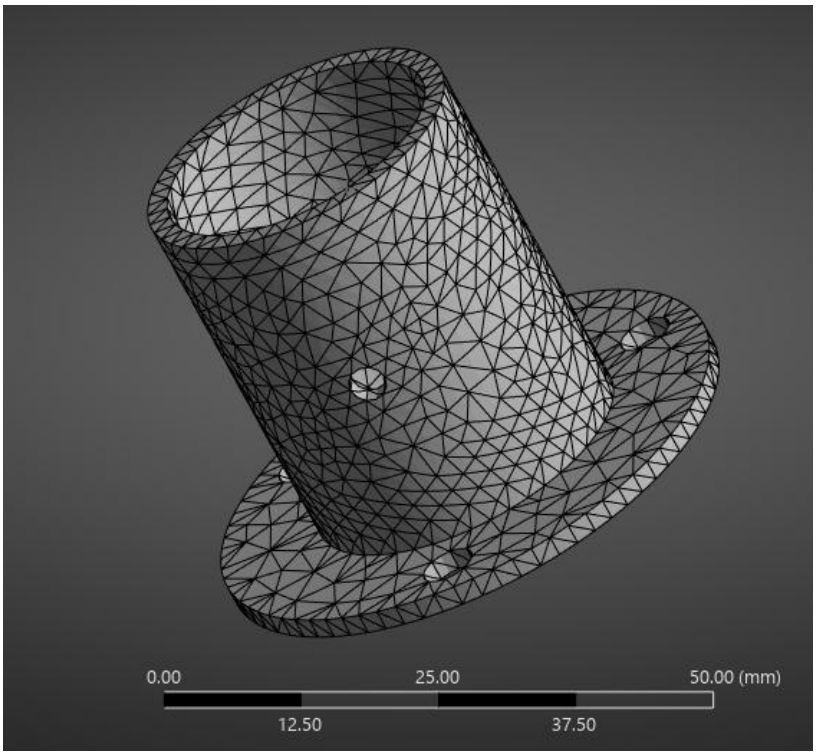

Figure X: Differential Tube Fitting Mesh

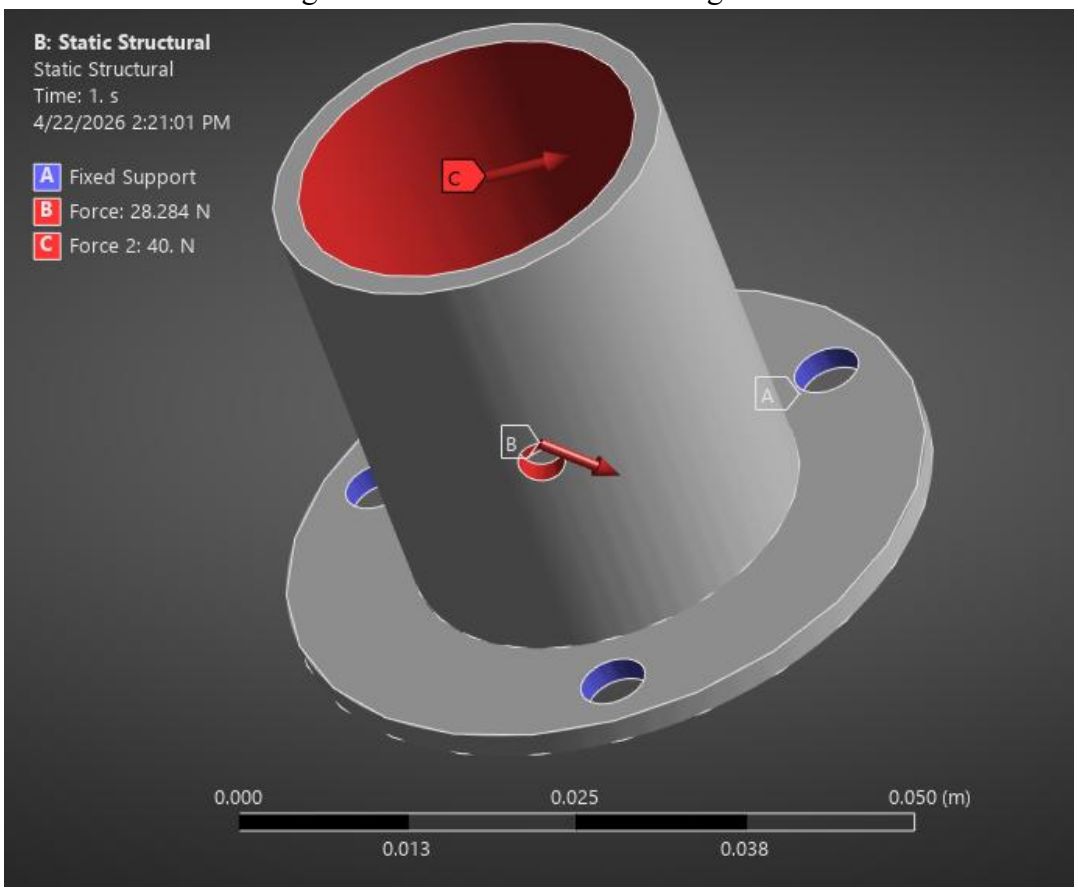

Figure X: Differential Tube Fitting Forces and Supports

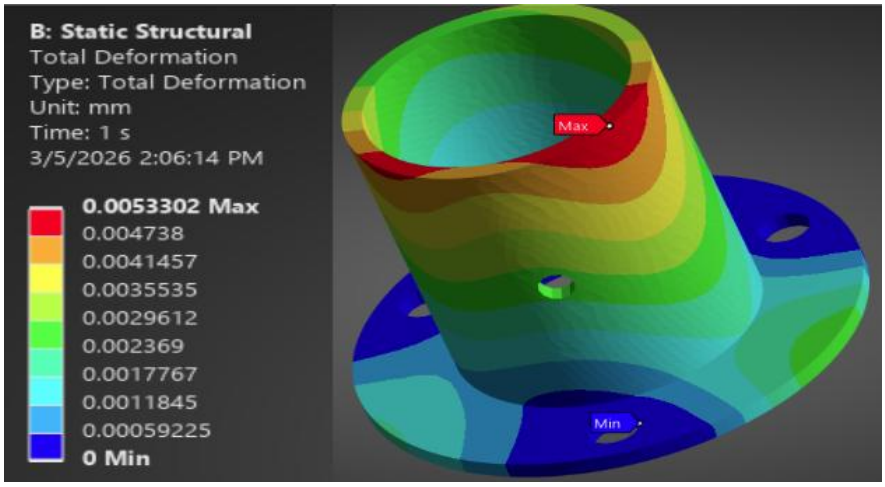

Figure X: Differential Tube Fitting Total Deformation

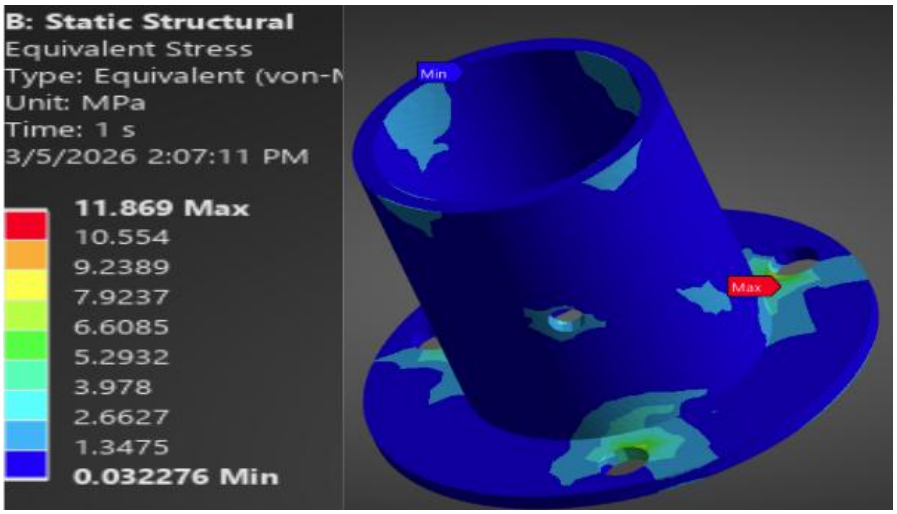

Figure X: Differential Tube Fitting Equivalent Stress

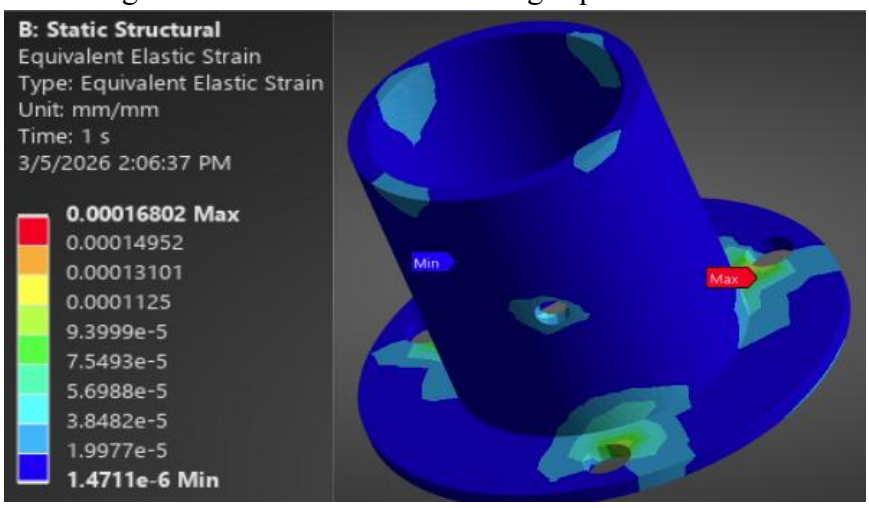

Figure X: Differential Tube Fitting Equivalent Strain

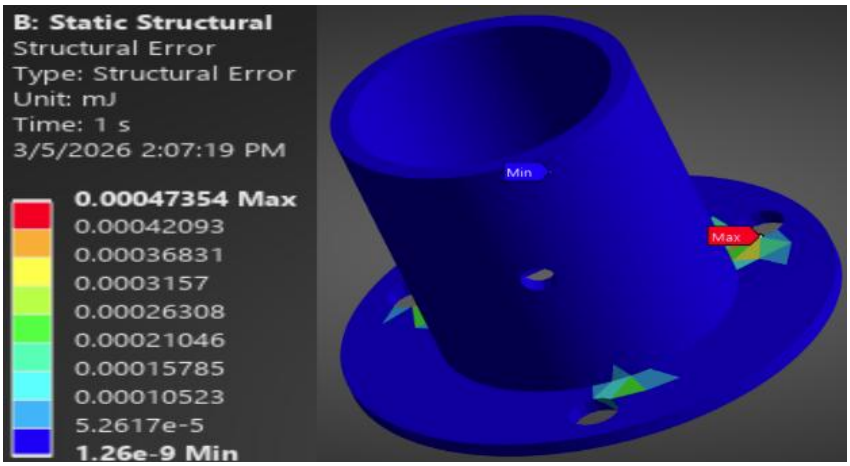

Figure X: Differential Tube Fitting Structural Error

Figure X: Differential Tube Fitting Factor of Safety